Lithos 380–381 (2021) 105865

Contents lists available at ScienceDirect

Lithos

journal homepage: www.elsevier.com/locate/lithos

Research Article

Anatexis origin of rare metal/earth pegmatites: Evidences from the Permian pegmatites in the Chinese Altai

Zheng-Hang Lv, Hui Zhang *, Yong Tang

Key Laboratory of High-temperature and High-pressure Study of the Earth's Interior, Institute of Geochemistry, Chinese Academy Sciences, Guiyang 550081, China

ARTICLE INFO

Article history:
Received 22 April 2019
Received in revised form 19 August 2020
Accepted 29 October 2020
Available online 2 November 2020

Keywords:
Anatexis
Rare metal
Rare earth
Pegmatite
Chinese Altai

ABSTRACT

The petrogenesis of the isolated pegmatites from granites is under debate. In the Chinese Altai, massive isolated pegmatites have been regarded as derivatives of granitic melts, which contradicts to the results of recent studies. In this work, the geology and mineralogy, as well as the zircon U-Pb chronology and Hf isotope geochemistry, of 10 Permian pegmatites are analyzed, and a comparative study of the Permian pegmatites and granites is conducted to reveal the petrogenesis of the Permian pegmatites in the Chinese Altai. The Permian pegmatites are concentrated in the Qiongkuer domain with a linear distribution and show structural control from regional anticlinoriums and connections to adjacent migmatites and luecogranite dykes. Their zircon U-Pb ages are 274–253 Ma, with the dominating age being late Permian. The pegmatites have three mineralization types including Li-Be-Ta-Nb ± Sn, Be-Nb-Ta ± REEs (rare earth elements) and REEs. The former two are comparable with the Triassic and Devonian-Carboniferous pegmatites in mineralization and Hf isotope composition, respectively, and the latter is unique in the Permian generation. The Permian pegmatites have comparable Hf isotope compositions with the juvenile and specific components in the Habahe Group, which indicates the dependency of mineralization on source from the heterogeneous Habahe Group metasedimentary rocks. The pegmatites also show decoupling spatial-temporal and differentiation-source correlations with the Permian granites, indicating no genetic relationship between them. Combining with the Permian high temperature metamorphism and previous tectonic-magmatic-metamorphic studies, we suggest that the Permian rare metal/earth pegmatites were likely generated by anatexis of the Habahe Group metasedimentary rocks under an extensional setting after the arc-arc collision between the Junggar arcs and the Chinese Altai.

1. Introduction

Granitic pegmatites hereafter referred to simply as pegmatites, are commonly regarded as the derivatives of granitic melt owing to their similarities in mineral assemblage and bulk composition (e.g., Černý, 1991a; Černý et al., 2012a; London, 2018). In some cases, a pegmatite can be linked to its parental granite according to the spatial, temporal or chemical connections between them. However, since such a relationship is not always present, the isolated pegmatites from granites have been hypothetically connected to the "deeply buried granites" (e.g., Černý, 1991a; London, 2008). However, the factors controlling the differentiation of granitic melts and the emplacement of pegmatite-forming melts are still unclear. Recent studies have proved that other than fractional crystallization, pegmatite formation can involve other mechanisms, such as anatexis (e.g., Dill, 2015a, 2015b; Lv et al., 2018a; Melleton et al., 2012; Müller et al., 2015, 2016, 2017; Simmons and Falster, 2016). The study of pegmatite petrogenesis is crucial from a scientific prospective because it reveals the origin of the pegmatite-forming melt. In addition, such studies have economic significance because the results serve as a guide for prospecting of rare metal ore deposits.

The Chinese Altai, one of the largest pegmatite provinces in the world, consists of two pegmatite belts, nine pegmatite fields, 38 mining areas, and more than 100,000 pegmatites (Zou and Li, 2006). It is known for production of rare metals Li, Be, Ta, Nb and Cs, since the finding of Koktokay No. 3 pegmatite in 1940s (Zhu et al., 2000). Abundant studies have been conducted on these pegmatites with focuses on their mineralogy (e.g., Liu and Zhang, 2005; Lv et al., 2018b; Tang and Zhang, 2015; Wang et al., 2006a, 2007a, 2009a; Wang et al., 1981; Yin et al., 2013; Zhang et al., 2004; Zhang A.C. et al., 2008; Zhang, 2001; Zhou et al., 2015a), chronology and isotope geochemistry (e.g., Chen et al., 1999; Liu, 2015; Lv et al., 2012, 2015, 2018a; Ma et al., 2015; Ren et al., 2011; Wang et al., 2001, 2002, 2003; Wang et al., 2007b; Zhang, 2001; Zhang et al., 2016; Zhou et al., 2018), melt and fluid inclusions (e.g., Wu et al., 1994; Lu et al., 1996; Zhang, 2001), classification (e.g., Luan et al., 1995; Lv et al., 2018a; Wu and Zou, 1989; Zou and Xu, 1975) and prospecting method (e.g., Luan et al., 1995; Lv et al.,

* Corresponding author.
E-mail address: zhanghui@vip.gyig.ac.cn (H. Zhang).

https://doi.org/10.1016/j.lithos.2020.105865
0024-4937/

2017, 2018c; Tang et al., 2013, 2018; Zhao et al., 2017). However, the petrogenesis of the rare metal pegmatites in the Chinese Altai remains poorly understood even though this topic is a crucial scientific issue. Early studies suggested that most of these rare metal pegmatites were formed by fractional crystallization of granitic melts (Wu and Zou, 1989; Zou and Li, 2006). However, our recent studies have proven that the rare metal pegmatites from the Qinghe, Koktokay, Kelumute, Kaluan, Azubai, Qunku and Bieyesamasi areas are commonly distinct from the neighboring or potential parent granites in ages and isotopic compositions (Liu, 2013; Lv et al., 2012, 2015, 2018a; Ma et al., 2015; Zhang et al., 2016). The petrogenesis of the massive pegmatites in the Chinese Altai requires reassessment.

Our previous studies have revealed that multiple generations of rare metal pegmatites formed during the Devonian synorogenic to Jurassic post- or anorogenic stage, with diagenetic and metallogenic peaks occurring in the Triassic (e.g., Liu, 2015; Lv et al., 2012, 2015, 2018a; Ma et al., 2015; Ren et al., 2011; Zhang et al., 2016). Comparatively, granites in the Chinese Altai show a diagenetic peak during the Devonian and a decreasing trend from the Devonian to the Jurassic (e.g., Wang et al., 2006b, 2009b, 2014a). It is widely accepted that the pegmatite group derived from the same batch of granitic melt is responsible for one generation of diagenetic and metallogenic events, such as the Triassic granite-pegmatite systems in Songpan-Ganzi and West Kunlun orogenic belts (Xu et al., 2020; Yan et al., 2018) and the Archean pegmatites and parental rock of the Ghost Lake batholith from the Mavis Lake in Canada (Breaks and Moore, 1992). However, pegmatite fields in the Chinese Altai commonly consist of three or two generations of rare metal pegmatites, such as the Devonian, Permian and Triassic pegmatites in the Jiamanhaba and Qiebielin pegmatite fields (Lv et al., 2018a; Ren et al., 2011). How the multiple generations of rare metal pegmatites were formed by fractional crystallization of granitic melts, if the requirements include sufficient material and energy bases such as granitic batholiths, successive fractional crystallization from granitic to pegmatite-forming melts, and a specific tectonic setting such as late- or post-orogenic (e.g., Černý, 1991a, 1991b). In this study, the geology, mineralogy, zircon U-Pb age, and Hf isotopic compositions of 10 Permian pegmatites are analyzed, and a comparative study between the pegmatites and granites in the Chinese Altai is conducted to reveal the mineralization, age, source and tectonic setting of the pegmatites, and to evaluate the genetic relationship between the pegmatites and granites in the Chinese Altai.

2. Geological background

2.1. Regional geology

The Chinese Altai is located in the middle segment of the western part of the Central Asian Orogenic Belt (CAOB) and is adjacent to Kazakhstan to the west, Russia to the north and Mongolia to the east (Fig. 1a). According to its stratigraphy, metamorphism, deformation pattern, and magmatic activity, the Chinese Altai is divided into four fault-bounded domains including the North Altai, the Central Altai, the Qiongkuer and the Erqis domains (Fig. 1b) (e.g., Cai et al., 2011a, 2011b; Long et al., 2007; Sun et al., 2008; Yuan et al., 2007). The North Altai domain (Unit I in Fig. 1b) is bounded to the south by the Hongshanzui-Nuoerte Fault (F1 in Fig. 1b); Devonian - lower Carboniferous metavolcanic and metasedimentary rocks (e.g., Wang et al., 2006b; Windley et al., 2002) are widely exposed in this domain. The igneous rocks mainly consist of Devonian granite porphyry and I-type granites (e.g., Lv et al., 2015; Qin et al., 2016; Yuan et al., 2001). The Central Altai domain (Unit II in Fig. 1b) is bounded by the Hongshanzui-Nuoerte and the Abagong-Kuerti faults to the north and south, respectively. As the principal segment of the Chinese Altai, it is composed of a thick turbidite and pyroclastic sequence of the Habahe Group (e.g.,BGMRX, 1993 ; Windley et al., 2002), upper Ordovician volcanic molasse and terrigenous clastic sequences of the Dongxileke and Baihaba Formations, and middle to upper Silurian metasandstone of the Kulumuti Formation (e.g., BGMRX, 1993; Windley et al., 2002). Granitoids are widely exposed and consist of major early to mid-Paleozoic (500–360 Ma) I- and S-type granites (e.g., Cai et al., 2011a, 2011b; Ma et al., 2015; Sun et al., 2008, 2009b; Windley et al., 2007; Wang et al., 2006b, 2009b; Wang et al., 2010; Yuan et al., 2007; Zhang et al., 2017) and minor Mesozoic granites (230–202 Ma) (e.g., Chen et al., 2017; Liu, 2015; Wang et al., 2014a). Mafic rocks that formed in the Devonian have a limited occurrence in the Koktokay area (e.g., Cai et al., 2012a). The Qiongkuer domain (Unit III in Fig. 1b) is bounded by the Abagong-Kuerti Fault to the north and the Fuyun-Xibodu Fault to the south. It is composed of Paleozoic clastic and volcanic rocks, which are subdivided into the early Devonian Kangbutiebao Formation and the Middle Devonian Altai Formation, respectively (e.g., BGMRX, 1993; Windley et al., 2002). A recent study revealed a deposition time of Cambrian to Ordovician (540–460 Ma) for the Altai Formation based on the detrital zircon ages (Broussolle et al., 2018). The igneous rocks exposed in this domain mainly consist of middle-late Paleozoic I-type granite (e.g., Tong et al., 2014; Sun et al., 2008; Wang et al., 2006b, 2009b, Wang T. et al., 2010; Yang et al., 2010; Yuan et al., 2007; Zheng et al., 2016), late Paleozoic A-type granite (e.g., Liu, 2017), and Devonian-Permian mafic dykes (e.g., Broussolle et al., 2018; Cai et al., 2010, 2016; Pirajno et al., 2008; Wan et al., 2013). The south Altai domain (Unit IV in Fig. 1b) is located between the Fuyun-Xibodu Fault to the north and the Erqis Fault to the south. The northwestern part of this domain is largely covered by Quaternary sediments. The southeastern part is occupied mainly by Devonian fossiliferous successions of the Kangbutiebao Formation that are in turn overlain by Late Carboniferous formations (BGMRX, 1993; Windley et al., 2002). A few Carboniferous-Permian granites are exposed in this domain (Tong et al., 2012, 2014).

Recent studies have suggested that the Chinese Altai is a magmatic arc formed by multiple subduction-accertion processes occurring at an active continental margin during the middle Cambrian to early Permian. During the middle Cambrian, the tectonic setting of the Chinese Altai changed from a passive to active continental margin. Subsequently, the Chinese Altai underwent a prolonged subduction process from Ordovician to Carboniferous marked by ocean ridge subduction, massive granitic magma activity, and high-temperature metamorphism during the Devonian (e.g., Cai et al., 2010, 2011a, 2011b, 2012a; Jiang et al., 2010; Sun et al., 2009b). With the continuous subduction of the Paleo-Asian Ocean slab, the Chinese Altai converged consecutively with the East and West Junggar arcs during the Permian (e.g., Broussolle et al., 2018; Cai et al., 2012b, 2016; Li et al., 2015). After the amalgamation of the Siberia and Tarim cratons, the Chinese Altai entered a post-orogenic stage during the Triassic (e.g., Cai et al., 2016; Xiao et al., 2008, 2009, 2015, 2018).

2.2. Geology and mineralogy of the pegmatites

According to previously reported statistics, approximately 100,000 dykes constitute the huge number of pegmatites exposed in the Chinese Altai (Wu and Zou, 1989). They are distributed mainly in the Halong-Qinghe (A in Fig. 1b) and the Jiamanhaba-Dakalasu (B in Fig. 1b) located in the Central Altai Qiongkuer domains, respectively. Of these, the former consists of five pegmatite fields, including Qinghe, Kuwei-Jiebiete, Keketuohai, Kelumute-Jideke and Kalaeerqisi (1 to 5 in Fig. 1b, respectively), and the latter consists of four pegmatite fields, including Dakalasu-Kekexier, Xiaokalasu-Qiebielin, Hailiutan-Yeliuman and Jiamanhaba (6 to 9 in Fig. 1b, respectively) (Wu and Zou, 1989; Zou and Li, 2006).

2.2.1. JMHB06 pegmatite

The JMHB06 pegmatite is located in the southeastern part of the Jiamanhaba pegmatite field, which is situated at the western end of the Kabaer-Xibodu Paleozoic magmatic arc and the northern limb of

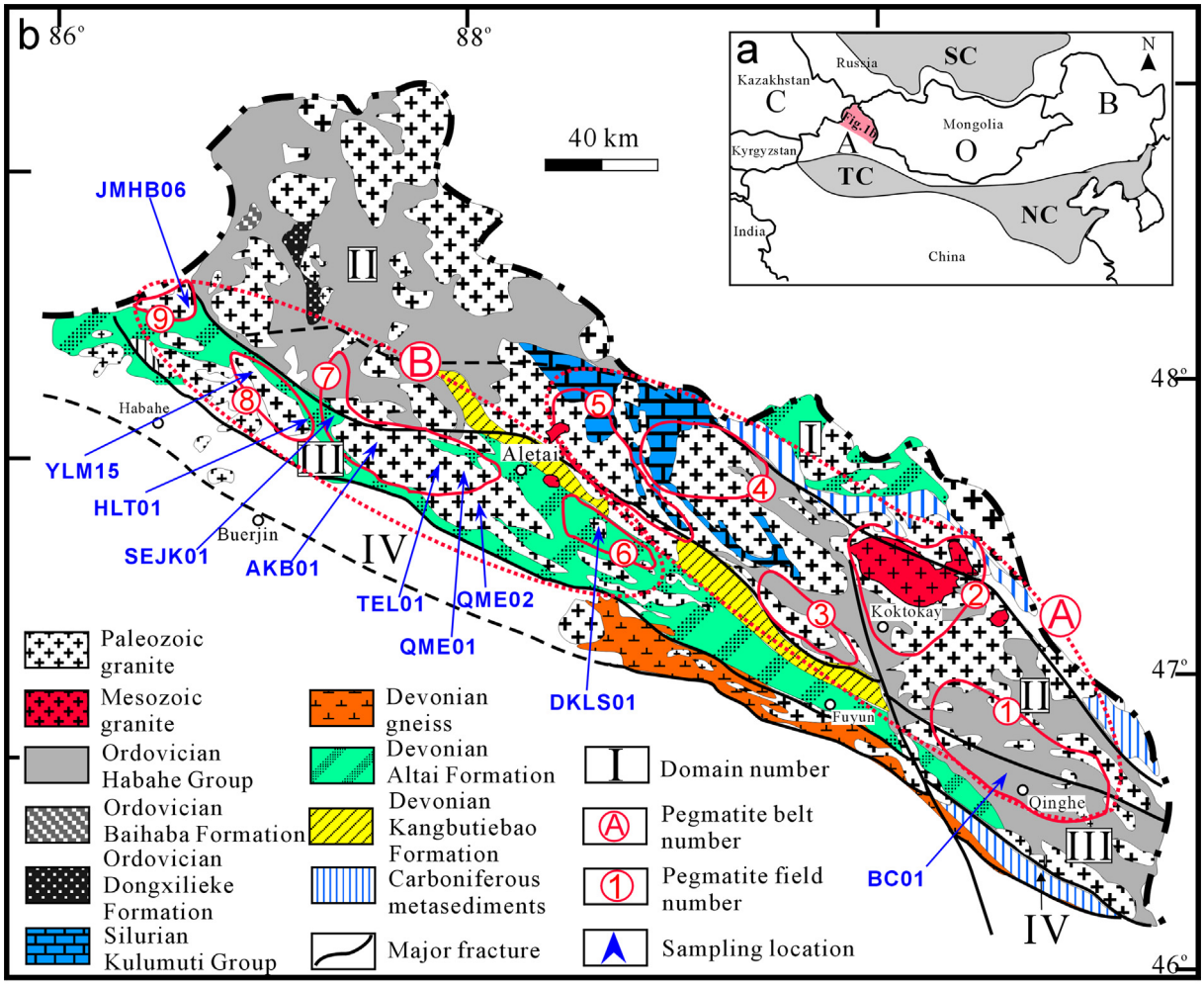

Fig. 1. Tectonic location (a) and geological sketch map of the Chinese Altai (b) (modified from Windley et al., 2002; Lv et al., 2018a). Abbreviation: CAOB = Central Asian Orogenic Belt; SC = Siberia Craton; TC = Tarim Craton; NC = North China Craton. Code: I, North Altai domain; II, Central Altai Domain; III, Qiongkuer domain; IV, Erqis domain. A, Halong-Qinghe pegmatite belt; B, Jiamanhaba-Xiaokalasu pegmatite belt. 1, Qinghe pegmatite field; 2, Koktokay pegmatite field; 3, Kuwei-Jiebiete pegmatite field; 4, Kelumute-Jideke pegmatite field; 5, Kalaeerqisi pegmatite field; 6, Dakalasu-Kekexier pegmatite field; 7, Xiaokalasu-Qiebielin pegmatite field; 8, Hailiutan-Yeliuman pegmatite field; 9, Jiamanhaba pegmatite field.

the Baogutu anticlinorium. The area is dominated by the Caledonian Jiamanhaba granite batholiths, which consists of biotite granite and plagiogranite (Zou and Li, 2006). The biotite granite is the major host rock for the pegmatites. Sedimentary rocks are rarely exposed, with only a limited outcrop of the Tuokesalei Formation exposed in the central area. This formation consists of marine terrigenous clastics with siliceous and carbonate rocks (Yang et al., 2013) and hosts a few of pegmatites. The Pegmatites in this field commonly have small outcrops with maximum lengths and widths of 300 m and 10 m, respectively. Most of these pegmatites consist mainly of K-feldspar, quartz, and muscovite and show simple internal zoning; only a few show Be±Nb-Ta mineralizations. Three generations of pegmatite have been recognized in this field, including Devonian (~395 Ma), Permian (~269 Ma), and Triassic (~238 Ma) (Lv et al., 2018a, 2018b, 2018c; Ren et al., 2011). The JMHB06 pegmatite intruded in gneissic biotite granite, as suggested by the sharp contact, development of a chilled border, and orientated growth of schorl in exocontact zone (Fig. 2a). It shows a limited outcrop and consists of four internal zones (Table 1). Some Be-, Nb- and Ta-rich minerals were observed in the outcrop or separated by artificial heavy concentrate testing (Fig. A.1). Details of the mineral association are presented in Table 2.

2.2.2. YLM15 and HLT01 pegmatites

The YLM15 and HLT01 pegmatites are located in the Yeliuman-Hailiutan pegmatite field. The pegmatite field is situated in the northwestern part of the Kabaer-Xibodu Paleozoic magmatic arc and the northern limb of the Qilimutale anticlinorium (Zou and Li, 2006). Granitic rocks including gneissic biotite granite, plagiogranite and medium-grained granite are widely exposed and host a few pegmatites. Zircon U-Pb dating indicates ages of Devonian to Ordovician (389–453 Ma) (Cai et al., 2011a; Sun et al., 2008, 2009b). Mafic rocks with U-Pb age of about 376 Ma are sporadically exposed (Cai et al., 2010). The Aletai Formation is exposed in the northern part of the area and hosts abundant pegmatites. The pegmatites in this area are commonly less fractionated, as proved by the dominating K-feldspar-quartz-muscovite mineral association, simple zonation, and mineralizations of Be±Nb-Ta. Two Ordovician-Silurian metapegmatites (476–426 Ma) were identified in previous works (Ren et al., 2011; Wang et al., 2001).

The YLM15 pegmatite is located in the Yeliuman mining area northwestern of the Hailiutan-Yeliuman pegmatite field, exhibits a vein intrusion in gneissic biotite granite (Fig. 2b). The HLT01 pegmatite is located in the Hailiutan-Chonghuer mining area southeastern of the

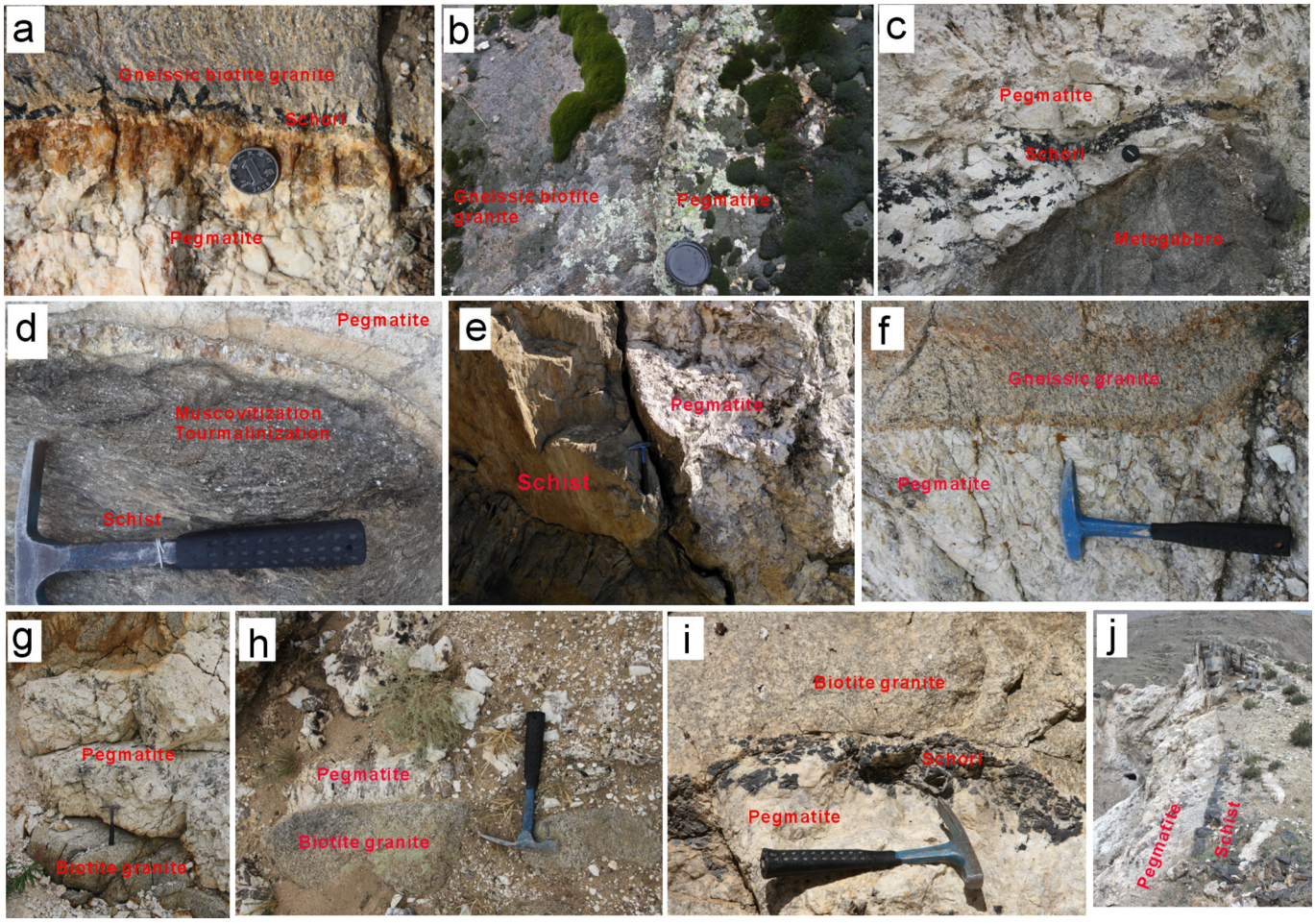

Fig. 2. Field photographs of the studied pegmatites and wall rocks, which show the contact relationship between the pegmatites and wall rocks. (a) JMHB06, (b) YLM15, (c) HLT01, (d) SEJK01, (e) TEL01, (f) QME01, (g) AKB01, (h) QME02, (i) DKLS01 and (j) BC01.

Hailiutan-Yeliuman pegmatite field as an intrusion in metagabbro along a northwest joint (Fig. 2c). They consist of 3–4 internal zones (Table 1) and have simple mineral assemblages (Table 2), with REE(Y)-rich minerals locally observed in the outcrops (Figs. A.2 and A3).

2.2.3. SEJK01, AKB01, TEL01, QME01 and 02 pegmatites

The SEJK01, AKB01, TEL01, QME01, and QME02 pegmatites are distributed throughout the northwestern to southeastern segments of the Xiaokalasu-Qiebielin pegmatite field. Tectonically, this pegmatite field is situated in the western of the Kabaer-Xibodu Paleozoic magmatic arc and the axis structure zone of the Qiebielin anticlinorium (Zou and Li, 2006). As the largest pegmatite distribution area in the Jiamanhaba-Dakalasu pegmatite belt, the Xiaokalasu-Qiebielin pegmatite field consists of the Xiaokalasu, Qiemuerqieke, Taerlang, Qiebielin, Aergake, Akesaiyi-Akesu, Akebasitawu, Saerjiake, Wulukete and Qieboluoyi-Akegonggaite mining areas and thousands of pegmatite dykes. Most of the pegmatites show simple internal zoning and limited rare metal mineralization, with some exhibiting Be±Nb-Ta mineralations. Only a few located, in Xiaokalasu, Qiebielin, and Saerjiake mining areas, show complex zonation and Li-Be-Ta-Nb mineralization. Two generations of pegmatites including Devonian (403 Ma, Lv et al., 2018a) and Triassic (249–240 Ma, Ren et al., 2011) have been confirmed. Granitoids are prevalent and dominated by early-middle Paleozoic Taerlang and Qiemuerqieke batholiths consisting of granodiorite, biotite granite, tonalite, and adamellite, with zircon U-Pb ages of 404–462 Ma (Cai et al., 2011a; Wan et al., 2011; Wang et al., 2013; Yuan et al., 2007). In addition, three small Permian granite plutons have been reported including Keyinbulake syenogranite (278 Ma, Li et al., 2012b), Aweitan porphyritic adamellite (271 Ma, Tong et al., 2014) and a two-mica granite situated close to the Aletai city (275 Ma, Sun et al., 2009a). Permian gabbro dykes are exposed only in Qiemuerqieke area (Wan et al., 2013). Metasedimentary rocks, including those of the Habahe Group and the Aletai Formation, are locally exposed in the northwestern and southeastern parts of the pegmatite field, respectively.

The SEJK01, AKB01, TEL01, and QME01 and 02 pegmatites are located in the Saerjiake, Akebasitawu, Taerlang and Qiemuerqieke mining areas, respectively, and exhibit as intrusions in biotite-quartz schist, biotite granite, quartz-biotite schist, gneissic two-mica granite and biotite granite, respectively (Fig. 2d-h). They consist of 3–5 internal zones (Table 1) and show various types of mineralization according to the mineral assemblages (Table 2) and typical ore and accessory minerals (Figs. A.4–8).

2.2.4. DKLS05 pegmatite

The DKLS05 pegmatite is exposed in the Dakalasu-Kekexier pegmatite field. Tectonically, this field is situated in the axis structure zone of the Kelan syncline and the northern of Kalasu fault zone (Zou and Li, 2006). Granites consist of the Ordovician gneissic biotite granite (465 Ma, Zou and Li, 2006); Devonian gneissic granite and epidote-bearing granite (412 Ma and 410.5 Ma, respectively; Broussolle et al., 2018); and Permian epidote-bearing granite (283.7 Ma), gneissic granite (279.1 Ma) (Broussolle et al., 2018), and porphyritic biotite granite (270 Ma; Liu et al., 2018). Metasedimentary rocks including the Aletai

Table 1
Geology and internal zonation of the studied pegmatites in the Chinese Altai.

Pegmatite	Pegmatite field	Mining area	Wall rock	Contact relationship	Shape	Length and width (m)	Strike	Mineralization	Zonation
JMHB06	Jiamanhaba	Jiamanhaba	Gneissic biotite granite	Sharp	Tabular	100 and 1–3	275°	Be-Ta-Nb	Graphic zone, blocky microcline zone, quartz-muscovite zone, quartz core zone
YLM15	Yeliuman- Hailiutan	Yeliuman	Gneissic biotite granite	Sharp	Vein	80 and 3–5	325°	REE	Graphic zone, microcline-quartz-muscovite-biotite zone, quartz core zone
HLT01		Hailiuitan	Metagabbro	Sharp	Tabular	200 and 5–10	330°	REE	Graphic zone, blocky orthoclase-microcline-quartz zone, orthoclase-muscovite-biotite zone, quartz core zone
SEJK01	Xiaokalasu-Qiebielin	Saerjiake	Biotite-quartz schist	Sharp	Tabular	600 and 3–5	330°	Li-Be-Ta-Nb	Graphic zone, blocky orthoclase-microcline zone, quartz- muscovite zone, quartz-cleavelandite- spodumene zone, quartz core zone
AKB01		Akebasitawu	Biotite granite	Sharp	Tabular	200 and 2–5	210°	Be-Nb-Ta-REE	Graphic zone, blocky orthoclase-microcline zone, quartz-muscovite zone
TEL01		Taerlang	Biotite-quartz schist	Sharp	Tabular	200 and 3–5	290°	Be-Nb-Ta-REE	Graphic zone, quartz-microcline-biotite zone, quartz-muscovite-biotite zone, quartz core zone
QME01		Qiemuerqieke	Gneissic two- mica granite	Sharp	Vein	50 and 3–5	342°	REE	Graphic zone, blocky microcline zone, quartz-muscovite zone, quartz core zone
QME02			Biotite granite	Sharp	Tabular	300 and 1–5	330°	Li-Be-Ta-Nb-Sn	Graphic zone, blocky microcline zone, quartz-muscovite zone, cleavelandite-quartz- muscovite zone, quartz core zone
DKLS01	Dakalasu-Kekexier	Dakalasu	Biotite granite	Sharp	E: Pod	60 and 5–15	290°	Be-Nb-Ta	Graphic zone, blocky microcline-quartz zone, muscovite aggregation zone, albite-muscovite-quartz zone
					W: Vein	100 and 3–5	220°		
BC01	Qinghe	Tagerbasitawu-Baicheng	Staurolite-biotite-quartz schist	Sharp	Pod	80 and 2–16	280°	Li-Be- Ta-Nb	Graphic zone, muscovite aggregation zone, microcline- orthoclase-quartz zone, quartz-muscovite-albite zone, cleavelandite-quartz-spodumene zone, quartz core zone

Table 2
The mineral assemblages of the Permian pegmatites in the Chinese Altai.

Mineral/pegmatite	JMHB06	YLM15	HLT01	SEJK01	AKB01	TEL01	QME01	QME02	DKLS01	BC01
Microline	35	35	25	30	35	35	30	35	45	30
Quartz	31	26	22	25	32	22	35	25	25	30
Muscovite	19	21	17	15	15	20	25	20	10	15
Orthoclase	6	8	23	10	8	9	4	6	10	7
perthite	5	4	8	3	6	7	3	3	5	2
Albite	3	2	1	15	3	1	2	10	2	15
Biotite	−	3	3	−	−	5	−	−	2	−
Beryl	+++	−	−	++++	+++	+++	−	+++	++++	++++
Ferrocolumbite	+	−	−	−	++	−	+	−	+++	++
Mangancolumbite	++	−	−	+++	+++	−	+	+++	++	+++
Ferrotantalite	−	−	−	−	++	−	−	−	++	−
Manganotantalite	++	−	−	+++	+	−	−	+	−	++
Spodumene	−	−	−	+++	−	−	−	−	−	++++
Lepidolite	−	−	−	++	−	−	−	+++	−	++
Betafite	++	−	−	−	+	−	−	−	+	−
(Ce)-Monazite	++	+++	++	+	++	++	++	−	−	+
Xenotime	++	++	+++	−	++	+	+++	−	+	−
Bertrandite	−	−	−	−	−	−	−	−	+	−
Bismutotantalite	−	−	−	+	−	−	−	−	−	−
Cassiterotantalite	−	−	−	−	−	−	−	++	−	−
Thoreaulite	−	−	−	−	−	−	−	+	−	−
Cassiterite	−	−	−	−	−	−	−	+	−	−
Uranmicrolite	++	−	−	+	++	−	−	++	+++	−
Bismutomicrolite	+	−	−	+	++	−	−	−	−	−
Uranpyrochlore	++	−	−	−	+	+	−	−	+	+++
Yttropyrochlore	−	−	−	−	++	−	−	−	−	−
Fergusonite	++	−	−	−	−	−	−	−	−	−
Tapiolite	−	−	−	−	−	−	−	−	+	−
Triphylite	−	−	−	++	−	−	−	−	−	+++
Sicklerite	−	−	−	++	−	−	−	−	−	+++
Spessartite	+++	+++	+++	++++	+++	+++	++++	+++	++	+++
Almandine	+	−	+	−	−	+	−	−	+++	−
Fluorapatite	+++	++	+++	−	+++	++++	+++	+	+++	++
Manganapatite	−	−	−	++++	−	−	−	++++	−	+++
Schorl	+++	+++	++++	++++	+++	++++	+++	++++	++++	+++
Tsilaisit	−	−	−	++	−	−	−	+++	−	−
Zircon	++	++	++	+++	++	++	++	++	++	+++
Amblygonite	−	−	−	+	−	−	−	−	−	+
Rutile	−	−	+	−	−	−	−	−	++	−
Ilmenite	++	−	+	−	−	−	+	−	++	+
magnetite	+	++	+	+	+	+++	++	+	+++	+
Cheralite	+	+	+	−	+	−	−	−	−	−
Bismutite	+	−	−	+	−	−	−	−	−	+
Thorite	−	+	+	−	−	+	−	−	+	−
Sphene	−	+	−	−	−	−	−	−	−	−
Pyrophanite	−	−	−	−	−	−	−	−	+	−
Topaz	+	+	+	−	−	+	+	−	−	+
Allanite	−	−	+	−	−	−	−	−	−	−
Epidote	−	+	+	−	−	−	−	+	−	−
Vernadite	−	−	++	−	−	−	−	+	−	+

Note: number means speculative volume percent; symbol ++++ means high content and can be commonly observed in pegmatites; +++ means medium content and can be locally observed; ++ means low content confirmed by artificial heavy concentrate tests; + means extremely low content confirmed by artificial heavy concentrate tests; − means not observed.

formation slate as well as schist and gneiss are widely exposed. More than 1000 pegmatites are exposed in this area (Zou and Li, 2006) and are commonly characterized by low fractionation and simple zoning; only a few show Be±Nb-Ta mineralization.

The DKLS01 pegmatite is the largest pegmatite in this pegmatite field and occurs as intrusion in porphyritic biotite granite with a sharp contact (Fig. 2i). It consists of the eastern and western segments with distinct shapes and strikes (Table 1), and contains abundant Be-, Nb- and Ta-rich minerals (Table 2 and Fig. A.9).

2.2.5. BC01 pegmatite

The BC01 pegmatite is situated in the Tagerbasitawu-Baicheng mining area, Qinghe pegmatite field. This field is located the plunging crown of the Qinggeli anticlinorium tectonically and consists of tens of mining areas and 8000 pegmatites (Zou and Li, 2006). The pegmatites with Be mineralization are distributed mainly in the Asikaerte and Buleke mining areas; those with muscovite mineralization are distributed in the Tiemulete, Buleke, Naransala, and Akebulake mining areas. Only a few pegmatites, with limited Li-Be±Nb-Ta ± Cs mineralization, are exposed in the Baicheng, Talati and Amulagong mining areas. Metasedimentary rocks of the Habahe Group are widely exposed in the pegmatite field and host a majority of pegmatites. Granitoids are rare in most mining areas, only a few small plutons are sporadically exposed and consist of plagioclase granite (485–507 Ma, Zhang et al., 2017), granodiorite (363–394 Ma, Ye et al., 2015; Song et al., 2017), monzogranite (395 Ma, Shi et al., 2015) and quartz diorite (381 Ma, Song et al., 2017).

The BC01 pegmatite occurs as an intrusion in staurolite-biotite-quartz schist with a sharp contact (Fig. 2j). It consists of six zones (Table 1) with prevalent development of albitization. Li-, Be-, Nb- and Ta-rich minerals are locally observed in the outcrop (Fig. A.10), and other minerals are also identified, as listed in Table 2.

3. Sampling and analytical methods

All samples numbered as JMHB06, YLM15, HLT01, SEJK01, AKB01, TEL01, DKLS01, BC01, QME01 and 02 were collected from the graphic texture zones of the corresponding pegmatites. The samples were grinded and zircons were picked out by hand to avoid contamination. Zircon target preparation, image acquisition under cathodoluminescence (CL), and in situ U-Pb, REEs and Hf isotope analyses were performed at the State Key Laboratory of Continental Dynamics, Northwest University, Xi'an, China. The U-Pb dating and content analysis of REEs was conducted on an Agilent7500a ICP-MS instrument equipped with a 193-nm ArF excimer laser, with working conditions as following: laser frequency of 10 Hz with energy of 34–40 mJ, beam diameter of 30 μm, background acquisition of 30 s and signal acquisition of 60 s. Helium was used as the carrier gas to provide efficient aerosol delivery to the torch (Yuan et al., 2004). The U, Th and Pb concentrations were calibrated using ^{29}Si as an internal standard and NIST 610 as an external standard. The zircon $^{206}Pb/^{207}Pb$, $^{206}Pb/^{238}U$ and $^{207}Pb/^{235}U$ ratios were calculated by ICPMS Data Cal (Liu et al., 2009). The concordia diagrams and weighted mean calculations were making by using the Isoplot program (Ludwig, 2003). The two standard zircons 91,500 and GJ-1 yielded weighted mean $^{206}Pb/^{238}U$ ages of 1064 ± 3.5 Ma ($n = 30$, 2σ) and 603 ± 3.0 Ma, respectively, which are in good agreement with the recommended ages (Wiedenbeck et al., 2004). The correction of common Pb was achieved according to the method of Andersen (2002). The uncertainty of individual analyses was reported at the 1σ level, and the weighted mean $^{206}Pb/^{238}U$ age was calculated at the 2σ level.

Zircon Hf isotopic analysis was conducted on a Nu Plasma HR MCICP-MS equipped with a GeoLas 2005 193-nm ArF excimer laser ablation system. The analyses were performed with a spot size of 44 μm, laser repetition rate 10 Hz and energy density of 15–20 J/cm^{-2}. Helium was used as the carrier gas. The detailed instrumental settings and analytical procedures were described by Diwu et al. (2011). Zircons 91,500 and GJ-1 were also analyzed as unknown samples to check the data quality. The obtained weighted 176Hf/177Hf ratios were 0.282326 ± 0.000098 ($n = 40$, 2σ) for 91,500 and 0.282039 ± 0.000010 (n = 40, 2σ) for GJ-1, which were consistent with the recommended ratios within 2σ error (0.282307 ± 0.000058 and 0.282015 ± 0.000019, respectively) (Elhlou et al., 2006; Griffin et al., 2006).

4. Results

4.1. Zircon morphology, cathodoluminescence (CL) and backscattered electron (BSE) features and Th/U ratios

The zircon grains from the ten pegmatites vary in size from 80 to 500 μm. They are brown in color and opaque with euhedral habits featuring {111} and {110} or only {111} crystal faces. According to the CL and BSE features, three types of zircon were identified. The type-1 zircon is featured by weak and homogenous luminance with no evident oscillatory zoning under CL and BSE images, such as the zircons from the HLT01 (Fig. 3c1 and 2), SEJK01 (Fig. 3d), TEL01 (Fig. 3f1 and 2), QME01 (Fig. 3g) QME02 (Fig. 3h1 and 2), DKLS01 (Fig. 3i) and BC01 (Fig. 3j1 and 2) pegmatites. The type-2 zircon is characterized by weak and mosaic luminance and spongy texture in CL and BSE images with abundant mineral inclusions or pores, such as the zircons from the JMHB06 (Fig. 3a), YLM15 (Fig. 3b), HLT01 (Fig. 3c3 and 4), QME02 (Fig. 3h3 and 4), and BC01 (Fig. 3j5 and 6) pegmatites. The type-3 zircon is featured by core-rim texture and relatively intense luminance in CL images, and exhibits as an inherited zircon core with blurry oscillatory zoning, such as the zircons from the AKB01 (Fig. 3e4) and BC01 (Fig. 3j4) pegmatites. Except the type-3 zircon, other zircons commonly have high U and/or Th contents and varying Th/U ratios. The zircons from the JMHB06 and YLM15 pegmatites commonly have high contents of Th (771–13,580 ppm and 142–1336 ppm) and U (3887–32,504 ppm and 4399–32,507 ppm, respectively) with varying Th/U ratios of 0.08–0.68 and 0.01 to 0.19, respectively. The zircons from the HLT01, SEJK01, AKB01, TEL01, QME01, QME02, and BC01 pegmatites have low contents of Th (mostly <100 ppm) and high contents of U (mostly >1000 ppm) with low Th/U ratios (mostly <0.1). Comparatively, the zircons from the DKLS01pegmatite have moderate contents of Th (253–2430 ppm) and U (1036–8777 ppm) with Th/U ratios of 0.08–0.68 (Table A.1). Comparatively, the type-3 zircons from the AKB01 and BC01 pegmatites have lower contents of Th (146–341 ppm) and U (220–3789 ppm), with Th/U ratios of 0.07–0.66 (Table A.1).

4.2. Rare earth elements (REEs) in zircon

The zircons from the ten pegmatites have varying contents of REEs (not including Y), with the average contents decreasing from 6391 ppm for the JMHB06 pegmatitie to 236 ppm for the BC01 pegmatite (Table C.1). However, the three types of zircon mentioned above show distinct REE patterns. The type-1 zircon shows enrichment of heavy rare earth elements (HREEs, Gd-Lu), Ce positive anomaly and Eu negative anomaly in the chondrite-normalized patterns (Fig. 5), with $(Sm/La)_N$ ratios of 4.8–132.5, Ce/Ce* ratios of 1.7–34.5 and Eu/Eu* ratios of 0.02–0.7 (Table C.1). The type-2 zircon shows relatively enrichment of light rare earth elements (LREEs, La-Eu), weakened Ce and Eu anomalies compare to the type 1 (Fig. 5a, b, c, f, h and i), with smaller $(Sm/La)_N$ and Ce/Ce* ratios of 2.5–12.5 and 0.9–2.8, respectively, and larger Eu/Eu* ratios of 0.1–1.4 (Table C.1). The type-3 zircon shows more evident enrichment of HREEs and Ce positive anomaly compare to the type-1 (Fig. 5e and j), with larger $(Sm/La)_N$ and Ce/Ce* ratios of 14.6–152.9 and 9.8–82.1, respectively (Table C.1). The types-1 and -2 both have evident tetrad effect in the HREE segment ($TE_{3,4} > 1.2$), which is distinct to the type-3 (Table C.1).

4.3. Zircon U-Pb ages and Hf isotopes

4.3.1. JMHB06

Fifteen zircons were selected for U - Pb age determination. Of these, thirteen type-1 zircons define an age population with $^{206}Pb/^{238}U$ ages ranging from 256 Ma to 264 Ma and a weighted mean $^{206}Pb/^{238}U$ age of 260.4 ± 4.0 Ma (Table A.1; Fig. 4a). The age of 260.4 ± 4.0 Ma is considered to represent the formation age of the pegmatite. Two type-2 zircons yield discordant ages with $^{206}Pb/^{238}U$ ages of 285–301 Ma (Spots 4 and 6, Table A.1). Of these thirteen zircons, twelve yielded consistent $^{176}Hf/^{177}Hf$ values ranging of 0.282747–0.282778. According to the crystallization age of 260.4 Ma, the calculated $\varepsilon_{Hf}(t)$ values range from +4.81 to +5.80 with T^C_{DM} model ages of 977–914 Ma (Table B.1).

4.3.2. YLM15

Five type-2 zircons yield discordant ages with $^{206}Pb/^{238}U$ ages ranging from 268 to 396 Ma (Spots 4, 5, 7, 9 and 14). Ten type-1 zircons define an age population with $^{206}Pb/^{238}U$ ages of 258–267 Ma and a weighted mean $^{206}Pb/^{238}U$ age of 262.9 ± 3.8 Ma (Table A.1; Fig. 4b), which is considered to represent the formation age of the pegmatite. The ten zircons yield consistent $^{176}Hf/^{177}Hf$ values ranging from 0.282810 to 0.282897. According to the crystallization age of 262.9 Ma, the calculated $\varepsilon_{Hf}(t)$ values range from +6.99 to +9.80 with T^C_{DM} model ages of 841–662 Ma (Table B.1).

4.3.3. HLT01

Fifteen zircons were selected for U - Pb age determination. Of these, ten type-1 zircons yield concordant $^{207}Pb/^{235}U$ and $^{206}Pb/^{238}U$ ages and define a weighted mean $^{206}Pb/^{238}U$ age of 253.8 ± 4.1 Ma (Table A.1; Fig. 4c). Five type-2 zircons yield discordant ages with $^{206}Pb/^{238}U$ ages of 256–335 Ma (Spots 5, 7, 9, 10 and 14, Table A.1). The age of 253.8 ± 4.1 Ma is considered to represent the formation time of the pegmatite. The ten zircons yield $^{176}Hf/^{177}Hf$ values ranging from 0.282768 to 0.282851. According to the crystallization age of

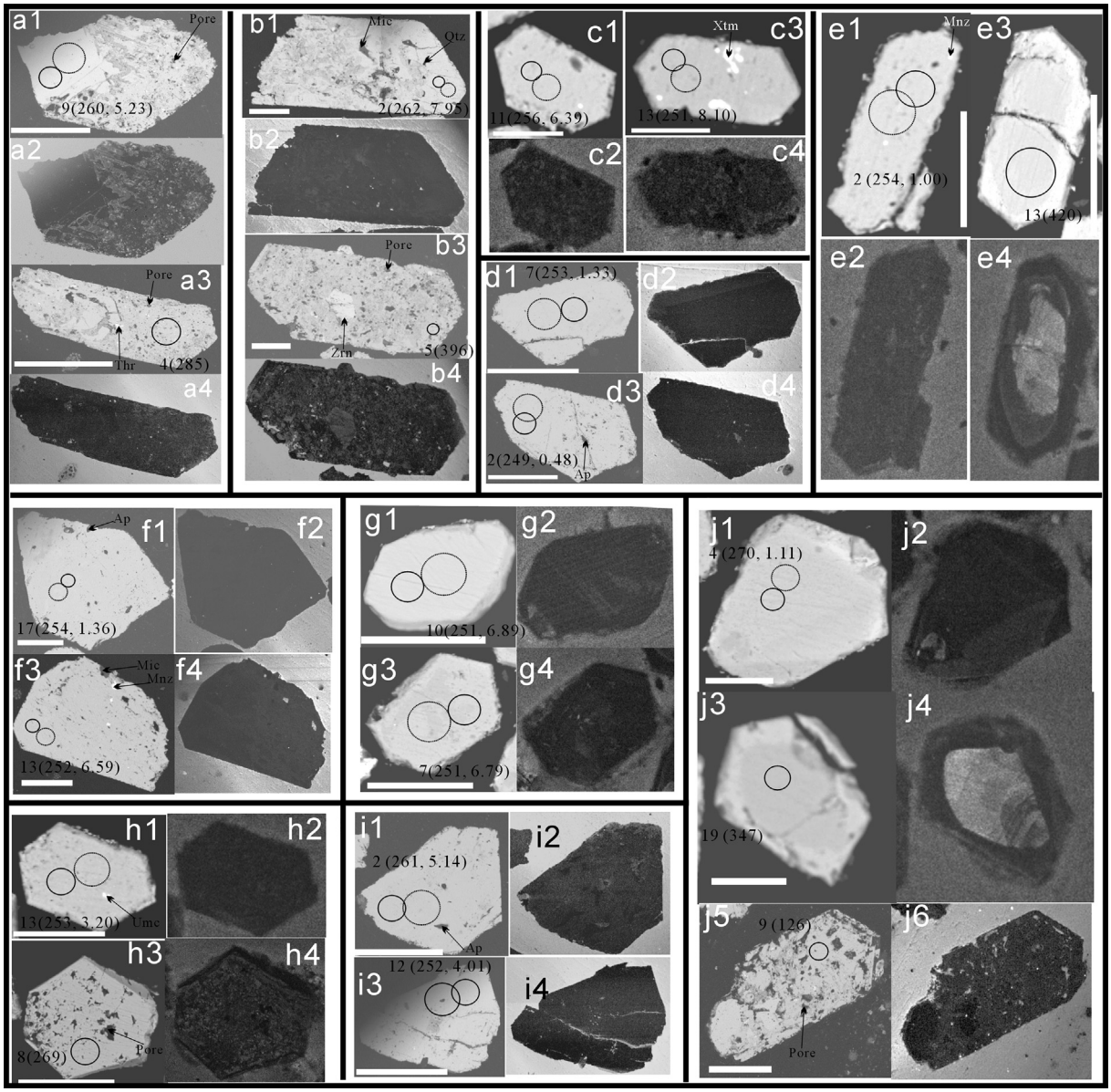

Fig. 3. Representative backscattered electron (BSE) and cathodoluminescence (CL) images of zircons from the studied pegmatites, showing the laser analytic spots, mineral inclusions, $^{206}Pb/^{238}U$ ages and/or $\varepsilon_{Hf}(t)$ values. (a) JMHB06, (b) YLM15, (c) HLT01, (d) SEJK01, (e) AKB01, (f) TEL01, (g) QME01, (h) QME02, (i) DKLS01 and (j) BC01. Scale bars correspond to 100 μm.

253.8 Ma, the calculated $\varepsilon_{Hf}(t)$ values range from +5.21 to +8.10 with T^C_{DM} model ages of 947–763 Ma (Table B.1).

4.3.4. SEJK01

Fifteen type-1 zircons were selected for U and Pb age determination. They define an age population with $^{206}Pb/^{238}U$ ages of 247–260 Ma and a weighted mean $^{206}Pb/^{238}U$ age of 252.7 ± 2.1 Ma (Table A.1; Fig. 4d). The age of 252.7 ± 2.1 Ma is considered to represent the formation time of the pegmatite. Ten of these zircons yield consistent $^{176}Hf/^{177}Hf$ values ranging from 0.282623 to 0.282661. According to the crystallization age of 252.7 Ma, the calculated εHf(t) values range from −0.32 to +1.52 with T^C_{DM} model ages of 1296–1180 Ma (Table B.1).

4.3.5. AKB01

Fifteen zircons were selected for U-Pb age determination. Three type-3 zircons yield older ages with $^{206}Pb/^{238}U$ ages of 418–420 Ma (Spots 9, 12 and 13). Twelve type-1 zircons define an age population with $^{206}Pb/^{238}U$ ages varying from 247 Ma to 258 Ma and a weighted mean $^{206}Pb/^{238}U$ age of 253.0 ± 3.0 Ma (Table A.1; Fig. 4e) which is considered to represent the formation time of the pegmatite. Of these twelve zircons, ten yield consistent $^{176}Hf/^{177}Hf$ ranging from 0.282638 to 0.282686. According to the crystallization age of 253 Ma, the calculated εHf(t) values range from +0.58 to +2.37 with T^C_{DM} model ages of 1239–1126 Ma (Table B.1).

4.3.6. TEL01

Twenty zircons were selected for U - Pb age determination. Of these, six type-2 zircons yield discordant ages with varying $^{206}Pb/^{238}U$ ages of 323–475 Ma (Spots 1, 2, 4, 8, 10 and 12, Table A.1). Fourteen type-1 zircons define an age population with $^{206}Pb/^{238}U$ ages varying from 244 Ma to 265 Ma and a weighted mean $^{206}Pb/^{238}U$ age of 255.5 ± 2.7 Ma (Table A.1; Fig. 4f), which is considered to represent the

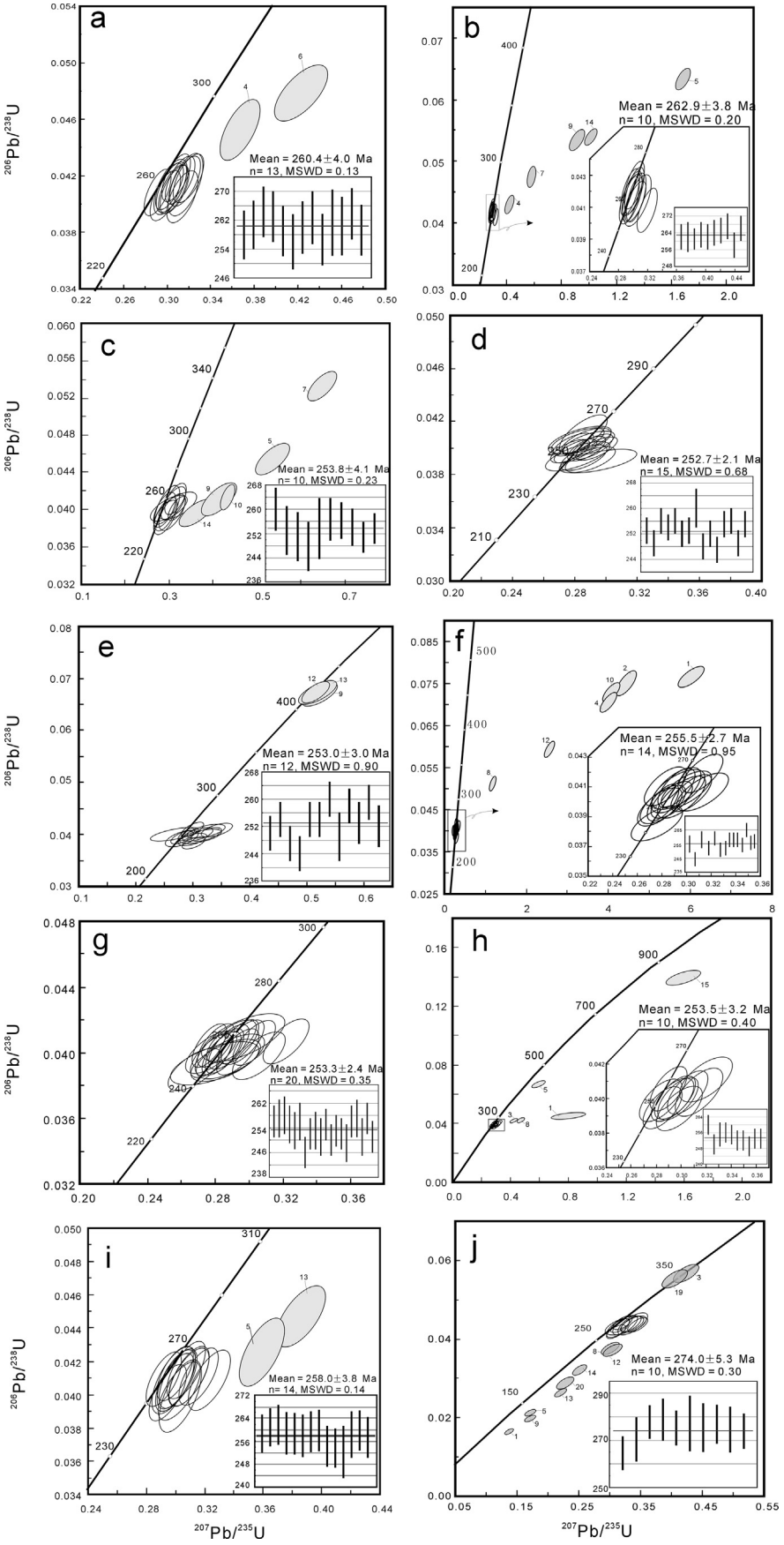

Fig. 4. Concordia and weighted average diagrams of the LA-ICP-MS U-Pb ages of zircons from samples JMHB06 (a), YLM15 (b), HLT01 (c), SEJK01 (d), AKB01 (e), TEL01 (f), QME01 (g), QME02 (h), DKLS01 (i) and BC01 (j). Mean ages were calculated from age spot without padding gray, error ovals are 1 sigma and mean ages given as 2 sigma.

formation age of the pegmatite. Of these fourteen zircons, ten yield $^{176}Hf/^{177}Hf$ values ranging from 0.282597 to 0.282834. According to the crystallization age of 255.5 Ma, the calculated $\varepsilon_{Hf}(t)$ values range from −0.60 to +7.61 with T^{C}_{DM} model ages of 1316–801 Ma (Table B.1).

4.3.7. QME01

Twenty type-1 zircons define an age population with $^{206}Pb/^{238}U$ ages varying from 249 Ma to 257 Ma and a weighted mean $^{206}Pb/^{238}U$ age of 253.3 ± 2.4 Ma (Table A.1; Fig. 4g) which reflects the formation time of the pegmatite. Ten of theses zircons yield $^{176}Hf/^{177}Hf$ values ranging from 0.282782 to 0.282911. According to the crystallization age of 253.3 Ma, the calculated $\varepsilon_{Hf}(t)$ values range from +5.82 to +10.19 with T^{C}_{DM} model ages of 907–629 Ma (Table B.1).

4.3.8. QME02

Fifteen zircons were selected for U - Pb age determination. Of these, five type-2 zircons yield discordant ages with varying $^{206}Pb/^{238}U$ ages from 268 Ma to 842 Ma (Spots 1, 3, 5, 8 and 15, Table A.1). Ten type-1 zircons define an age population with $^{206}Pb/^{238}U$ ages varying from 249 Ma to 260 Ma and a weighted mean $^{206}Pb/^{238}U$ age of 253.5 ± 3.2 Ma (Table A.1; Fig. 4h), which is considered to represent the formation time of the pegmatite. Eight of these zircons yield consistent $^{176}Hf/^{177}Hf$ values ranging from 0.282701 to 0.282714. According to the crystallization age of 253.5 Ma, the calculated $\varepsilon_{Hf}(t)$ values range from +2.58 to +3.20 with T^{C}_{DM} model ages of 1114–1074 Ma (Table B.1).

4.3.9. DKLS01

Sixteen zircons were selected for U-Pb age determination. Of these, two type-2 zircons yield discordant ages with $^{206}Pb/^{238}U$ ages of 270–282 Ma (Spots 5 and 13). Fourteen type-1 zircons define an age population with $^{206}Pb/^{238}U$ ages ranging from 252 Ma to 262 Ma and a weighted mean $^{206}Pb/^{238}U$ age of 258.0 ± 3.8 Ma (Table A.1; Fig. 4i). Thus, the age of 258.0 ± 3.8 Ma is considered to represent the formation time of the pegmatite. Of these fourteen zircons, twelve yield consistent $^{176}Hf/^{177}Hf$ values ranging from 0.282726 to 0.282775. According to the crystallization age of 258 Ma, the calculated $\varepsilon_{Hf}(t)$ values range from +4.01 to +5.76 with T^{C}_{DM} model ages of 1026–915 Ma (Table B.1).

4.3.10. BC01

Twenty zircons were selected for U-Pb age determination. Two type-3 zircons yield older $^{206}Pb/^{238}U$ ages of 347–355 Ma (Spots 3 and 19). Eight type-2 zircons yield discordant ages with $^{206}Pb/^{238}U$ ages ranging from 105 Ma to 238 Ma (Spots 1, 3, 5, 8, 9, 11, 12 and 14). Ten type-1 zircons define an age population with $^{206}Pb/^{238}U$ ages of 264–278 Ma and a weighted mean $^{206}Pb/^{238}U$ age of 274.0 ± 5.3 Ma (Table A.1; Fig. 4j), which is considered to represent the formation age of the pegmatite. The ten zircons yielded consistent $^{176}Hf/^{177}Hf$ values of 0.282600–0.282633. According to the crystallization age of 274 Ma, the calculated εHf(t) values range from −0.07 to +1.11 with T^{C}_{DM} model ages of 1296–1222 Ma (Table B.1).

5. Discussion

5.1. Age, mineralization, and classification of the Permian pegmatite

5.1.1. Genesis of zircon and significance of U-Pb age

Some isotopic systems of minerals have been applied in pegmatite dating, such as (1) zircon U-Pb, (2) monazite U-Pb, (3) molybdenite Re-Os, (4) columbite U-Pb, (5) apatite U-Pb and (6) muscovite Ar-Ar and K-Ar. However, zircon U-Pb dating is preferentially adopted for the studied pegmatites, with consideration of the varying closure temperatures of the isotopic systems in minerals [T1 (900–700 °C; Cherniak and Watson, 2000; Ortega-Rivera et al., 1997) ≥ T2 (750–720 °C; Copeland et al., 1988) > T3 (700–600 °C; Raith and Stein, 2000) > T4 (> lower amphibolite facies, Romer and Smeds, 1994) ≥ T5 (620–450 °C; Chamberlain and Bowring, 2000; Krogstad and Walker, 1994) > T6 (425 °C and 380 °C, respectively; Harrison et al., 2009)], the dominating formation temperature of pegmatite (about 650–450 °C), the hydrothermal fluid activities, the multiple-generations and the prevalence of dating mineral in highly-fractionated pegmatites. Although the zircons formed in highly-fractionated pegmatites are commonly rich in U and Th, those formed in early stage (e.g., graphic zone and aplite zone) mostly have low U and Th, and are suitable for dating, according to our previous works (e.g., Lv et al., 2012, 2018a). The reasons for the failure in zircon U-Pb dating of highly-fractionated pegmatites, include limited zircon grains have been separated, rock samples for zircon separation were collected from the zones with high U and/or Th or alteration zones, and rough preparation works for dating (target, polishing and zircon CL and BSE imaging, etc.).

The zircons from the studied pegmatites commonly have low Th/U ratios <0.1 (Table A.1). Except inherited zircons, no zircon shows oscillatory zoning in the BSE and CL images (Fig. 3), which indicates their distinction from typical igneous zircons (e.g., Wu and Zheng, 2004). In the BSE and CL images, the type-1 zircons show uniform luminance (e.g., Fig. 3a1, d1, f1, g1, i1 and j1), which indicates that they are primary in composition and structure with limited modification by metamictization or fluid alteration (e.g., Corfu et al., 2003). In the chondrite-normalized REE patterns (Fig. 5), the type-1 zircons show depletion of LREEs and enrichment of HREEs, positive Ce anomalies (Ce/Ce^{*} = 2.0–34.5) and negative anomalies (Eu/Eu^{*} = 0.1–0.7) with the tetrad effect shown in the HREE segment ($TE_{3,4}$ > 1.2) (Table C.1). The development of tetrad effect indicates that the pegmatite-forming melts were highly fractionated and enriched in hydrous fluids (Irber, 1999). As shown in Fig. 6, most of the zircons show intermediate abundances of La and $(Sm/La)_N$ and Ce/Ce^{*} ratios (Table C.1) between the referred magmatic and hydrothermal zircons (Hoskin, 2005) (Fig. 6a and b). All of these features suggest that the type-1 zircons are neither igneous nor hydrothermal in origin, which is consistent with the nature of pegmatite-forming melts featuring the coexistence of melt and hydrous fluid phases (e.g., Thomas and Davidson, 2016). Therefore, the type-1 zircons may represent the primary zircons crystallized form pegmatite-forming melts. The $^{206}Pb/^{238}U$ and $^{207}Pb/^{235}U$ ages obtained from these zircons are concordant with concordance ≥90% (Table A.1), and may represent the formation ages of the pegmatites.

Comparatively, the type-2 zircons show mosaic luminance and spongy textures featuring abundant pores and mineral inclusions in BSE and CL images (e.g., Fig. 3a3, b3, h3 and j5). These features indicate that modifications in composition and structure occurred after crystallization (e.g., Corfu et al., 2003). In addition, except for those of the BC01 pegmatite, the type-2 zircons show higher abundances of REEs, particularly LREEs (Fig. 5a, b, c, f, h and i), and lower ratios of $(Sm/La)_N$ (2.5–12.5) and Ce/Ce^{*} (0.9–2.8) than those with concordant ages (Table C.1), which overlap with the range of hydrothermal zircon (Fig. 6a and b). All of these features suggest that the type-2 zircons were altered by hydrothermal fluid after metamictization. The $^{206}Pb/^{238}U$ and $^{207}Pb/^{235}U$ ages obtained from the type-2 zircons are discordant with concordance <90% (Table A.1) and older than the concordant ages of type-1 zircons from the same sample, which indicates that the U-Pb systems were destroyed and mixed by common Pb (e.g., Wu and Zheng, 2004). The zircons of type 2 from the BC01 pegmatite show mosaic luminance and spongy textures, have higher and lower contents of U and REEs (Table C.1), respectively, and younger ages than those of the type-1 zircons from the same pegmatite (Table A.1 and Fig. 4j). The younger ages are discordant with concordance of 78.3–89.5% (Table A.1), and show negative correlations with the U and Th contents (Fig. 7), which contrasts to the positive correlation caused by “high-U/Th effect”, indicating a loss of radiogenic Pb after metamictization (e.g., Li, 2016). The type-3 zircons are definitely inherited zircons according to the core-rim texture in CL images and distinct REE patterns to other types of zircons (e.g., Corfu et al., 2003;

Hoskin, 2005), and their ages are irrelevant to the formation time of pegmatites.

Previous works suggest that high abundances of U or Th in zircons, depending on the crystallization age, could induce metamictization of the zircon by radiation damage, which further results in a loss of radioactive Pb and misinterpretation of the U-Pb age (e.g., Wu and Zheng, 2004). Some of our zircon samples have high abundances of U or Th (Table A.1), which indicates that they underwent metamictization featured by mosaic luminance and spongy texture in CL images. Following the calculation method of Nasdala et al. (2001), the radiation dosages in the studied zircons have calculated with varying α-doses (D_α) of 0.08–32.7 × 10^{18} α/g (Table D.1). However, we believe that the concordant ages obtained from the type-1 zircons can represent the crystallization times of the zircons according to 1) most analyzed zircons (> 63%) have α-dose accumulations lower than 4 × 10^{18} α/g, which indicates limited metamictization (Nasdala et al., 2004); 2) the α-doses do not show correlation to the concordance of U-Pb ages (Fig. 8), which means that metamictization and late annealing processes do not always induce a loss of radiogenic Pb (e.g., Nasdala et al., 2001, 2004); 3) the concordant ages do not show positive correlations to the contents of U and Th in the zircons (Fig. 7), which contradicts the disturbance from the "high-U/Th effect" (e.g., Li, 2016).

A few Permian pegmatites in the Chinese Altai have been reported by previous works (Ren et al., 2011; Zhou et al., 2018), some of which suggest formation in the early Permian according to the Ar-Ar ages of muscovite (Zhou et al., 2018). However, such ages for the pegmatites should be reassessed carefully for the following reasons. Firstly, the muscovite Ar-Ar ages are commonly tens of millions of years younger than zircon U-Pb ages, as indicated by previous dating results. For example, the Talati pegmatite has been dated by zircon U-Pb and muscovite Ar-Ar method at 385.9 ± 3.5 Ma (sampling from the rim zone, Lv et al., 2018a) and 286.4 ± 1.6 Ma (sampling from the outer intermediate zone, Zhou et al., 2018), respectively. Such a large gap (ca. 100 Ma) is hard to explain by slow cooling or late hydrothermal fluid activity. Similar age gaps between U-Pb ages and Ar-Ar or K-Ar ages were also observed in the Koktokay No. 3 pegmatite (ca. 30–70 Ma, Chen et al., 1999; Chen, 2011; Wang et al., 2007b; Zhou et al., 2015b) and the Kelumute No. 112 pegmatite (ca. 60–80 Ma, Lv et al., 2012; our unpublished data) in the Chinese Altai, and other pegmatites worldwide (e.g., Barnes, 2010; Kontak et al., 2005; Melleton et al., 2012). Secondly, the Ar-Ar ages of 297–265 Ma determined for the pegmatites (Zhou et al., 2018) overlap with the time span of high-temperature granulite-facies metamorphisms during the Permian (299–271 Ma; Hu et al., 2006; Li et al., 2014; Tong et al., 2013; Wang et al., 2009c, 2014b), which indicates that the Ar-Ar ages might be reset by high-temperature metamorphisms and reflect the cooling times after peak metamorphism. For example, the Talati pegmatite is proposed to form at 385.9 ± 3.5 Ma by zircon U-Pb age, and the Ar-Ar system in muscovite may suffered from thermal disturbance (e.g., with T > 425 °C, Harrison et al., 2009) from high-temperature metamorphism at 299 Ma (e.g., Wang et al., 2009c), which induced the open of Ar-Ar system in muscovite and further to the loss of radiogenic Ar. After that, the Ar-Ar system rebooted during the cooling process at temperature below 425 °C and about 286 Ma.

In this work, the JMHB06, YLM15, HLT01, SEJK01, AKB01, TEL01, QME01, QME02, DKLS01, and BC01 pegmatites, were dated by zircon U-Pb as 260.4 ± 4.0 Ma, 262.9 ± 3.8 Ma, 253.8 ± 4.1 Ma, 252.7 ± 2.1 Ma, 253.0 ± 3.0 Ma, 255.5 ± 2.7 Ma, 253.3 ± 2.4 Ma, 253.5 ± 3.2 Ma, 258.0 ± 3.8 Ma and 274.0 ± 5.3 Ma, respectively. These ages can represent the formation times of the pegmatites according to the genesis of zircons and other evidence mentioned above. Therefore, our dating results demonstrate that the studied pegmatites formed mainly in the late Permian.

5.1.2. Mineralization

The Chinese Altai has been a main production site for rare metals such as Li, Be, Ta, and Cs since the Koktokay No. 3 pegmatite was discovered in the 1940s. Many rare metal ore deposits of the hundreds found in this area have been exploited. Recent studies have revealed that the major rare metal pegmatites exposed in the Central Altai domain were formed during the Triassic (238–208 Ma). These includes the super-large Li-Be-Ta-Nb-Cs ore deposits and Li ore deposits of the Koktokay No. 3 and Kaluan pegmatites, respectively; the large Li-Be-Ta-Nb ore deposits of the Kelumute No. 112 and Koktokay No. 1 pegmatites; and the mid-sized Li-Be ore deposits and Be ore deposits of the Kukalagai No. 650 and Asikaerte pegmatites (Chen, 2011; Liu, 2015; Lv et al., 2012; Ma et al., 2015; Ren et al., 2011). In addition, a few pegmatites exposed in the Qiongkuer domain with limited Li ± Be-Ta-Nb mineralization were formed during the Middle Devonian to Early Carboniferous (Lv et al., 2018a). However, the mineralization of Permian pegmatite remains unclear owning to a lack of sufficient chronology and mineralogy researches.

According to the mineral associations of the pegmatites (Table 2), the Permian pegmatites in the Chinese Altai have three types of mineralization. The SEJK01, QME02 and BC01 pegmatites have a complex mineralization of Li-Be-Ta-Nb ± Sn. The JMHB01, AKB01, TEL01, and DKLS01 pegmatites have dominat mineralization of Be-Nb-Ta, with a certain degree of REE mineralization. The YLM15, HLT01, and QME01 pegmatites show only REE (including Y) mineralization, particularly HREE, as proved by the centimeter-level xenotime grain in the HLT01 pegmatite (Fig. A.3c). Compared with the Devonian-carboniferous and Triassic pegmatites, some of the Permian pegmatites show evident REE mineralization, which indicates that the Permian pegmatites have a certain potential to form REE ore deposits in the Chinese Altai.

5.1.3. Classification

Although a classification scheme for pegmatites involving LCT (enrichment of Li, Cs and Ta), NYF (enrichment of Nb, Y and F) and mixtures of the two types (Černý, 1991b; Černý et al., 2012a; Černý and Ercit, 2005) is widely applied, it is indigestible for study, procpecting, and exploration works (Dill, 2016; Müller et al., 2018). For this reason, we recommend the CMS (Chemical composition-Mineral assemblage-Structural geology) model (Dill, 2016) because it clarifies the correlations between tectonic dynamics and the origins of pegmatitic rocks. More importantly, however, this model can be used to distinguish pegmatites from other pegmatitic quartz-feldspathic rocks including pegmatoids, metapegmatites, granitic pegmatites and pseudopegmatites. According to this classification, a total of five types of pegmatitic rocks have been identified in the Chinese Altai: pegmatites, granitic pegmatites, metapegmatites, pegmatoids, and pseudopegmatites (Lv et al., 2018a). The studied pegmatites in this work are distinguished from the Yelaman and Nasenqia metapegmatites (Wang et al., 2001) and the Tiemulete pegmatoids (Lv et al., 2018a) by their igneous origin and evident internal zonations. In addition, they are distinguished from the Liangkeshu pseudopegmatite (Jiang, 2012) by their primary and pegmatitic textures and from the Shangkelan granitic pegmatite (Zou and Li, 2006) by a lack of parental granite in the same region (Section 5.2).

5.2. Relationships between the Permian pegmatites and granites in the Chinese Altai

According to the classical petrogenesis model for pegmatites, LCT pegmatites always show regional zonation from barren to complex mineralization with a maximum distance of 10 km from their parental S-type granites (Selway et al., 2005). The NYF pegmatites commonly show no regional zonation, and are distributed in or near their parental A-type granites (Černý, 1991b; Černý and Ercit, 2005). However, the regional zonation of pegmatites does not prove the existence of parental rocks. In the Chinese Altai, the regional zonation of pegmatites is

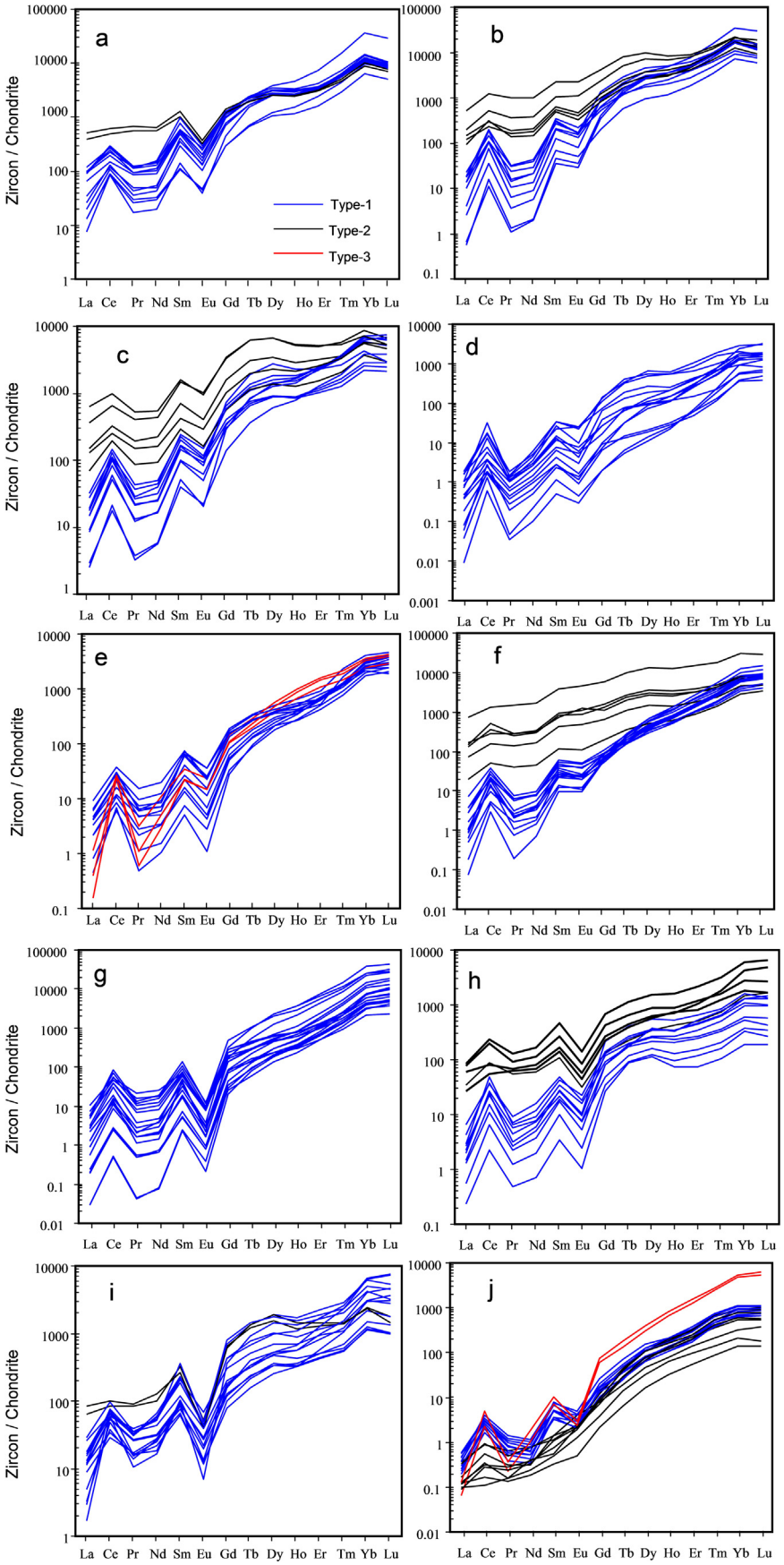

Fig. 5. Chondrite-normalized rare earth elements (REE) patterns of zircons from the JMHB06 (a), YLM15 (b), HLT01 (c), SEJK01 (d), AKB01 (e), TEL01 (f), QME01 (g), QME02 (h), DKLS01 (i) and BC01 (j) pegmatites. Type-1, —2 and — 3 represent primary, secondary and inherited zircon, respectively.

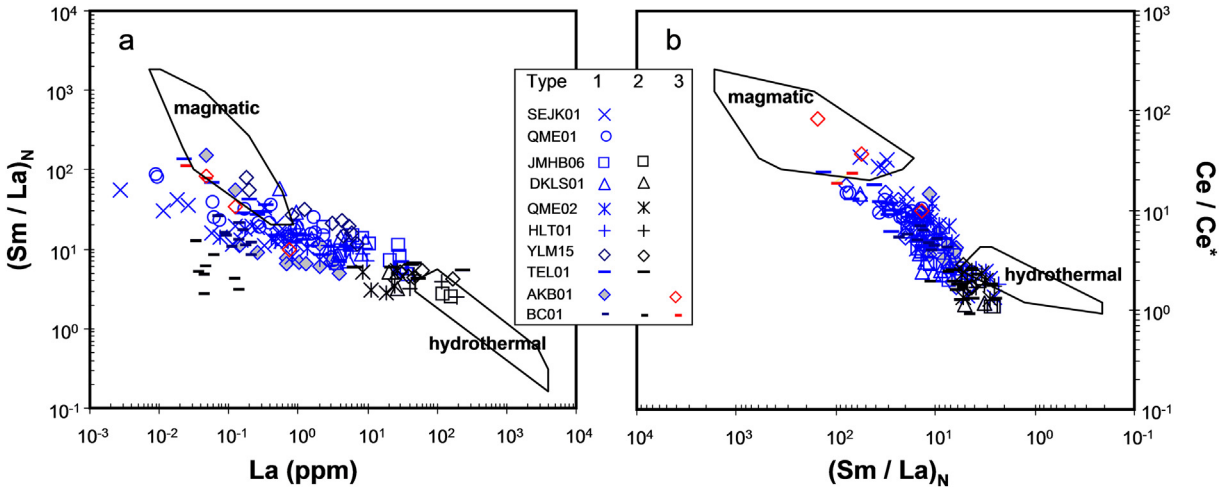

Fig. 6. La *vs.* $(Sm/La)_N$ (a) and Ce/Ce* *vs.* $(Sm/La)_N$ (b) diagrams for genetic discrimination of zircons from the studied pegmatites. Ranges of magmatic and hydrothermal zircons referred to Hoskin (2005). $(Sm/La)_N$ means chondrite-normalized Sm/La ratio, Ce/Ce* calculated according to $Ce_N/(La_N*Sm_N)^{0.5}$. The types of zircon are same to those in Fig. 5.

observed only to the west of the Halong granite batholiths, which consists of biotite granite and two-mica granite (Zou and Li, 2006). From east to west, four pegmatite zonations have been identified by local geologists since the 1950s: a barren pegmatite zone, a Be-Nb-Ta pegmatite zone, a Li-Be-Nb-Ta pegmatite zone, and a quartz vein zone. The Halong granite has been chronically regarded as the parental rock of the pegmatites. However, our recent chronology, isotope geochemistry and whole rock composition studies revealed that the Halong granite has zircon U-Pb ages of 403–398 Ma with $\varepsilon_{Hf}(t)$ values of +9.9 to +15.2 in addition to metaluminous compositions, indicating I-type granite. Conversely, the Azubai Be-rich pegmatites, the Jiamukai-Qunku Be-Nb-Ta pegmatites and the Kaluan Li-rich pegmatites have zircon U-Pb ages of 227–192 Ma with εHf(t) values of −0.6 to +6.3 (Ma et al., 2015; Zhang et al., 2016), which precludes a genetic relationship between the Halong granite and the rare metal pegmatites. Therefore, detailed geochemical and isotopic studies are required even if the potential parental granite of the pegmatite is indicated by field geological observations.

In this section, comparative studies of the Permian pegmatites and granites are conducted to clarify the temporal-spatial and differentiation-source relationships between them.

5.2.1. Temporal-spatial distributions of the Permian pegmatites and granites

According to the statistics on the Permian pegmatites and granites in the Chinese Altai, the ages and spatial features of the pegmatites show significant distinctions from the granites. Spatially, the granites are located mainly in the southeastern areas of the Qiongkuer and South Altai domains. The pegmatites are concentrated mostly in the northwestern part of the Qiongkuer domain (Fig. 9). Temporally, the granites formed mainly during the early Permian (285–265 Ma), and the pegmatites are commonly formed in the late Permian (265–250 Ma; Table 3; Fig. 10). Essentially, the Permian granite is absent in most pegmatite fields (Fig. 9). In the areas adjacent to the Xiaokalasu-Qiebielin pegmatite field, two Permian granites including the Keyinbulake syenogranite (No. 25 in Fig. 9) and the Aletai two-mica granite (No. 24 in Fig. 9) in addition to the Aweitan porphyritic adamellite (No. 23 in Fig. 9) have been dated by zircon U-Pb as 278.6 ± 3.5 Ma, 275.1 ± 1.7 Ma, and 271 ± 2 Ma, respectively (Li et al., 2012b; Sun et al., 2009a; Tong et al., 2014). However, the U–Pb ages of the adjacent pegmatites, including the SEJK01, AKB01 and Xiaokalasu pegmatites (Nos. 30, 31 and 35 in Fig. 9, respectively) are 252.7 ± 2.1 Ma, 253.0 ± 3.0 Ma (this work),

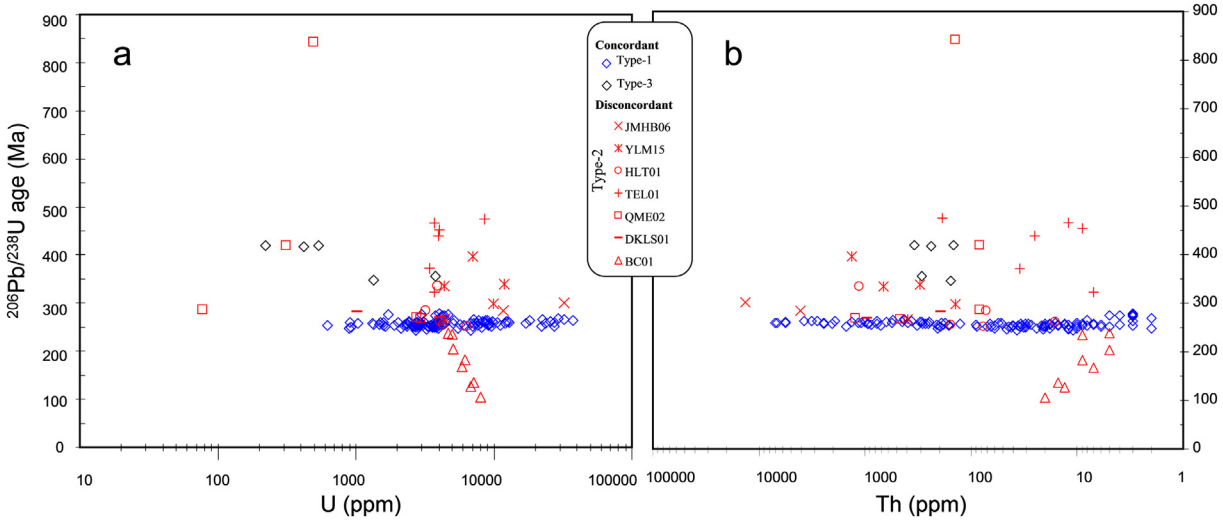

Fig. 7. $^{206}Pb/^{238}U$ ages *vs.* Contents of U (a) and Th (b) in zircons from the studied pegmatites. No evident correlation is observed in the diagrams, indicating the limited influence of "high U/Th effect" on the concordant ages (blue diamond shape). The types of zircon are same to those in Fig. 5.

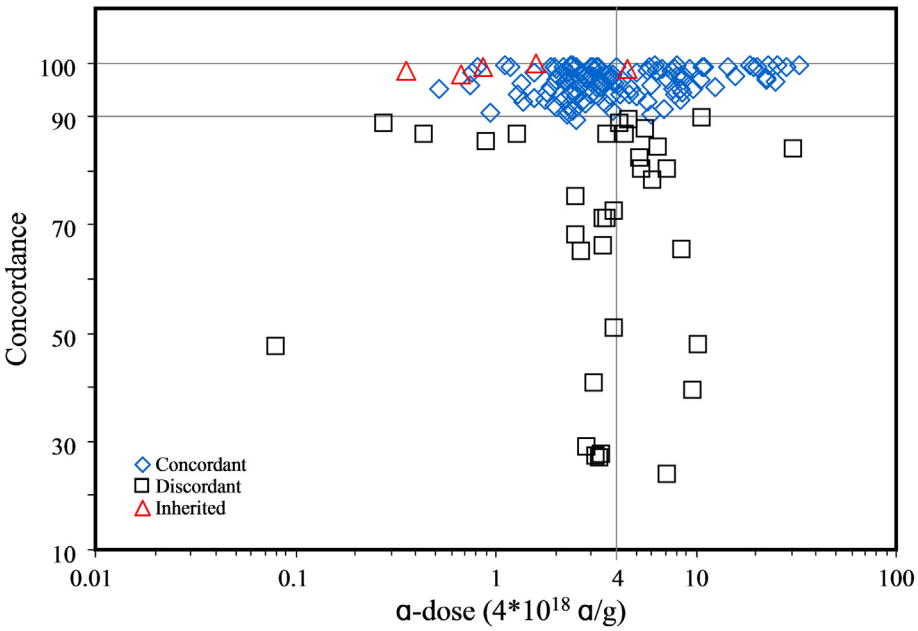

Fig. 8. Concordance between $^{206}Pb/^{238}U$ and $^{207}Pb/^{235}U$ ages *vs.* α-doses (radiation dosages) of zircons from the studied pegmatites. It shows weak correlation between the concordance of age and α-dose in the studied zircons.

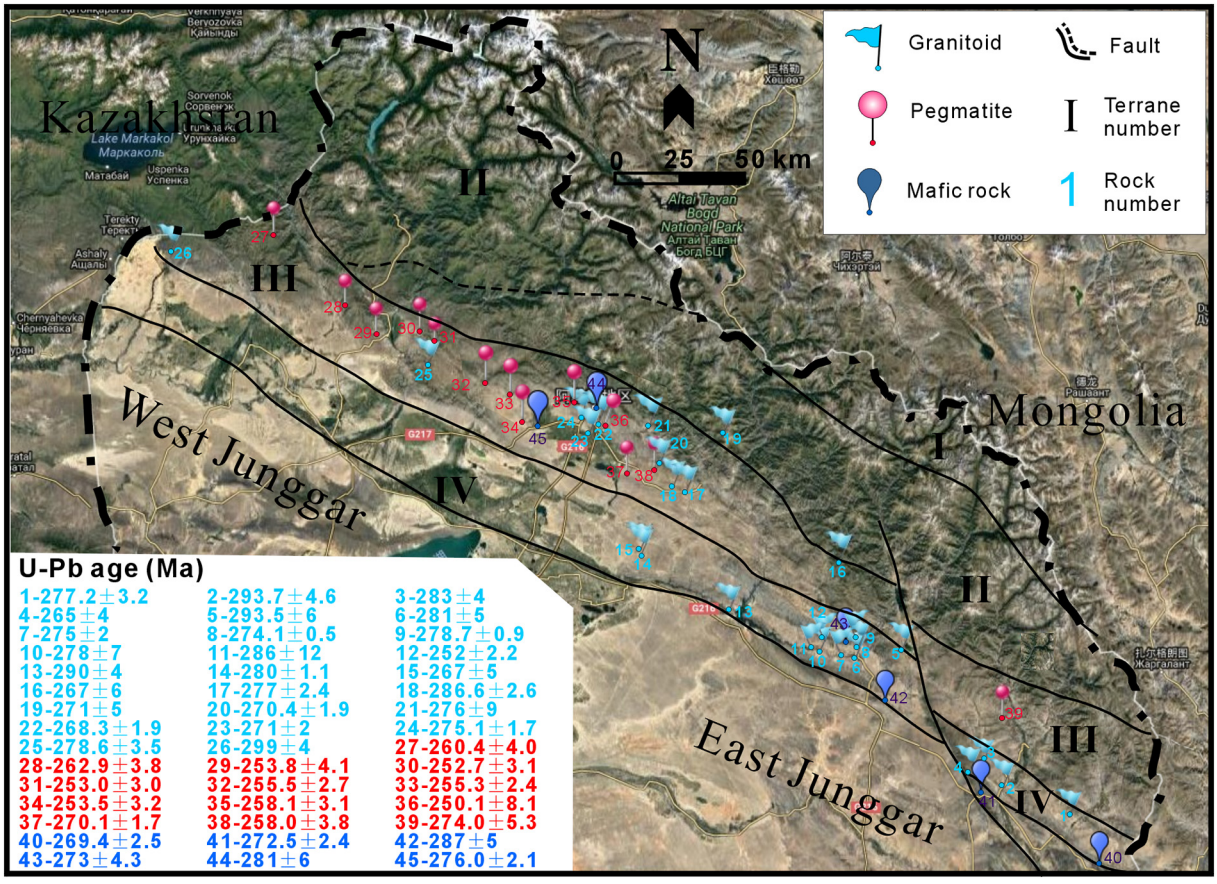

Fig. 9. The satellite map of the Chinese Altai from Google Earth, with showing of the precise locations of the Permian pegmatites, granitoids and mafic rocks. The rock numbers refer to Table 3.

Table 3
The age statistics on the Permian magmatic-metamorphic events in the Chinese Altai.

Number	Domain	Location	Sample	Lithology	Age	Error	Reference
1	SA	Chaergan	06Q4	Granite dyke	277	3.2	Zhang et al., 2010
2	SA	Areletuobie	11ALT17	Monzogranite	293.7	4.6	He et al., 2018
3	SA	Mayinebo	0410TW2	Biotite granite	283	4	Zhou et al., 2007
4	SA	Yulekenhalasu	ZR01	Beschtauite	265	4	Xue et al., 2016
5	SA	Wuqiagou	o9-2	Gnesisic granite dyke	293.5	6	Zhang et al., 2015
6	SA	Fuyun	A13	Biotite monzogranite	281	5	Tong et al., 2006
7	SA	Fuyun	A14	Biotite granite	275	2	
8	SA	Kuerqis		Gneissic granite	274.1	0.5	Yang et al., 2012
9	SA	Kuerqis		Gneissic granite	278.7	0.9	
10	SA	Ertix river	sample 7	Unfoliated granite	278	7	Briggs et al., 2007
11	SA	Fuyun	sample 4	Granitic Dyke	286	12	
12	SA	Mayinebo	08AL18	Granite dyke	252	2.2	Zhang et al., 2012
13	SA	daqiaonan	152	Biotite granite	267	5	Tong et al., 2014
14	SA	xibodu	3055	Monzogranite	267	6	
15	SA	Kezile	KZ	Monzogranite	290	4	Zhao et al., 2016
16	QD	Kadelat	Kadelat-07	Quartz monzonite	280	1.1	Zhang et al., 2018
17	QD	Bukesala	KL4	Biotite monzogranite	277	2.4	Gao et al., 2010
18	QD	Jiaerbasidao		Biotite granite	286.6	2.6	Yang et al., 2013
19	CA	Adenbluk	A4	Porphyritic granite	271	5	Tong et al., 2014
20	QD	Dakalasu		Biotite granite	270.4	1.9	Liu et al., 2018
21	QD	Lamazhao	258	Biotitite monzogranite	276	9	Wang et al., 2005
22	QD	Jiangjunshan		Biotite granite	268.3	1.9	Liu et al., 2018
23	QD	Aweitan	A3	Porphyritic adamellite	271	2	Tong et al., 2014
24	QD	Aletai city	D05126-1	Two-mica granite	275.1	1.7	Sun et al., 2009a
25	QD	Keyinbulake		Two mica syengranite	278.6	3.5	Li et al., 2012a
26	QD	Woduoke	09HTW1	Quartz diorite	299	4	Zhou et al., 2015
27	QD	Jiamanhaba	JMHB06	Pegmatite	260.4	4	This work
28	QD	Yeliuman	YLM15	Pegmatite	262.9	3.8	
29	QD	Hailiutan	HLT01	Pegmatite	253.9	4.1	
30	QD	Saerjiake	SEJK01	Pegmatite	252.7	3.1	
31	QD	Akebasitawu	AKB01	Pegmatite	253	3	
32	QD	Taerlang	TEL01	Pegmatite	255.5	2.7	
33	QD	Qiemuerqieke	QME01	Pegmatite	255.3	2.4	
34	QD	Qiemuerqieke	QME02	Pegmatite	253.5	3.2	
35	QD	Xiaokalasu	Xkls	Pegmatite	258.1	3.1	Zhou et al., 2018
36	QD	Jiangjunshan	JJS-1	Pegmatite	250.1	8.1	Liu, 2017
37	QD	Dakalasu	DKLS01	Pegmatite	258	3.8	This work
38	QD	Tangbahu	FH08-1	Pegmatite	258	3.8	Ren et al., 2011
39	QD	Baicheng	BC01	Pegmatite	274	5.3	This work
40	SA	Dasazi	07AL06	Gabbro	272.5	2.4	Zhang et al., 2010
41	SA	Mayinebo	07AL03	Gabbro	269.4	2.5	
42	SA	Kalatongke	02KK101	Norite	287	5	Han et al., 2004
43	SA	Fuyun	C12FY27	Gabbro-norite	273	4.3	Cai et al., 2016
44	QD	Kekesazi	2011ALT018	Gabbro	281.2	1.8	Zhang et al., 2014
45	QD	Qiemuerqieke		Gabbro	276	2.1	Wan et al., 2013
46	QD	Qinghe	02XA	Andesitic gneiss	281.2	3.1	Hu et al., 2006
47	QD	Altai	A915	Metapelitic schist	299.2	3.4	Wang et al., 2014b
48	QD	Dakalasu	A152	Pelitic granulite	292.8	2.3	Wang et al., 2009c
49	QD	Dakalasu	LT10F-41	Pelitic granulite	271	5	Tong et al., 2013
50	SA	Fuyun	Fy0402/052117	Pelitic granulite	277	2	Li et al., 2014

Note: SA = South Altai, QD = Qiongkuer domain; CA = Central Altai.

and 258.1 ± 3.1 Ma (Zhou et al., 2018), respectively. In the Jiangjunshan mining area, the alkaline biotite granite (No. 22 in Fig. 9) and the JJS01 pegmatite (No. 36 in Fig. 9) are dated as 268.3 ± 1.9 Ma and 250.1 ± 8.1 Ma, respectively (Liu, 2017; Liu et al., 2018). In the Dakalasu pegmatite field, the biotite granite (No. 20 in Fig. 9) has been dated as 270.4 ± 1.9 Ma (Liu et al., 2018), which is evidently older than the DKLS01 pegmatite, at 258.0 ± 3.8 Ma (No. 38 in Fig. 14).

A decoupling temporal-spatial relationship has also been proved regionally and globally. In the Koktokay, Bieyesamasi, Kelumute, Kaluan, Azubai and Jiamukai mining areas in the Chinese Altai, Paleozoic granites (450–370 Ma) are prevalent; however, the pegmatites formed during the Mesozoic (238–160 Ma) (Lv et al., 2012, 2015; Ma et al., 2015; Ren et al., 2011; Zhang et al., 2016). In the Central Asian Orogenic Belt, most of the Li-rich pegmatites show evident time gaps of a few tens to hundreds of millions of years compared with the granites which are generally regarded as parental rocks, according to the age statistics on Li-rich pegmatites and the adjacent granites (Zagorsky et al., 2014).

The isolated pegmatites with no parental granites exposed in the same region are hypothetically proposed to have a "deep-buried parent granite" (Černý, 1991a; London, 2018). However, the confirmed granite-related pegmatites are always juxtaposed with their parental granites. For example, the Archean Ghost Lake granite batholith and the Mavis Lake pegmatite group in the Superior province of northwestern Ontario, Canada, are concurrently exposed (Breaks and Moore, 1992). Similar situations are also observed in the Mesozoic Jiajika two-mica granite and in the surrounding pegmatite zones in Sichuan province, China (Fu et al., 2015; Xu et al., this issue). The coexposure of pegmatite groups and the associated source granites under the same denudation level could indicate that the pegmatites are (sub)horizontally but (sub)vertically differentiated from the source granite. In the Hagendorf-Pleystein pegmatite Province, Central Europe, the "deep-buried parental granite" of the pegmatites has been excluded by geophysical surveys and core rock samples from boreholes (Dill, 2015a).

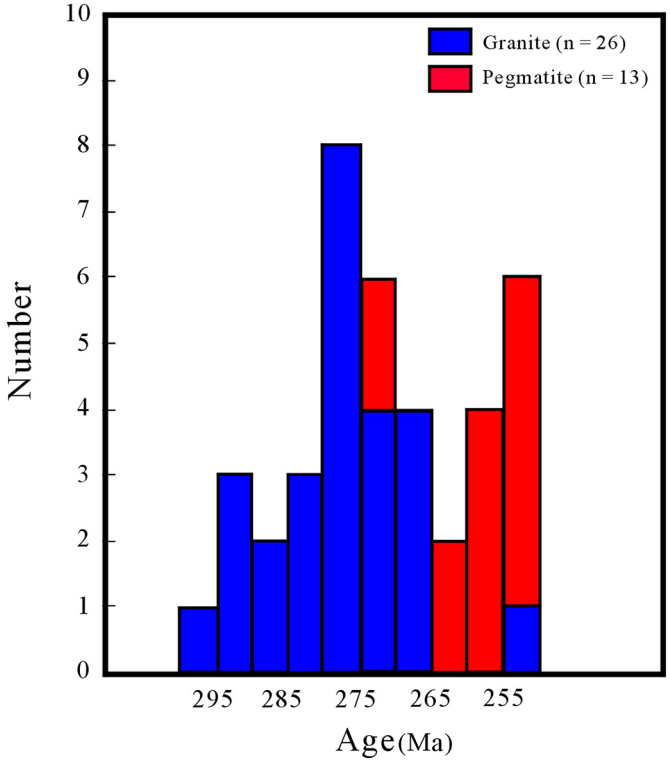

Fig. 10. Histogram of zircon U-Pb ages of the Permian pegmatites and granites from the Chinese Altai. Data source refers to Table 3.

5.2.2. Differentiation and metallogenetic potentiality of the Permian granite

The fertile granite, which is regarded as parental rock of the rare metal pegmatite consists mainly of rock-forming minerals of alkaline feldspar, muscovite, and quartz, with minor tourmaline, Mn-rich garnet, cordierite, Hf-rich zircon, and rare metal minerals such as beryl and ferrocolumbite (Černý, 1991b; Selway et al., 2005). The geochemistry indicates that this fertile granite is commonly peraluminous to strongly peraluminous and is characterized by high differentiation with low REE abundance and ratios of K/Rb < 100, Mg/Li < 10, Zr/Hf < 15, and Nb/Ta < 8 (Ballouard et al., 2016; Selway et al., 2005). The unique indicator for the fertile granite could be the general development of lanthanide tetrad effects in the chondrite-normalized REE patterns of the bulk compositions (Černý et al., 2012b) and REE-bearing minerals such as zircon (Yang et al., 2014). All of these features can be used to distinguish fertile granite from barren granite.

In the Chinese Altai, the Permian granitoids consist of monzogranite, biotite granite, two-mica granite and quartz diorite (Table 2). Most of the granitoids are approximately circular or linear in shape with limited deformation, and they generally cut pre-Permian structures. The granitoid mineralogy consists mainly of plagioclase, K-feldspar, quartz, and biotite, and the geochemistry indicates high-K calc-alkaline to alkaline and metaluminous to weakly peraluminous compositions. Most of these granitoids are identified as I- and A-type (e.g., Gao et al., 2010; He et al., 2018; Liu et al., 2018; Tong et al., 2014; Wang et al., 2005). S-type granite is rare and is distributed in the Mayinebo and Kadelat areas, southeastern part of the Chinese Altai (e.g., Zhang et al., 2018; Zhou et al., 2007) (Table 2). According to our statistics, these granitoids commonly show high ratios of K/Rb > 100, Mg/Li > 10, Zr/Hf > 15 and Nb/Ta > 8 (Fig. 11), which are distinctive of parental granites of rare metal pegmatites. In addition, these Permian granitoids have high REE contents with no lanthanide tetrad shown in the chondrite-normalized REE patterns of the bulk compositions (See references in Table 3). All of these features indicate that the Permian granitoids in the Chinese Altai are weakly differentiated and are too barren to be precursors of the rare metal pegmatites. However, the Yulekenhalasu beschtauite (Xue et al., 2016) the Keyinbulake syenogranite (Li et al., 2012b), and the Kuerqis gneissic granites (Yang et al., 2012) are proposed to relate with Cu, Cu-Zn and Fe mineralization, respectively.

5.2.3. Zircon Hf isotopic compositions of the Permian pegmatites and granites

It is generally known that the parental granite and its derivative pegmatite are expected to possess comparable isotopic compositions. The Lu-Hf isotope system has an extremely high blocking temperature and is hardly affected by the fractional crystallization process (e.g., Kinny and Maas, 2003). A comparative study of the zircon Hf isotope in the Permian pegmatites with that of the granites in the Chinese Altai is presented here to identify their source relationship. According to previous studies, early-middle Permian I-type granites (295–270 Ma) have zircon $\varepsilon_{Hf}(t)$ values of +5.7 to +12.3 and young T^{C}_{DM} model ages of 933–527 Ma, which partly overlap with the isotopic compositions of the Permian gabbros (Fig. 12) and are proposed to be generated by differentiation of mantle-derived magmas with variable degrees of crustal contamination (e.g., He et al., 2018; Tong et al., 2014). The middle Permian A-type granites (about 270 Ma) have dispersive zircon $\varepsilon_{Hf}(t)$ values of −7.0 to +4.6 with T^{C}_{DM} model ages of 948 Ma to 1668 Ma, which is ascribed to mantle-derived magma mixed with ancient crustal materials (e.g., Liu et al., 2018). The early Permian S-type granites (about 280 Ma) have $\varepsilon_{Hf}(t)$ values of −7.46 to +2.56 with T_{DM} model ages of 1770 Ma to 843 Ma, and are suggested to derive from partial melting of Mesoproterozoic metasediments (e.g., Zhang et al., 2018) with contamination by basalt magma (Zhou et al., 2007).

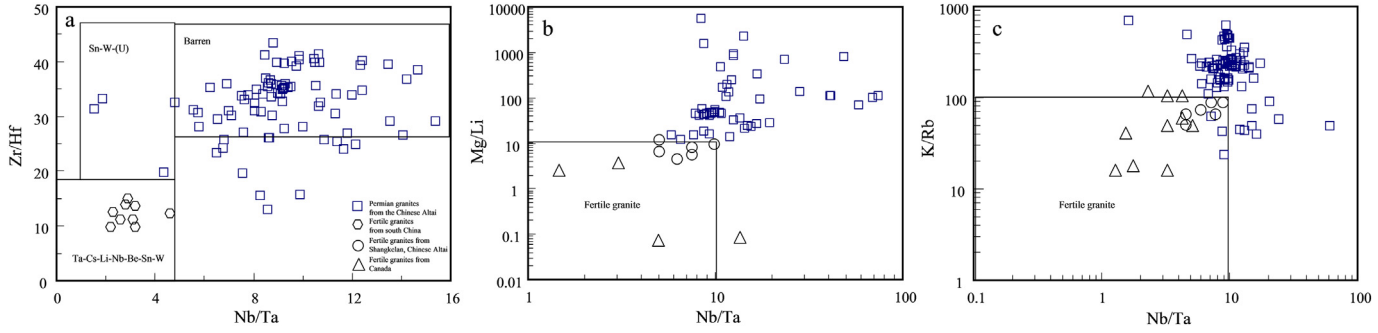

Fig. 11. Nb/Ta *vs.* Zr/Hf (a), Mg/Li (b), and K/Rb (c) diagrams of the Permian granites from the Chinese Altai and typical fertile granites worldwide, show the low differentiation degree of the former. Data of the Permian granites from the Chinese Altai refers to Cai et al. (2016); Gao et al. (2010); He et al. (2018); Liu et al. (2018); Tong et al. (2006, 2014); Wang et al. (2005); Zhang et al. (2018); Zhou et al. (2007, 2015b). data of the Shangkelan granites from Zou and Li (2006); data of the fertile granites from Superior and Manitoba, Canada refers to Černý et al. (2012b) and Selway et al. (2005), respectively; data of the fertile granites from South China is our unpublished data.

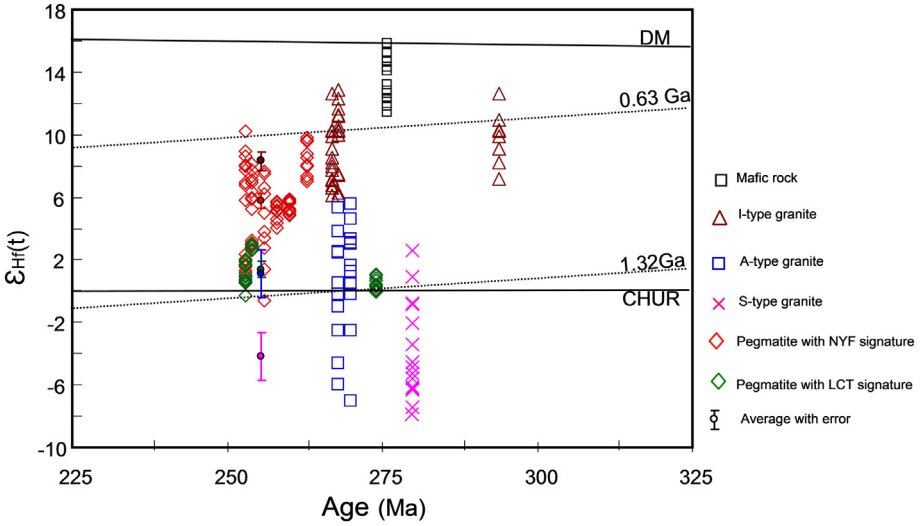

Fig. 12. Diagram of εHf(t) values *vs.* crystallizing ages of zircons from the Permian pegmatites (this work), mafic rocks (Cai et al., 2016; Wan et al., 2013), and I-type (He et al., 2018; Tong et al., 2014), A-type (Liu et al., 2018) and S-type (Zhang et al., 2018) granites in the Chinese Altai. DM = depleted mantle, CHUR = chondrite uniform reservoir.

The zircon Hf isotope compositions of the Permian pegmatites partly overlap with that of the I-, A- and S-type granites due to the scattered Hf isotope compositions of the latter (Fig. 12). In order to check the source connection between them precisely, the $\varepsilon_{Hf}(t)$ values and T_{DM} model ages of the pegmatites and granites at 255 Ma were recalculated, and the weighted mean Hf isotope compositions are used to compare. The pegmatites with 'NYF' signatures (JMHB06, HLT01, YLM15, AKB01, TEL01, QME01, and DKLS01) have weighted mean ε_{Hf}(255 Ma) value and model age of 5.45 ± 0.29 and 932 ± 19 Ma, respectively. The Hf isotopic composition is distinct from those of the A- (with ε_{Hf}(255 Ma) and T_{DM} age of 0.9 ± 1.5 and 1220 ± 92 Ma, respectively) and I-type (with ε_{Hf}(255 Ma) and T_{DM} age of 8.06 ± 0.6 and 735 ± 43 Ma, respectively) granites (Fig. 12). The pegmatites with 'LCT' signatures (SEJK01, QME02, and BC01) have weighted mean ε_{Hf}(255 Ma) value and model age of 1.16 ± 0.52 and 1204 ± 33 Ma, respectively, which is evidently distinct from that of the S-type granites (with ε_{Hf}(255 Ma) and T_{DM} model age of −4.4 ± 1.5 and 1553 ± 94 Ma, respectively) and close to that of the A-type granites (Fig. 12). Distinct Hf isotopic compositions of the Permian pegmatite and granite have also been observed locally with juxtaposition of the Permian granite and pegmatite. The Dakalasu pegmatites have been regarded as the derivative of the biotite granite and two-mica granite (Zou and Li, 2006). However, the DKLS01 pegmatite shows distinct Hf isotopic compositions with $\varepsilon_{Hf}(t)$ values of +4.01 to +5.76 (this work) from that in the biotite granite at −7.0 to +4.6 (Liu et al., 2018). Therefore, the source connections between the 'NYF' pegmatite and the A-type granite and between the 'LCT' pegmatite and the S-type granite were not observed in the Permian pegmatites and granites of the Chinese Altai.

In summary, the decoupling temporal-spatial and differentiation-isotope correlations between the Permian pegmatites and granites do not support a genetic relationship between them.

5.3. Source of the Permian pegmatites

Compared with the Hf isotopic compositions of zircons from the Devonian-Carboniferous and Triassic pegmatites in the Chinese Altai, the Permian pegmatites have a wider range of zircon $\varepsilon_{Hf}(t)$ values (Table 4; Fig. 12). However, all pegmatites of the three periods are comparable in their mineralizations and zircon Hf isotopic compositions. According to these features, the Permian pegmatites are classified into three types (Fig. 13a, b), including the Li-Be-Ta-Nb ± Sn mineralized pegmatites (SEJK01, QME02, and BC01) with dominat $\varepsilon_{Hf}(t)$ values ranging from 0 to +3 and maximum T_{DM} model ages of 1.09 Ga (type-1); Be-Nb-Ta ± REE mineralized pegmatites (JMHB06, AKB01, TEL01, and DKLS01) with major $\varepsilon_{Hf}(t)$ values ranging from +3 to +7 and T_{DM} model ages of 1.09 Ga to 0.86 Ga (type-2); and the REE mineralized pegmatites (YLM15, HLT01, and QME01) with major $\varepsilon_{Hf}(t)$ values ranging from +7 to +10 and T_{DM} model ages of 0.86–0.63 Ga (type-3) (Table 3; Fig. 13). The zircon Hf isotopes of the type-1 pegmatite are consistent with those of the Triassic pegmatites characterized by Li-Be-Ta-Nb ± Cs mineralization; those of the type-2 pegmatite are consistent with zircon Hf isotopic compositions of the Devonian-Carboniferous pegmatites featuring Be-Ta-Nb ± Li mineralization; and those of the type-3 pegmatites are unique in all pegmatite generations (Fig. 13a and b). Therefore, the correlation between the mineralization type and zircon Hf isotopic compositions indicates that the mineralization of the pegmatites is controlled predominately by their sources.

Recent studies have suggested that the Precambrian basement is absent in the Chinese Altai and that the crustal component is significantly heterogeneous (e.g., Jiang et al., 2016; Liu et al., 2012; Long et al., 2008, 2010). The Chinese Altai was an early Paleozoic magmatic arc developed at an active continental margin (e.g., Xiao et al., 2008, 2009, 2015, 2018) and consists mainly of early Paleozoic sedimentary, granitic and volcanic rocks (e.g., Cai et al., 2011a, 2011b; Jiang et al., 2011; Long et al., 2007, 2008, 2010; Sun et al., 2008; Sun et al., 2009a, 2009b; Wang et al., 2011; Yuan et al., 2007). The early Paleozoic sedimentary strata, particularly those of the Habahe Group, are proposed as the major crust components of the Chinese Altai (e.g., Jiang et al., 2015, 2016). Regarding the petrography, the western segment of the Habahe Group consists of schist, gneiss, siltstone, slate, and mudstone, and the central segment is composed of schist, gneiss, migmatite, and minor marble. The eastern segment of the Habahe Group includes lower garnet-sillimanite-biotite-plagioclase gneiss, garnet-biotite schist, migmatite, and leptynite and the upper staurolite-biotite schist, biotite-quartz schist, and chlorite-quartz schist (BGMRX, 1993; Long et al., 2010). Regarding the provenance, the U-Pb age and Hf isotope compositions of detrital zircons from the Habahe Group indicate multiple sources composed of a dominant magmatic source eroded from the Caledonian orogenic system, a mixed source of Neoproterozoic metasedimentary and juvenile igneous rocks from the Tuva-Mongol block and a mixed source of Paleoproterozoic-Neoarchean granitoid and metasedimentary rocks from the southern Siberian craton (Fig. 14) (Jiang et al., 2011; Liu et al., 2012; Long et al., 2010). In metamorphic grade, the lower, middle, and upper crust corresponds to granulite, amphibolites, and greenschist

Table 4
The mineralizations and zircon U-Pb ages and Hf isotopic compositions of rare metal/earth pegmatites in the Chinese Altai.

Location	Pegmatite field	Pegmatite	Mineralization	Scale	Age (Ma)	$\varepsilon_{Hf}(t)$	T^{C}_{DM} (Ma)	Referrence
Qingkuer domain	Qinghe	TLT01	Be-Nb-Ta-Li	Small	386	+3.99 ~ +5.06	1166–1057	Lv et al., 2018a
	Jiamanhaba	JMHB02	Be-Nb-Ta	Small	395	+4.69 ~ +8.28	1088–860	
	Qinghe	AMLG01	Be-Nb-Ta-Li	Small	358	+5.5 ~ +7.28	1008–895	
	Qiebielin-Xiaokalasu	QBL02	Be-Nb-Ta	Small	403	+3.12 ~ +7.22	1186–934	
	Qinghe	TMLT01	Be-Nb-Ta	Small	333	+3.20 ~ +5.30	1135–1001	
	Jiamanhaba	JMHB06	Be-Ta-Nb	Unknown	260	+4.81 ~ +5.87	977–910	This work
	Haikiutan-Yeliuman	YLM15	REE	Unknown	263	+7.17 ~ +9.80	830–662	
		HLT01	REE	Unknown	254	+5.21 ~ +8.10	947–763	
	Qiebielin-Xiaokalasu	SEJK01	Li-Be-Ta-Nb	Unknown	253	−0.32 ~ +1.52	1296–1180	
		ACB01	Be-Nb-Ta-REE	Unknown	253	+0.58 ~ +2.37	1239–1126	
		TEL01	Be-Nb-Ta-REE	Unknown	256	−0.61 ~ +7.63	1316–795	
		QME01	REE	Unknown	253	+5.82 ~ +10.19	907–629	
		QME02	Li-Be-Ta-Nb-Sn	Unknown	254	+2.58 ~ +3.20	1114–1074	
	Dakalasu	DKLS01	Be-Nb-Ta	Small	258	+4.01 ~ +5.76	1026–915	
	Qinghe	BC01	Li-Be-Ta-Nb	Small	274	−0.07 ~ +1.11	1296–1222	
Central Altai domain	Kelumute	KLMT112	Li-Be-Ta-Nb	Large	238–211	+0.92 ~ +2.35	1190–1112	Lv et al., 2012
	Koktokai	KKT03	Li-Be-Ta-Nb-Cs	Super-large	220–209	+1.25 ~ +2.39	1174–1102	Chen, 2011; Wang et al., 2007a, 2007b
	Kalaeerqisi	KKLG650	Li-Be-Ta-Nb	Medium	228–211	−0.51 ~ +1.99	1276–1131	Ma et al., 2015
		KLA805	Li-Ta-Nb	Large	216	0.00 ~ +2.50	1248–1090	
		KLA806	Li-Ta-Nb		224	+0.65 ~ +2.02	1213–1126	
		KLA803	Li-Ta-Nb		225	−0.60 ~ +2.20	1275–1095	Zhang et al., 2016

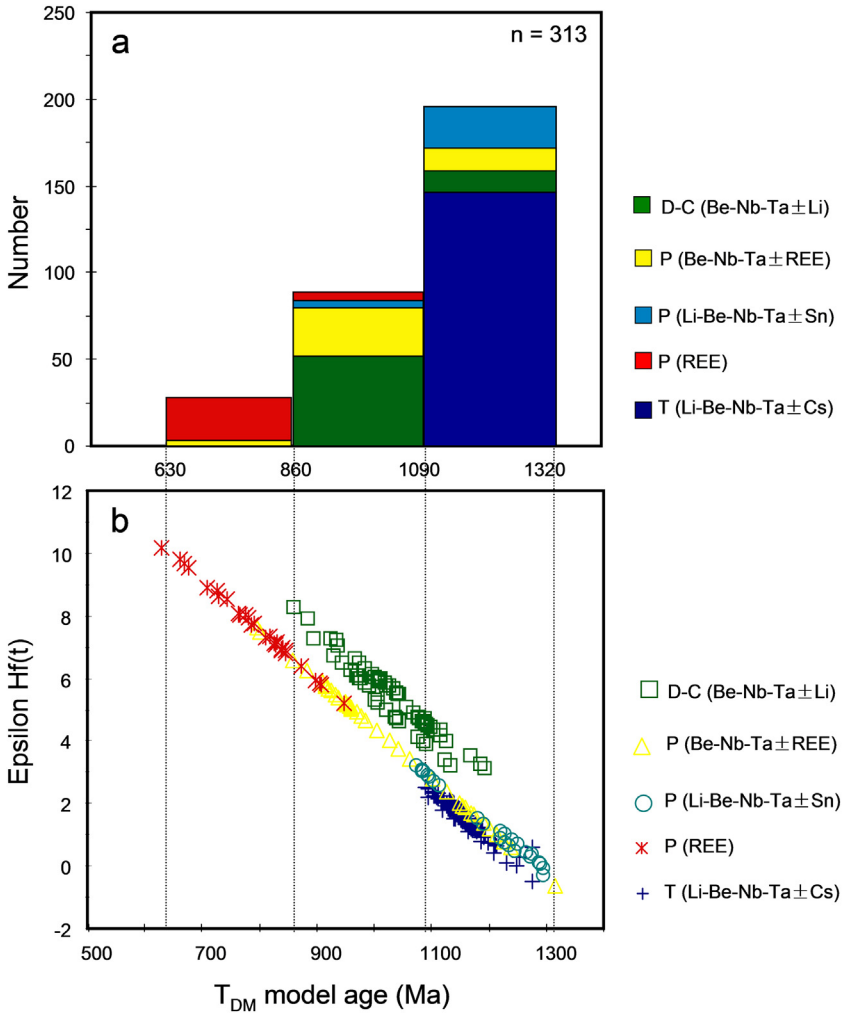

Fig. 13. Histogram of T^{C}_{DM} model ages (a) and $\varepsilon_{Hf}(t)$ values vs. T^{C}_{DM} model ages of zircons (b) from rare metal/earth pegmatites in the Chinese Altai. The diagrams show that various generations of pegmatites are comparable in Hf composition and mineralization. D, C, P and T are abbreviations of Devonian, Carboniferous, Permian and Triassic, respectively.

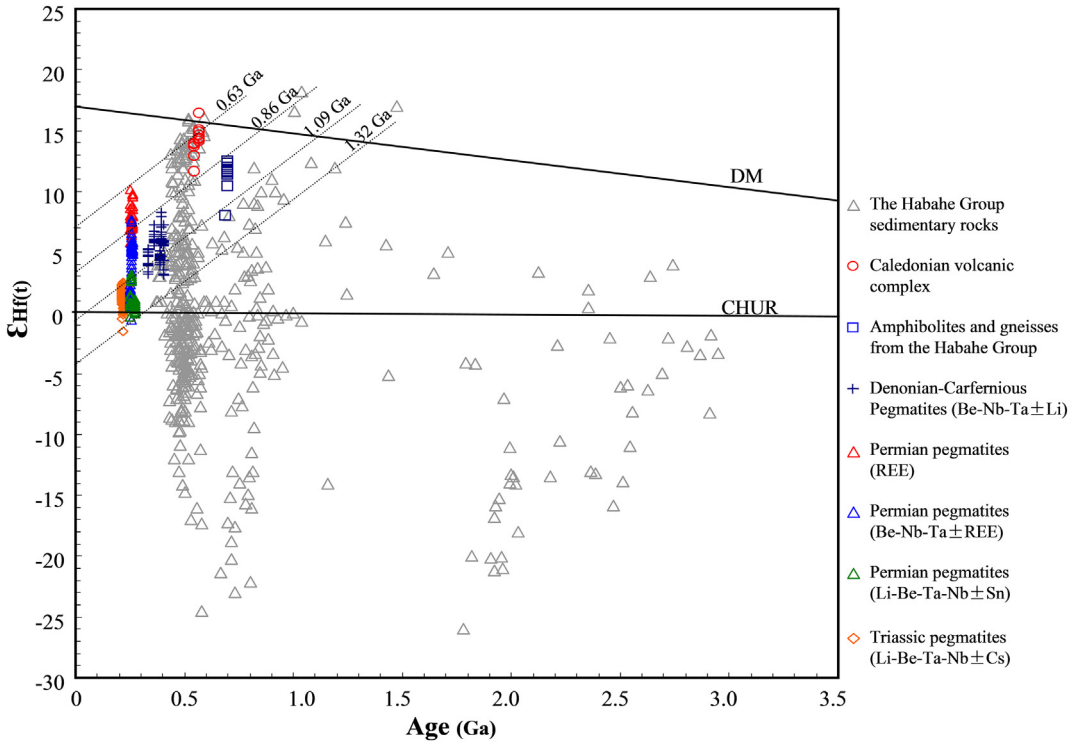

Fig. 14. Diagram of εHf(t) values *versus* crystallizing ages of zircons from the rare metal/earth pegmatites (Chen, 2011; Lv et al., 2012, Lv et al., 2018a, 2018b, 2018c; Ma et al., 2015; Zhang et al., 2016 and this work) and Habahe Group metasedimentary rocks (Jiang et al., 2011; Long et al., 2007, 2010, 2012) in the Chinese Altai. The εHf(t) values of the Caledonian volcanic complex from the Lake Zone, Mongolia (Kovach et al., 2011) and amphibolites and gneisses from the Chinese Altai (Hu et al., 2000) are calculated according to the reduction formula of εHf = 1.36εNd + 2.95 (Vervoort et al., 1999). DM = depleted mantle, CHUR = chondrite uniform reservoir.

facies metamorphism, respectively (Broussolle et al., 2018; Jiang et al., 2016). In rare metal/earth abundance, different rock samples from the Habahe Group show large variations including 15.6–91.2 ppm Li, 1.0–5.5 ppm Be, 6.0–84.2 ppm Nb, 0.4–5.1 ppm Ta, 2.4–12.5 ppm Cs, and113-273 ppm REEs (Shen, 2015).

The source diversity of the Habahe Group raises the possibility of generation of various pegmatites according to the mineralization and Hf isotopic composition. According to the zircon Hf isotope compositions, the three generations of pegmatites totally overlap with the juvenile crust materials in the Habahe Group (Fig. 14). The Permian-Triassic pegmatites with Li-Be-Ta-Nb ± Cs ± Sn mineralization might be derived from a slightly depleted source dominated by the Caledonian and Neoproterozoic igneous rocks with model ages of 1.09–1.32 Ga (Fig. 14). Although lack of the isotope study on the Caledonian spodumene pegmatites (483–497 Ma, Kuznetsova and Shokalsky, 2011) from the Southern Sangilen pegmatite belt in the Tuva-Mongol block, they could be one potential source for the Permian-Triassic Li-rich pegmatites in the Chinese Altai due to the large source of the Habahe Group from the Tuva-Mongol block (Jiang et al., 2011; Liu et al., 2012; Long et al., 2010). Comparatively, the Devonian-Permian pegmatites with Be-Nb-Ta ± Li ± REE mineralization might be derived from a moderately depleted source dominated by the Caledonian igneous rocks with model ages of 0.86–1.09 Ga (Fig. 14). The source is represented by the amphibolites or gneisses in the Habahe Group, with consistent $\varepsilon_{Nd}(t)$ values of 3.7–7.0 at 700 Ma (Hu et al., 2000) and corresponding $\varepsilon_{Hf}(t)$ and model ages of 8.0–12.5 and 0.87–1.1 Ga, respectively, according to the reduction formula $\varepsilon_{Hf} = 1.36\varepsilon_{Nd} + 2.95$ (Vervoort et al., 1999). As proved by previous study, the Be-Nb-Ta-REE-rich pegmatites in the Evje-Iveland pegmatite field, Norway, were generated by anatexis of amphibolites (Müller et al., 2017). Compared with that in other pegmatites, the Permian REE-rich pegmatites have largely depleted Hf isotopic compositions which is similar to the the Caledonian juvenile crust materials with model ages of 0.63–0.86 Ma (Fig. 14). We deduce that they might be formed by partial melting of the juvenile crust components eroded from the Caledonian orogenic system, with or without mixing by mantle components. The juvenile components are presented by the basaltic to andesitic volcanic complex from the Lake Zone, Mongolia. These rocks were formed at 570–540 Ma, with $\varepsilon_{Nd}(t)$ values of 6.4–9.9 (with corresponding $\varepsilon_{Hf}(t)$ values of 11.6–16.4, according to Vervoort et al., 1999) and T_{DM} model age of 0.55–0.80 Ga, and are suggested to be derived from depleted mantle (Kovach et al., 2011).

In summary, the Permian pegmatites have similar Hf isotope compositions to the juvenile components in the Habahe Group, and the multi-types of mineralization of pegmatite can be explained by the heterogeneous components in the Habahe Group.

5.4. Permian metamorphism and implications for pegmatite origin

Currently, anatectic pegmatites are confirmed in the Variscan (e.g., Dill, 2015a, 2016; Melleton et al., 2012) and Grenville (e.g., Müller et al., 2016, 2017) orogens in Europe, the Laxfordian orogen in Scotland (e.g., Shaw et al., 2016), and the Alleghanian in the United States (e.g., Simmons and Falster, 2016). The pegmatites commonly are located in highly metamorphic terrenes such as upper amphibolite to granulite facies and show temporal and spatial connections to high-temperature metamorphism (e.g., Melleton et al., 2012; Müller et al., 2017). The Chinese Altai has undergone two periods of high temperature metamorphisms at 391–377 Ma (e.g., 720–650 °C, Jiang et al., 2010) and 299–271 Ma (e.g., 960–800 °C, Li et al., 2014; Tong et al., 2013; Wang et al., 2009c, 2014b). The Permian high temperature metamorphism is featured by granulite facies and shows a linear distribution in the Qiongkuer domain. Granulite facies metamorphism can cause crustal anatexis and further to formations of migmatites (e.g., Wei et al., 2007; Zhuang, 1994), luecogranite dykes (e.g., Wang, 2011) and pegmatites (e.g., Melleton et al., 2012; Müller et al., 2017; Shaw et al., 2014). The pegmatites studied in this work (274–253 Ma) were formed

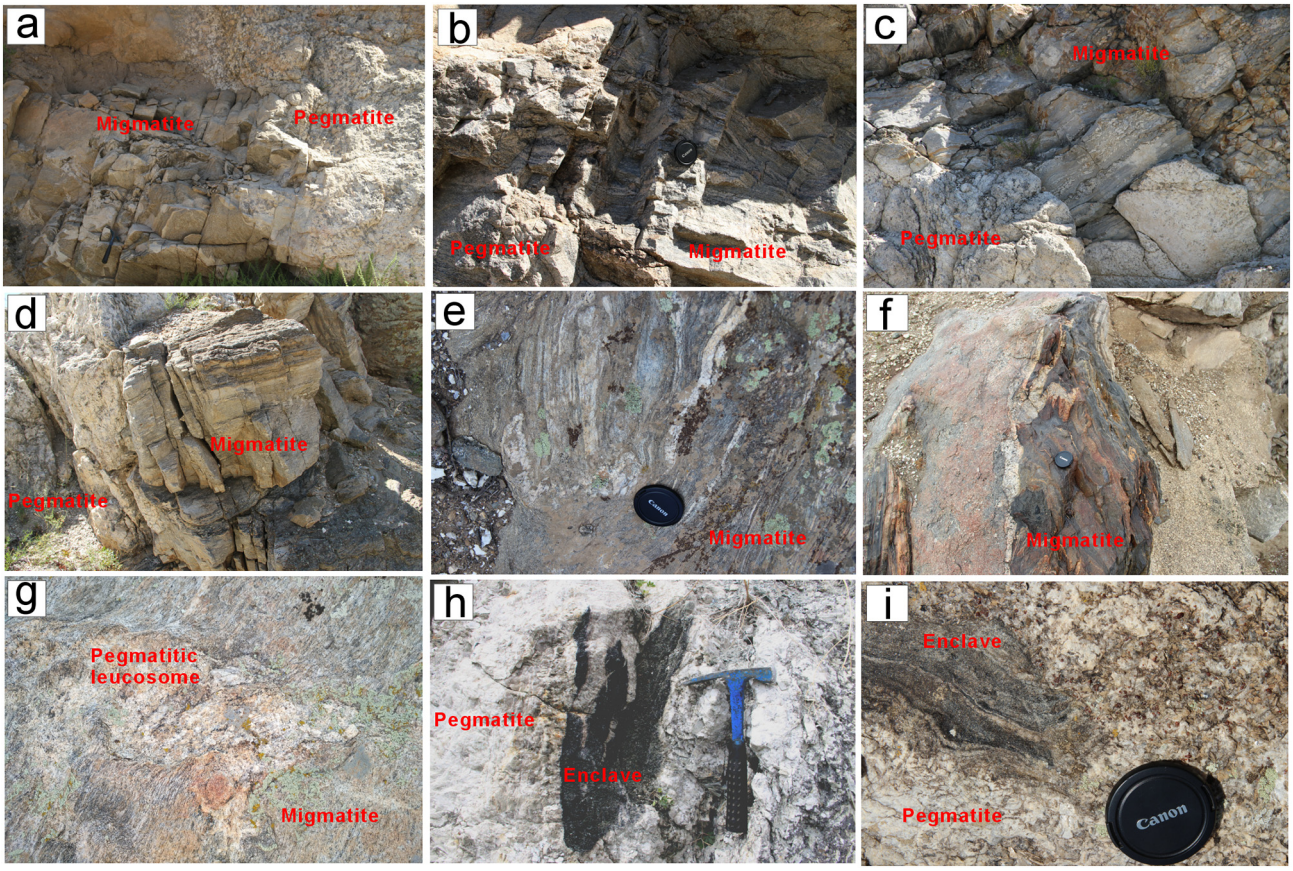

Fig. 15. Field pictures of migmatites in pegmatite mining areas (a-g) and enclaves in pegmatites (h and i). Physical contacts between pegmatites and migmatites in Jiamanhaba (a and b), Hailiutan (c) and Qiebielin (d) areas. Migmatites exposed in Qiemuerqieke (e) and Dakalasu (f) areas. Local pegmatitic leucosome in migmatite in Qiemuerqieke area (g). Enclaves hosted in HLT01 (h) and JMHB01 (i) pegmatites.

slightly late to ultra-high temperature metamorphism (299–271 Ma; Hu et al., 2006; Li et al., 2014; Tong et al., 2013; Wang et al., 2009c, 2014b), which corresponds to the retrograde metamorphism stage. In addition, physical contact between pegmatites and migmatites are observed in the Yeliuman (Fig. 15a and b), Hailiutan (Fig. 15c), and Qiebielin (Fig. 15d) mining areas. In the Qiemuerqieke and Dakalasu areas, migmatites are also observed and close to the QME01 and DKLS01 pegmatites (Fig. 15e and f), with local development of pegmatitic leucosome (Fig. 15g). In the HLT01 and JMHB01 pegmatites, metamorphic rock enclaves (Fig. 15h and i) are also observed, respectively.

Migmatite is one of the robust evidences for anatexis of the crust and widely observed in the Chinese Altai (Wang et al., 2009c; Wei et al., 2007; Zhuang, 1994). The melts formed during migmatization, can form intrusive dykes or bodies after concentration, segregation and extraction (e.g., Kriegsman, 2001). The intrusive dykes may undergo melt loss and fractional crystallization in different level during the mobilization process (e.g., White and Powell, 2002). In the Chinese Altai, abundant luecogranite dykes are proved to form by low degree partial melting of pelitic rocks during crust anatexis (Liu, 2016; Wang, 2011; Zhang et al., 2012). Some luecogranite dykes juxtapose with rare metal pegmatites in the Xiaokalasu and Dakalasu mining areas, show increasing numbers with metamorphism grades. The recent chronology studies revealed that the luecogranite dykes have three generations with zircon U-Pb ages of 255–280 Ma, 216–233 Ma and 197–204 Ma, respectively (Liu, 2016; Wang et al., 2011), which are consistent with the ages of the Permian, Triassic and Jurassic pegmatites (Ren et al., 2011; Lv et al., 2012; Zhang et al., 2016; this work). The luecogranite dykes are rich in Si (73.55–81.78%) and Al (ASI = 1.0–2.16), poor in Fe, Mg and Ca (mostly below 1%), and varying in K and Na. According to the trace element compositions (without analysis of Li and Be) of the dykes (Liu, 2016; Wang, 2011), three types of dykes are identified. The type 1 is rich in Cs, Rb, Ta, Zr, Hf and Sn, and depleted in Ba, Sr and REEs. Tetrad effect is hard to determine in the REE patterns due to the extremely low contents of REEs. The type 2 is rich in Th, U and REEs, but depleted in Ba, Nb and Sr, and shows development of tetrad effect in the REE pattern. The type 3 has lower contents of Cs, Rb, Ta, Zr and Hf, and higher contents of REEs than the type 1, with development of tetrad effect (Fig. B.1). Although the whole rock compositions of the rare metal/earth pegmatites are hardly to determinate due to internal zonation and large size of rock-forming minerals, they are comparable to the three types of luecogranite dykes in geochemistry based on their mineral associations (Table 2). Some luecogranite dykes in the Xiaokalasu area host pegmatitic feldspar and quartz minerals (Liu, 2016), indicating the lithoface transition from luecogranite to pegmatite. Similar case is also observed in the Alpine orogenic belt. The rare metal pegmatites in the Austroalpine unit, Eastern Alps, Central Europe, have been demonstrated to have a genetic relationship with the adjacent leucogranite dykes, according to the geology, petrography, geochemistry and geochronology studies. They both are suggested to form by crustal anatexis rather than crystal fractionation of parental granite melts during the Alpine orogeny (Knoll et al., 2018).

It is necessary to emphasize that the source protolith has dominating controls on the mineralization types of both anatectic and granite-related pegmatites (e.g., Müller et al., 2017; Shearer et al., 1992). The studied pegmatites in this work show distinct types of mineralization and Hf isotope compositions (Fig. 13), which is a strong support. In addition, varying degrees of partial melting during crustal anatexis may also affect the abundance of rare elements in melts due to the discrepant

decompositions of carrier minerals under different P-T conditions (Shearer et al., 1992). For example, Shearer et al. (1992) propose that high degrees of partial melting (> 40%) of the sedimentary protoliths in Black Hills, South Dakota, will contribute to formation of abundant granitic melts and granites, but low degrees (5–20%) partial melting facilitates to generation of LCT pegmatite-forming melts. Analogously, the NYF pegmatites in the Evje-Iveland pegmatite field, southern Norway, are suggested to form by 15–30% partial melting of gneisses and metagabbros (Snook, 2014). According to the phase equilibrium modeling, the Permian pelitic migmatites in the Chinese Altai can produce about 30% melt under the metamorphic peak condition with P = 6.0–6.3 kbar and T = 815–825 °C (granulite-facies). During the prograde metamorphism, about 4%, 14.1% and 29.41% melt are expected to generate by the water-saturated solidus melting, muscovite dehydration melting and biotite dehydration melting, respectively (Wang, 2011). As the product of partial melting, the luecogranite dykes exposed in Xiaokalasu and Dakalasu mining areas are comparable with the Permian pegmatites in geology, formation time, major (rich in Si, metaluminous to peraluminous) and trace (rare metal/earth elements) compositions (Table 2; Fig. B.1), indicating a genetic relationship. With consideration of (1) the max percentage of melt produced by dehydration melting of muscovite and biotite (e.g., 10% and 30%, respectively, White et al., 2001); (2) the critical degree of partial melting required for melt connectivity (e.g., about 4%, Lupulescu and Watson, 1999); and (3) the dominating carrier minerals of rare elements in metasedimentary rocks, such as muscovite for Li, Be, Rb and Cs, biotite for Be, Nb, Ta and LREE, Ti-rich minerals (e.g., ilmenite) for Nb and Ta, and monazite, xenotime, apatite, garnet, zircon, pyroxene and amphibole for REEs (e.g., London, 2008; Müller et al., 2017), it is reasonable to deduce that dehydration melting of muscovite and biotite could be main mechanisms responsible for generation of rare metal/earth pegmatites. Therefore, we suppose that the Permian pegmatites with Li-Be-Ta-Nb mineralization (SEJK01, QME02 and BC01) could be formed by dehydration melting of muscovite with melting degrees of ca. 5–10%. Comparatively, the pegmatites with mineralizations of Be-Nb-Ta-REE (JMHB06, AKB01, TEL01 and DKLS01) and REE (HLT01, YLM15 and QME01) show increasing Fe, Ti and REE, and more depleted Hf isotope compositions (Table 2; Fig.13), indicating more mafic components involved in their source protoliths. In addition, some elliptic biotites surrounded by magnetite, quartz and microcline were observed in the TEL01 and DKLS01 pegmatites, indicating biotite has been involved in partial melting. Furthermore, the REE-rich pegmatite has a larger quantity than the Li-rich pegmatite in the Chinese Altai, which requires enhancing degrees of partial melting. They are thus supposed to produce by dehydration melting of biotite with melting degrees of ca.10–30%.

Except the Permian high temperature metamorphism, the connection of pegmatite with migmatite and luecogranite dyke in the Chinese Altai (see Section 5.4), there are some other evidences to support the anatexis origin of the Permian pegmatites. Firstly, our previous study on fluid inclusions demonstrated that the BC01, SEJK01, YLM15 and the Xiaokalasu Li-rich pegmatite were emplaced at depths of 11.4–14.5 km (Huang et al., 2016). These depths are significantly deeper than the typical depths of 4–8 km for rare metal pegmatites (Ginsburg, 1984), indicating deep sources from the middle or lower crust. Secondly, recent Li isotope study suggests that the pegmatites in the Qinghe field originated from low degrees of partial melting of host rock of schists involving muscovite dehydration melting (Chen et al., 2020). Thirdly and most importantly, the studied rare metal/earth pegmatites are distinct from the granite-related pegmatites on mineralogy and mineralization. The pegmatites formed by crystal fractionation of graniric melts are lack of restite minerals due to the efficient extraction of melts from the mostly crystalline magmas (e.g., London, 2005). However, the studied pegmatites contain a certain amount of exotic minerals, such as biotite restites in the TEL01 and DKLS01 pegmatites, inherited zircons in the AKB01 and BC01 pegmatites (Fig. 3e and j). Moreover, metamorphic rock enclaves are also observed in the JMHB06 and HLT01 pegmatites (Fig. 15h and i). In addition, compare with the granite-related pegmatites, the anatectic pegmatite are almost lack of W ± Sn mineralization (Dill, 2015a, 2015b). For example, the Shangkelan pegmatite is the only confirmed granite-related pegmatite in the Chinese Altai so far. It was formed at early Jurassic and shows temporal-spatial and differentiation connections with neighboring muscovite-albite granite, and Be-Nb-W mineralization (Zou and Li, 2006). Analogously, W ± Sn mineralization is also widely observed in the highly fractionated granites and their derivatives, such as the Mesozoic Jiajika rare metal pegmatites in Songpan-Ganzi orogenic belt (e.g., Hao et al., 2015), and the Neoproterozoic Fanjingshan and Yuanbaoshan Nb-Ta-Sn-W leucogranites (e.g., Xiang et al., 2020) and Mesozoic Limu Ta-Nb-Sn-W pegmatites (e.g., Huang et al., 2020) in South China. Comparatively, W ± Sn mineralization is almost missing in the isolated rare metal/earth pegmatites in the Chinese Altai, and only observed as W- or Sn-rich trace minerals in few pegmatites (e.g., Sn-rich minerals in the QME02 pegmatite). All of these evidences support the anatexis origin of the studied pegmatites, although more works need to be re-evaluated in future works.

In summary, we suggest that the Permian pegmatites could be generated by anatexis (low-percentage partial melting) of the newly accreted sediments in the Habahe Group, and the mineralization type of the pegmatite evidently depends on the sources from the Habahe Group and partial melting degrees of source.

5.5. Tectonic setting and petrogenesis of the Permian pegmatites

Several tectonic models for the Permian Chinese Altai have been proposed by previous works, such as post-orogenic extension (e.g., Tong et al., 2006; Wang et al., 2009b, 2014a) and mantle plume (e.g., Tong et al., 2014; Zhang et al., 2012). However, these models are insufficient for explaining the magmatic-metamorphic-tectonic events in the Permian Chinese Altai (e.g., Cai et al., 2016; Wan et al., 2013; Xiao et al., 2008, 2009, 2015, 2018). For example, all the known Permian magmatic-metamorphic events are restricted in the Qiongkuer domain and South Altai with a zonal arrangement (Fig. 9), indicating a local tectonic thermodynamics motion, such as arc-arc collision. As a part of the accretionary orogenic belt of CAOB, the Chinese Altai has undergone prolonged accretion processes and multiple extension events which including the Permian post-accretion extension (e.g., Cai et al., 2016; Xiao et al., 2015, 2018). On the basis of Permian magmatic-metamorphic-tectonic studies (Fig. 16), a Permian tectonic scenario for the Chinese Altai and a petrogenesis model of the pegmatites are proposed below:

With the continuous subduction of the Ob-Zaisan ocean plate, the East Junggar arc converged with the eastern Chinese Altai during the early Permian (Broussolle et al., 2018; Cai et al., 2016). The arc-arc collision resulted in upright folding and perturbation of the mantle lithosphere's thermal structure (Broussolle et al., 2018) as well as high-temperature metamorphisms (e.g., Hu et al., 2006; Wang et al., 2009c, 2014b). Afterward, the clockwise rotation of the Mongolia collage (Xiao et al., 2018) induced sinistral strike-slip along the Irtish tectonic belt (Li et al., 2014) and the break-off of the subduction slab (Li et al., 2012a) owing to intense extrusion stress. The upwelling of the asthenosphere via a slab window induced the extension of the southern Chinese Altai and significant injections of heat energy and mantle-derived materials. This give rise to the generations of ultramafic and/or mafic rocks in the Kalatongke and Qiemuerqieke areas (Cai et al., 2016; Li et al., 2012a; Wan et al., 2013), high-temperature metamorphism (e.g., Li et al., 2014; Tong et al., 2013) and abundant I- and A-type

granites in the southeastern Chinese Altai (e.g., Liu et al., 2018; Tong et al., 2014). In the Qinghe area, local anatexis of the Habahe Group metasedimentary rocks induced by decompression resulted in the formation of the BC01 rare metal pegmatite (Fig. 17a). Comparatively, the oblique arc-arc collision between the West Junggar arc and the western Chinese Altai lagged behind and might have occurred during the middle Permian, followed by regional uplift (270–265 Ma) of the southern Chinese Altai (Li et al., 2015). Afterward, the lasting clockwise rotation of the Mongolia collage and the roll-back of the subduction slab (Xiao et al., 2018) resulted in the extension of the southwestern Chinese Altai. This in turn gave rise to anatexis of various components from the Habahe Group and formation of pegmatite-forming melts (Fig. 17b). These melts might have been partly mixed during mobilization process along faults and lithological boundaries and have intruded into the fissures of upper sedimentary rocks and the joints of Paleozoic granites to ultimately form the late Permian pegmatites in the Qiongkuer domain, Chinese Altai.

With respect to the differences on the two types of pegmatites formed under slab breakoff and slab rollback setting, respectively, no study has performed to reveal that so far. Therefore, we try to make it clear in this work. According to the Fig. 9 and 16, the early Permian pegmatites were rarely formed in the southeast Altai, whereas high temperature metamorphism, and abundant I- and A-type granites and mafic rocks were synchronously generated during slab breakoff. It indicates that the significant input of materials and heat from mantle via slab window (e.g., Li et al., 2012a), and high degrees of partial melting dominated the reworking of middle-lower crust. If pegmatites were formed by crystal fractionation of the granitic melts, they should have a NYF affinity. However, the BC01 pegmatite shows a LCT affinity. In contrast, the late Permian pegmatites were largely formed during the retrograde stage of high temperature metamorphism and extension induced by slab rollback in the northwest Altai, whereas the synchronous granites and mafic rocks were almost absent (Fig. 9), indicating limited input of mantle materials in late Permian. All these suggest that the significant input of mantle materials in crust adverses to the formation of pegmatites. It is maybe the reason for LCT pegmatites overwhelm NYF pegmatites in quantity on Earth. About the differences on geochemistry and source of the two types of pegmatites, it is hard to distinguish from the mineral associations (Table 2) and Hf isotope compositions (Fig. 13) of the BC01, QME02 and SEJK01 pegmatites. But the late Permian pegmatites were much more formed and studied than the early pegmatites, more sources derived pegmatites (e.g., JMHB06, AKB01, TEL01, DKLS01, HLT01, YLM15 and QME01) are definitely distinct to the BC01 pegmatite on mineralogy and geochemistry.

6. Conclusion

(1) The studied pegmatites have zircon U-Pb ages of 274–253 Ma, with the dominant age being late Permian, which demonstrates the occurrence of the Permian pegmatites in the Chinese Altai.
(2) The Permian pegmatites have three mineralization types including Li-Be-Ta-Nb ± Sn, Be-Nb-Ta ± REEs and REEs. The first and second types are comparable with the Triassic and Devonian-Carboniferous pegmatites in mineralization and Hf isotope composition, respectively, and the latter is unique in the Permian generation, indicating the dependency of mineralization on source.
(3) A comparative study between the Permian pegmatites and granites show decoupling spatial-temporal and differentiation-source correlations, which disproves their genetic relationship.

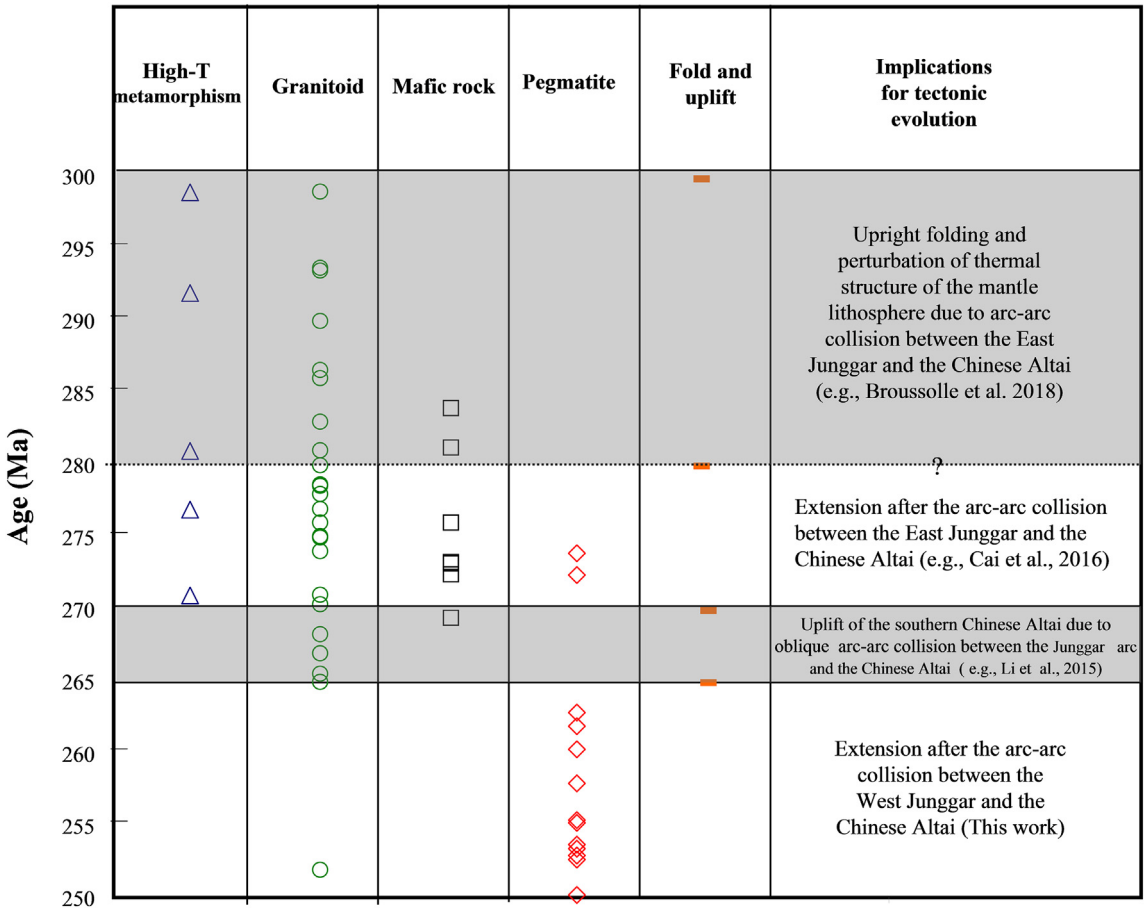

Fig. 16. Age statistics on the Permian magmatic-metamorphic-tectonic events in the Chinese Altai. Age date refers to Table 3.

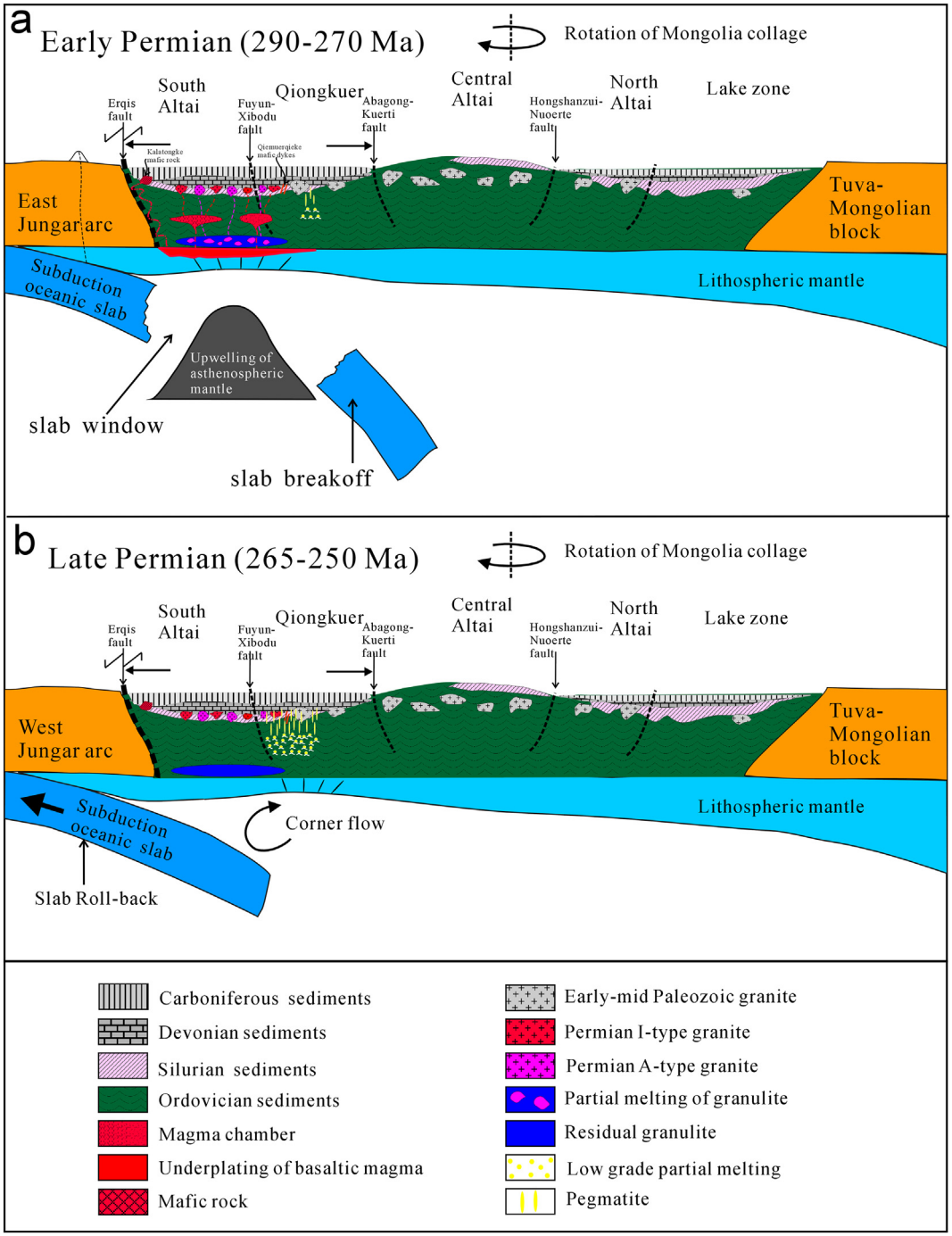

Fig. 17. The petrogenetic model for the Permian pegmatites in the Chinese Altai at Early Permian (290–270 Ma) (a) and Late Permian (265–250 Ma) (b). Modified from Jiang et al. (2016), Li et al. (2012b), and Lv et al. (2018a).

(4) The comparable Hf isotope compositions of the pegmatites with the juvenile components in the Habahe Group indicate a source connection between them. Combing with the connection of the pegmatites with migmatites and luecogranite dykes in the Chinese Altai and previous magmatic-metamorphic-tetonic works, we suggest that the Permian pegmatites were likely generated by anatexis of the Habahe Group metasedimentary rocks under a post-accretion extensional setting following the arc-arc collision between the Junnger arcs and the Chinese Altai.pt

Supplementary data to this article can be found online at https://doi.org/10.1016/j.lithos.2020.105865.

Declaration of Competing Interest

The authors declare that they have no known competing financial interests or personal relationships that could have appeared to influence the work reported in this paper.

Acknowledgments

This study is jointly supported by the National Science Foundation of China under Grants 91962222, 41873030, 41403016 and 41372104 and the Strategic Priority Research Program (B) of the Chinese Academy of Sciences (XDB18000000). Profs. Xiaoming Liu and Honglin Yuan are appreciated for their assistance with the LA-ICP-MS analyses. Guest Editor Yigang Xu and three anonymous reviewers are appreciated for their constructive comments to help us improve the manuscript. Prof. Wei Wang is acknowledged for the discussion on the metamorphism in the Chinese Altai.

References

Andersen, T., 2002. Correction of common Pb in U-Pb analyses that do not report ^{204}Pb. Chem. Geol. 192, 59–79.

Ballouard, C., Poujol, M., Boulvais, P., Branquet, Y., Tartese, R., Vigneresse, J.L., 2016. Nb-Ta fractionation in peraluminous granites: a marker of the magmatic-hydrothermal transition. Geology 44 (3), 231–234.

Barnes, E.M., 2010. The rare element Little Nahanni Pegmatite Group, NWT: Studies of Emplacement, and Magmatic Evolution From Geochemical and Li Isotopic Evidence. University of British Columbia, Vancouver, British Columbia, pp. 1–247 Ph.D. dissertation.

BGMRX (Bureau of Geology and Mineral Resources of Xinjiang Uygur Autonomous Region), 1993. Regional Geology of Xinjiang Uygur Autonomous Region. People's Republic of China, Ministry of Geology and Mineral Resources. Geological Memoirs, Series. vol. 1(32). Geological Publishing House, Beijing, pp. 6–206 (in Chinese).

Breaks, F.W., Moore, J.M., 1992. The Ghost Lake Batholith, Superior Province of northwestern Ontario; a fertile, S-type, peraluminous granite-rare-element pegmatite system. Can. Mineral. 30 (3), 835–875.

Briggs, S.M., Yin, A., Manning, C.E., Chen, Z.L., Wang, X.F., Grove, M., 2007. Late Paleozoic tectonic history of the Ertix Fault in the Chinese Altai and its implications for the development of the Central Asian Orogenic System. Geol. Soc. Am. Bull. 119, 944–960.

Broussolle, A., Aguilar, C., Sun, M., Schulmann, K., Štípská, P., Jiang, Y., Yu, Y., Xiao, W.J., Wang, S., Míková, J., 2018. Polycyclic Palaeozoic evolution of accretionary orogenic wedge in the southern Chinese Altai: evidence from structural relationships and U-Pb geochronology. Lithos 314, 400–424.

Cai, K., Sun, M., Yuan, C., Xiao, W., Zhao, G., Long, X., Wu, F., 2010. Geochronological and geochemical study of mafic dykes from the northwest Chinese Altai: implications for petrogenesis and tectonic evolution. Gondw. Res. 18, 638–652.

Cai, K.D., Sun, M., Yuan, C., Zhao, G.C., Xiao, W.J., Long, X.P., Wu, F.Y., 2011a. Geochronology, petrogenesis and tectonic significance of peraluminous granites from the Chinese Altai, NW China. Lithos 127, 261–281.

Cai, K.D., Sun, M., Yuan, C., Zhao, G.C., Xiao, W.J., Long, X.P., Wu, F.Y., 2011b. Prolonged magmatism, juvenile nature and tectonic evolution of the Chinese Altai, NW China: evidence from zircon U-Pb and Hf isotopic study of Paleozoic granitoids. J. Asian Earth Sci. 42, 949–968.

Cai, K.D., Sun, M., Yuan, C., Zhao, G.C., Xiao, W.J., Long, X.P., 2012a. Keketuohai mafic ultramafic complex in the Chinese Altai, NW China: petrogenesis and geodynamic significance. Chem. Geol. 294, 26–41.

Cai, K., Sun, M., Yuan, C., Xiao, W., Zhao, G., Long, X., Wu, F., 2012b. Carboniferous mantle-derived felsic intrusion in the Chinese Altai, NW China: implications for geodynamic change of the accretionary orogenic belt. Gondw. Res. 22, 681–698.

Cai, K., Sun, M., Jahn, B.M., Xiao, W., Long, X., Chen, H., Xia, X., Chen, M., Wang, X., 2016. Petrogenesis of the Permian intermediate-mafic dikes in the Chinese Altai, Northwest China: implication for a postaccretion extensional scenario. J. Geol. 124, 481–500.

Černý, P., 1991a. Rare-element granite pegmatites. Part I: anatomy and internal evolution of pegmatite deposits. Geosci. Canada 18, 49–67.

Černý, P., 1991b. Rare-element granitic pegmatites. Part II: regional to global environments and petrogenesis. Geosci. Canada 18, 68–81.

Černý, P., Ercit, T.S., 2005. The classification of granitic pegmatites revisited. Can. Mineral. 43, 2005–2026.

Černý, P., London, D., Novák, M., 2012a. Granitic pegmatites as reflections of their sources. Elements 8, 289–294.

Černý, P., Halden, N.M., Ferreira, K., Meintzer, R.E., Brisbin, W.C., Chackowsky, L.E., Corkery, M.T., Longstaffe, F.J., Trueman, D.L., 2012b. Extreme fractionation and deformation of the leucogranite-pegmatite suite at Red Cross lake, Manitoba, Canada. II. Petrology of the leucogranites and pegmatites. Can. Mineral. 50, 1807–1822.

Chamberlain, K.R., Bowring, S.A., 2000. Apatite-feldspar U-Pb thermochronometer: a reliable, mid-range ~450°C diffusion-controlled system. Chem. Geol. 172, 173–200.

Chen, J.F., 2011. Geochemistry of the plate part in Altai No. 3 Pegmatite and Its Formation and Evolution. A Dissertation Submitted to Graduate University of Chinese Academy of Sciences for the Degree of Master of Philosophy. pp. 1–86 (in Chinese with English abstract).

Chen, F.W., Li, H.Q., Wang, D.H., Cai, H., Chen, W., 1999. New chronological evidence for Yanshanian diagenetic mineralization in China's Altay orogenic belt. Chin. Sci. Bull. 44, 1142–1148.

Chen, Y.X., Gao, F., Pei, X.Z., Tian, H.B., Li, Z.C., Li, R.B., Wang, M., He, J.L., 2017. Chronology, geochemistry and tectonic implication of the Huiteng granitic pluton in the Altay area, Xinjiang. Acta Petrol. Sin. 33 (10), 3076–3090 (in Chinese with English abstract).

Chen, B., Huang, C., Zhao, H., 2020. Lithium and Nd isotopic constraints on the origin of Li-poor pegmatite with implications for Li mineralization. Chem. Geol. 551, 119769.

Cherniak, D.J., Watson, E.B., 2000. Pb diffusion in zircon. Chem. Geol. 172, 5–24.

Copeland, P., Parrish, R.R., Harrison, T.M., 1988. Identification of inherited radiogenic Pb in monazite and its implications for U-Pb systematics. Nature 333 (6175), 760–763.

Corfu, F., Hanchar, J.M., Hoskin, P.W.O., Kinny, P., 2003. Atlas of Zircon Textures. Rev. Mineral. Geochem. 53, 469–500.

Dill, H., 2015a. The Hagendorf-Pleystein Province: the center of pegmatites in an ensialic orogen. Springer 15, 1–465.

Dill, H.G., 2015b. Pegmatites and aplites: Their genetic and applied ore geology. Ore Geol. Rev. 69, 417–561.

Dill, H.G., 2016. The CMS classification scheme (Chemical composition-Mineral assemblage-Structural geology)-linking geology to mineralogy of pegmatitic and aplitic rocks. Neues Jahrbuch für Mineralogie-Abhandlungen 193, 231–263.

Diwu, C., Sun, Y., Guo, A., Wang, H., Liu, X., 2011. Crustal growth in the North China Craton at ~2.5 Ga: evidence from in situ zircon U-Pb ages, Hf isotopes and wholerock geochemistry of the Dengfeng complex. Gondw. Res. 20, 149–170.

Elhlou, S., Belousove, E., Griffin, W.L., Pearson, N.J., O'Reilly, S.Y., 2006. Trace element and isotopic composition of GJ-red zircon standard by laser ablation. Geochim. Cosmochim. Acta 70 (18).

Fu, X.F., Yuan, L.P., Wang, D.H., Hou, L.W., Pan, M., Hao, X.F., Liang, B., Tang, Y., 2015. Mineralization characteristics and prospecting model of newly discovered X03 rare metal vein in Jiajika orefield, Sichuan. Mineral Depos. 34 (6), 1172–1186 (in Chinese with English abstract).

Gao, F.P., Zhou, G., Lei, Y.X., Wang, D.S., Chen, J.X., Zhang, H.F., Wu, X.B., Liu, G.R., Zhao, Z.H., 2010. Early Permian granite age and geochemical characteristics in Shaerbulake of Xinjiang's Altay area and its geological significance. Geol. Bull. China 29 (9), 1281–1293 (in Chinese with English abstract).

Ginsburg, A.I., 1984. The geological condition of the location and the formation of granitic pegmatites. Proceedings of the 27th International Geological Congress, Non-Metallic Mineral Ores. 15, pp. 245–260.

Griffin, W.L., Pearson, N.J., Belousova, E.A., Saeed, A., 2006. Comment: Hf-isotope heterogeneity in zircon 91500. Chem. Geol. 233, 358–363.

Han, B.F., Ji, J.Q., Song, B., Chen, L.H., Li, Z.H., 2004. SHRIMP zircon U-Pb ages of Karatongke No.1 and Huangshandong Cu-Nibearing mafic-ultramafic complexes, North Xinjiang, and geological implications. Chin. Sci. Bull. 49, 2424–2429 (in Chinese with English abstract).

Hao, X.F., Fu, X.F., Liang, B., Yuan, L.P., Pan, M., Tang, Y., 2015. Formation ages of granite and X03 pegmatite vein in Jiajika, western Sichuan, and their geological significance. Mineral Depos. 34 (6), 1199–1208 (in Chinese with English abstract).

Harrison, T.M., Celerier, J., Aikman, A.B., Herman, J., Heiziler, M.T., 2009. Diffusion of ^{40}Ar in muscovite. Geochim. Cosmochim. Acta 73, 1039–1051.

He, D., Dong, Y., Xu, X., Chen, J., Liu, X., Li, W., Li, X., 2018. Geochemistry, geochronology and Hf isotope of granitoids in the Chinese Altai: implications for Paleozoic tectonic evolution of the Central Asian Orogenic Belt. Geosci. Front. 9 (5), 1399–1415.

Hoskin, P.W.O., 2005. Trace element composition of hydrothermal zircon and the alteration of Hadean zircon from the Jack Hills, Australia. Geochim. Cosmochim. Acta 69, 637–648.

Hu, A.Q., Jahn, B.M., Zhang, G.X., Chen, Y.B., Zhang, Q.F., 2000. Crustal evolution and Phanerozoic crustal growth in northern Xinjiang: Nd isotopic evidence. Part I. Isotopic characterization of basement rocks. Tectonophysics 328, 15–51.

Hu, A.Q., Wei, G.J., Deng, W.F., Chen, L.L., 2006. SHRIMP zircon U-Pb dating and its significance for gneisses from the southeast area to Qinghe Country in the Altai, China. Acta Petrol. Sin. 22, 1–10 (in Chinese with English abstract).

Huang, Y.S., Zhang, H., Lv, Z.H., Tang, Y., Tang, H., 2016. Research on emplacement depths of Permian and Triassic pegmatites in Altay, Xinjiang, China: indications from fluid inclusions. Acta. Mineral. Sin. 36 (4), 571–585.

Huang, W.T., Wu, J., Liang, H.Y., Zhang, J., Ren, L., Chen, X.L., 2020. Ages and genesis of W-Sn and Ta-Nb-Sn-W mineralization associated with the Limu granite complex, Guangxi, China. Lithos 352-353, 105321.

Irber, W., 1999. The lanthanide tetrad effect and its correlation with K/Rb, Eu/Eu*, Sr/Eu, Y/Ho, and Zr/Hf of evolving peraluminous granite suites. Geochim. Cosmochim. Acta 63, 489–508.

Jiang, L.P., 2012. The study on fluid inclusion of Liangkeshu pegmatite iron deposit in Altay. Urumchi: A Dissertation Submitted to Xinjiang University for the Degree of Master of. Philosophy, pp. 1–50 (in Chinese with English abstract).

Jiang, Y., Sun, M., Zhao, G., Yuan, C., Xiao, W., Xia, X., Long, X., Wu, F., 2010. The ~390 Ma high-T metamorphic event in the Chinese Altai: a consequence of ridge-subduction? Am. J. Sci. 310, 1421–1452.

Jiang, Y., Sun, M., Zhao, G., Yuan, C., Xiao, W., Xia, X., Long, X., Wu, F., 2011. Precambrian detrital zircons in the Early Paleozoic Chinese Altai: their provenance and implications for the crustal growth of central Asia. Precambrian Res. 189, 140–154.

Jiang, Y., Štípská, P., Sun, M., Schulmann, K., Zhang, J., Wu, Q., Long, X., Yuan, C., Racek, M., Zhao, G., Xiao, W., 2015. Juxtaposition of Barrovian and migmatite domains in the Chinese Altai: a result of crustal thickening followed by doming of partially molten lower crust. J. Metam. Geol. 33, 45–70.

Jiang, Y., Schulmann, K., Sun, M., Štípská, P., Guy, A., Janoušek, V., Lexa, O., Yuan, C., 2016. Anatexis of accretionary wedge, Pacific-type magmatism, and formation of vertically stratified continental crust in the Altai Orogenic Belt. Tectonics 35 (12), 3095–3118.

Kinny, P.D., Maas, R., 2003. Lu-Hf and Sm-Nd isotope systems in zircon. Rev. Mineral. Geochem. 53 (1), 327–341.

Knoll, T., Schuster, R., Huet, B., Mali, H., Onuk, P., Horschinegg, M., Ertl, A., Giester, G., 2018. Spodumene pegmatites and related leucogranites from the Austroalpine Unit (Eastern Alps, Central Europe): Field relations, petrography, geochemistry, and geochronology. Can. Mineral. 56 (4), 489–528.

Kontak, D.J., Creaser, R.A., Heaman, L.M., Archibald, D.A., 2005. U-Pb tantalite, Re-Os molybdenite, and $^{40}Ar/^{39}Ar$ muscovite dating of the Brazil Lake pegmatite, Nova Scotia: a possible shear-zone related origin for an LCT-type pegmatite. Atlantic Geol. 41, 17–29.

Kovach, V.P., Yarmolyuk, V.V., Kovalenko, V.I., Kozlovskyi, A.M., Kotov, A.B., Terent'Eva, L.B., 2011. Composition, sources, and mechanisms of formation of the continental crust of the Lake Zone of the Central Asian Caledonides. II. Geochemical and Nd isotope data. Petrology 19 (4), 399–425.

Kriegsman, L.M., 2001. Partial melting, partial melt and partial back reaction in anatectic migmatites. Lithos 56 (1), 75–96.

Krogstad, E.J., Walker, R.J., 1994. High closure temperatures of the U-Pb system in large apatites from the Tin Mountain pegmatite, Black Hills, South Dakota, USA. Geochim. Cosmochim. Acta 58, 3845–3853.

Kuznetsova, L.G., Shokalsky, S.P., 2011. Lithium deposits in the rare-metal pegmatites of Tuva. In: Lyakhov, N.Z., Vladimirov, A.G., Isupov, V.P. (Eds.), Proc. All-Russ. Conf. "Lithium of Russia: Mineral Resources, Innovative Technology, and Environmental Safety" with Int. Participation, Novosibirsk, pp. 65–70 (in Russian).

Li, Q.L., 2016. "High-U effect" during SIMS zircon U-Pb dating. Bull. Mineral. Petrol. Geochem. 35 (3), 405–412 (in Chinese with English abstract).

Li, C., Zhang, M., Fu, P., Qian, Z., Hu, P., Ripley, E., 2012a. The Kalatongke magmatic NiCu deposits in the Central Asian Orogenic Belt, NW China: product of slab window magmatism? Miner. Deposita 47, 51–67.

Li, X.R., Liu, F., Yang, F.Q., 2012b. Geologyical times and tis signification of the two mica syenogranite in the Keyinblak Cu-Zn deposit area in Altay, Xinjiang. Xinjiang Geol. 30 (1), 5–11 (in Chinese with English abstract).

Li, Z., Yang, X., Li, Y., Santosh, M., Chen, H., Xiao, W., 2014. Late Paleozoic tectonometamorphic evolution of the Altai segment of the Central Asian Orogenic Belt: constraints from metamorphic P-T pseudosection and zircon U-Pb dating of ultrahigh-temperature granulite. Lithos 204, 83–96.

Li, P., Yuan, C., Sun, M., Long, X., Cai, K., 2015. Thermochronological constraints on the late Paleozoic tectonic evolution of the southern Chinese Altai. J. Asian Earth Sci. 113, 51–60.

Liu, H., 2013. Geochemical Study on Petrogenesis of Aral Granite and the Keketuohai No. 3 Pegmatite Vein, Altay, Xinjiang. A Dissertation Submitted to the Kunming University of Science and Technology for the Degree of Master of Philosophy. pp. 1–60 (in Chinese with English abstract).

Liu, W.Z., 2015. The Geochemical Evolution of the Asikaerte Granite-Pegmatite System and Its Implication for the Metallogenesis of Be and Mo, XinJiang, China. A Dissertation Submitted to Institute of Geochemistry for the Degree of Master of Philosophy, Guiyang. pp. 1–71 (in Chinese with English abstract).

Liu, J.N., 2016. Study of Leucogranite Dykes in the Altai Metamorphic Zones. A Dissertation Submitted to China University of Geosciences for Master Degree. pp. 1–86 (in Chinese with English abstract).

Liu, Y.L., 2017. Petrogenesis and Continental Dynamics of Permian Pegmatites and Post-collision Granites in the Chinese Altay Orogenic Belt. A Dissertation Submitted to Institute of Geochemistry for the Degree of Doctor of Philosophy, Guiyang. pp. 1–110 (in Chinese with English abstract).

Liu, C.Q., Zhang, H., 2005. The lanthanide tetrad effect in apatite from the Altay No. 3 pegmatite, Xingjiang, China: an intrinsic feature of the pegmatite magma. Chem. Geol. 214, 61–77.

Liu, Y.S., Gao, S., Hu, Z.C., Gao, C.G., Zong, K.Q., Wang, D.B., 2009. Continental and oceanic crust recycling-induced melt-peridotite interactions in the Trans-North China Orogen: U-Pb dating, Hf isotopes and trace elements in zircons from mantle xenoliths. J. Petrol. 51, 537–571.

Liu, W., Liu, X.J., Xiao, W.J., 2012. Massive granitoid production without massive continental-crust growth in the Chinese Altay: insight into the source rock of granitoids using integrated zircon U-Pb age, Hf-Nd-Sr isotopes and geochemistry. Am. J. Sci. 312 (6), 629–684.

Liu, Y.L., Zhang, H., Tang, Y., Zhang, X., Lv, Z.H., Zhao, J.Y., 2018. Petrogenesis and tectonic setting of the Middle Permian A-type granites in Altay, Northwestern China: evidences from geochronological, geochemical, and Hf isotopic studies. Geological Journal 53 (2), 527–546.

London, D., 2005. Granitic pegmatites: an assessment of current concepts and directions for the future. Lithos 80, 281–303.

London, D., 2008. Pegmatites. 10. The Canadian Mineralogist Special Publication, pp. 1–347.

London, D., 2018. Ore-forming processes within granitic pegmatites. Ore Geol. Rev. 101, 349–383.

Long, X.P., Sun, M., Yuan, C., Xiao, W.J., Lin, S.F., Wu, F.Y., Xia, X.P., Cai, K.D., 2007. Detrital zircon age and Hf isotopic studies for metasedimentary rocks from the Chinese Altai: implications for the Early Paleozoic tectonic evolution of the Central Asian Orogenic Belt. Tectonics 26, TC5015. https://doi.org/10.1029/2007TC002128.

Long, X.P., Sun, M., Yuan, C., Xiao, W.J., Cai, K.D., 2008. Early Paleozoic sedimentary record of the Chinese Altai: implications for its tectonic evolution. Sediment. Geol. 208, 88–100.

Long, X.P., Yuan, C., Sun, M., Xiao, W.J., Zhao, G.C., Wang, Y.J., Cai, K.D., 2010. Detrital zircon ages and Hf isotopes of the early Paleozoic Flysch sequence in the Chinese Altai, NW China: new constraints on depositional age, provenance and tectonic evolution. Tectonophysics 480, 213–231.

Long, X., Yuan, C., Sun, M., Safonova, I., Xiao, W., Wang, Y., 2012. Geochemistry and UPb detrital zircon dating of Paleozoic graywackes in East Junggar, NW China: insights into subduction–accretion processes in the southern Central Asian Orogenic Belt. Gondw. Res. 21, 637–653.

Lu, H.Z., Wang, Z.G., Li, Y.S., 1996. Magma/fluid transition and genesis of pegmatite dike No. 3 at Altay, Xinjiang. Acta. Mineral. Sin. 16, 1–7 (in Chinese).

Luan, S.W., Mao, Y.Y., Fan, L.M., Wu, X.B., Lin, J.H., 1995. Rare metal Mineralization and Exploration in the Keketuohai Area. Chengdu University of Science and Technology Press, Chengdu, pp. 1–278 (in Chinese with English abstract).

Ludwig, K.R., 2003. User's manual for Isoplot/Ex, Version 3. 00. A Geochronological Toolkit for Microsoft Excel. Berkeley Geochronol. Center Spec. Publ. 4, 1–70.

Lupulescu, A., Watson, E.B., 1999. Low melt fraction connectivity of granitic and tonalitic melts in a mafic crustal rock at 800 °C and 1 GPa, Contrib. Mineral. Petrol. 134, 202–216.

Lv, Z.H., Zhang, H., Tang, Y., Guan, S.J., 2012. Petrogenesis and magmatic-hydrothermal evolution time limitation of Kelumute No. 112 pegmatite in Altay, Northwestern China: evidence from zircon U-Pb and Hf isotopes. Lithos 154, 374–391.

Lv, Z.H., Zhang, H., Tang, Y., 2015. The study of genetic relationship between Bieyesamasi No. L1 pegmatite Li-Nb-Ta ore deposit and wall rock granite, Xinjiang. Acta Mineral. Sin. S1, 323 (in Chinese).

Lv, Z.H., Zhang, H., Zhao, J.Y., 2017. Magmatic-hydrothermal evolution and Li mineralization in pegmatite: constraints from composition of garnet from Kelumute No. 112 Pegmatite, Xinjiang Autonomous Region, China. Acta Minerl. Sin. 37, 247–257 (in Chinese with English abstract).

Lv, Z.H., Zhang, H., Tang, Y., Liu, Y.L., Zhang, X., 2018a. Petrogenesis of syn-orogenic rare metal pegmatites in the Chinese Altai: evidences from geology, mineralogy, zircon U-Pb age and Hf isotope. Ore Geol. Rev. 95, 161–181.

Lv, Z.H., Zhang, H., Tang, Y., 2018b. Lanthanide tetrads with implications for liquid immiscibility in an evolving magmatic-hydrothermal system: Evidence from rare earth elements in zircon from the No. 112 pegmatite, Kelumute, Chinese Altai. J. Asian Earth Sci. 164, 9–22.

Lv, Z.H., Zhang, H., Tang, Y., Zhao, J.Y., Liu, Y.L., Guo, L., 2018c. The distribution of phosphorous in various types of pegmatites from Altai, Xinjiang and its Implication. Bull. Mineral. Petrol. Geochem. 37, 260–270 (in Chinese with English abstract).

Ma, Z.L., Zhang, H., Tang, Y., Lv, Z.H., Zhang, X., Zhao, J.Y., 2015. Zircon U-Pb geochronology and Hf isotopes of pegmatites from the Kaluan mining area in the Altay, Xinjiang and their genetic relationship with the Halong granite. Geochimica 44, 9–26 (in Chinese with English abstract).

Melleton, J., Gloaguen, E., Frei, D., Novak, M., Breiter, K., 2012. How are the emplacement of rare-element pegmatites, regional metamorphism and magmatism interrelated in the Moldanubian Domain of the Variscan Bohemian Massif, Czech Republic? Can. Mineral. 50, 1751–1773.

Müller, A., Ihlen, P.M., Snook, B., Larsen, R., Flem, B., Bingen, B., Williamson, B.J., 2015. The chemistry of quartz in granitic pegmatites of southern Norway: petrogenetic and economic implications. Econ. Geol. 110, 137–157.

Müller, A., Romer, R.L., Szuszkiewicz, A., Ilnicki, S., Szełęg, E., 2016. Can pluton-related and pluton-unrelated granitic pegmatites be distinguished by their chemistry? Second Eugene E. Foord Pegmatite Symposium, pp. 67–69

Müller, A., Romer, R.L., Pedersen, R.-B., 2017. The Sveconorwegian Pegmatite Province - thousands of pegmatites without parental granites. Can. Mineral. 55, 283–315.

Müller, A., Simmons, W., Beurlen, H., Thomas, R., Ihlen, P.M., Wise, M., Roda-Robles, E., Neiva, A.M.R., Zagorsky, V., 2018. A proposed new mineralogical classification system for granitic pegmatites-Part I: history and the need for a new classification. Can. Mineral. 56, 1–25.

Nasdala, L., Wenzel, M., Vavra, G., Irmer, G., Wenzel, T., Kober, B., 2001. Metamictisation of natural zircon: accumulation versus thermal annealing of radioactivity-induced damage. Contrib. Mineral. Petrol. 141, 125–144.

Nasdala, L., Reiners, P.W., Garver, J.I., Kennedy, A.K., Stern, R.A., Balan, E., Wirth, R., 2004. Incomplete retention of radiation damage in zircon from Sri Lanka. Am. Mineral. 89, 219–231.

Pirajno, F., Mao, J., Zhang, Z., Zhang, Z., Chai, F., 2008. The association of mafic-ultramafic intrusions and A-type magmatism in the Tian Shan and Altay orogens, NW China: implications for geodynamic evolution and potential for the discovery of new ore deposits. J. Asian Earth Sci. 32, 165–183.

Ortega-Rivera, A., Farrar, E., Hanes, J.A., Archibald, D.A., Gastil, R.G., Kimbrough, D.L., Zentilli, M., López-Martinez, M., Féraud, G., Ruffet, G., 1997. Chronological constraints on the thermal and tilting history of the Sierra San Pedro Mártir pluton, Baja California, México, from U/Pb, 40Ar/39Ar, and fission-track geochronology. Geol. Soc. Am. Bull. 109 (6), 728–745.

Qin, J.H., Geng, X.X., Wen, C.Q., Guo, J.X., Ren, Y.C., 2016. Zircon LA-ICP-MS U-Pb age of intrusion from Xiaotuergen copper deposit in Altay, Xinjiang, and its geological significance. Mineral Depos. 35, 18–32 (in Chinese with English abstract).

Raith, J.G., Stein, H.J., 2000. Re-Os dating and sulfur isotopic composition of molybdenite from tungsten deposits in western Namaqualand, South Africa: implications for ore genesis and the timing of metamorphism. Miner. Deposita 35, 741–753.

Ren, B.Q., Zhang, H., Tang, Y., Lv, Z.H., 2011. LA-ICPMS U-Pb zircon geochronology of the Altai pegmatites and its geological significance. Acta. Mineral. Sin. 31, 587–596 (in Chinese with English abstract).

Romer, R.L., Smeds, S.-A., 1994. Implications of U-Pb ages of columbite-tantalites from granitic pegmatites for the Palaeoproterozoic accretion of 1.90-1.85Ga magmatic arcs to the Baltic Shield. Precambrian Res. 67, 141–158.

Selway, J.B., Breaks, F.W., Tindle, A.G., 2005. A review of rare-element (Li-Cs-Ta) pegmatite exploration techniques for the Superior Province, Canada, and large worldwide tantalum deposits. Explor. Min. Geol. 14, 1–30.

Shaw, R.A., Goodenough, K.M., Roberts, N.M.W., Horstwood, M.S.A., Chenery, S.R., Gunn, A.G., 2016. Petrogenesis of rare-metal pegmatites in high-grade metamorphicterranes: A case study from the Lewisian Gneiss Complex of northwest Scotland. Precam. Res. 281, 338–362.

Shearer, C.K., Papike, J.J., Jolliff, B.L., 1992. Petrogenetic links among granites and pegmatites in the Harney Peak rare-element granite-pegmatite system, Black Hills, South Dakota. Can. Mineral. 30, 785–809.

Shen, R.F., 2015. Geochemical Characteristics of Paleozoic Strata and Their Implications for Depositional Environment and Rare Metal Background in Altay orogen, north Xinjiang, China. A Dissertation Submitted to Institute of Geochemistry for the Degree of Master of Philosophy, Guiyang. pp. 1–78 (in Chinese with English abstract).

Shi, W.X., Zhang, J.D., Liu, W.G., Feng, H.G., Yu, Y., 2015. Chronology and petrology characteristics of early devonian gnessic granites from east Altai orogenic belt. Xinjiang Geol. 33 (4), 456–462 (in Chinese with English abstract).

Simmons, W.B., Falster, A.U., 2016. Evidence for an anatectic origin of an LCT type pegmatite: Mt. Second Eugene E. Foord Pegmatite Symposium, Mica, Maine, p. 103.

Song, P., Tong, Y., Wang, T., Qin, Q., Zhang, J.J., Ning, D.X., 2017. Zircon U-Pb ages and genetic evolution of Devonian granitic rocks in the southeastern Chinese Altai and its tectonic implications: new evidence for magmatic evolution of calc-alkaline-high-K calc-alkaline-alkaline rocks. Acta Geol. Sin. 91 (1), 55–79 (in Chinese with English abstract).

Snook, B.R., 2014. Towards exploration tools for high purity quartz: an example from the south norwegian evje-iveland pegmatite belt. A thesis for the degree of Doctor of Philosophy in Earth Resources. University of Exeter, pp. 1–284.

Sun, M., Yuan, C., Xiao, W.J., Long, X.P., Xia, X.P., Zhao, G.C., Lin, S.F., Wu, F.Y., Kroner, A., 2008. Zircon U-Pb and Hf isotopic study of gneissic rocks from the Chinese Altai: progressive accretionary history in the early to middle Palaeozoic. Chem. Geol. 247, 352–383.

Sun, G.H., Li, J.Y., Yang, T.N., Li, Y.P., Zhu, Z.X., Yang, Z.Q., 2009a. Zircon SHRIMP U-Pb dating of two linear granite plutons in southern Altay Mountains and its tectonic implications. Geol. China 36 (5), 976–987 (in Chinese with English abstract).

Sun, M., Long, X., Cai, K., Jiang, Y., Wang, B., Yuan, C., Zhao, G.C., Xiao, W., Wu, F., 2009b. Early Paleozoic ridge subduction in the Chinese Altai: insight from the abrupt change in zircon Hf isotopic compositions. Sci. China 52, 1345–1358.

Tang, Y., Zhang, H., 2015. Lanthanide tetrads in normalized rare element patterns of zircon from the Koktokay No. 3 granitic pegmatite, Altay, NW China. Am. Mineral. 100, 2630–2636.

Tang, Y., Zhang, H., Su, G.Z., 2013. Phosphorus in alkali feldspars as an indicator for prospecting for pegmatite-type rare-metal ore deposits in Altay, NW China. Geochemistry 13, 3–10.

Tang, Y., Wang, H., Zhang, H., Lv, Z.H., 2018. K-feldspar composition as an exploration tool for pegmatite-type rare metal deposits in Altay, NW China. J. Geochem. Explor. 185, 130–138.

Thomas, R., Davidson, P., 2016. Revisiting complete miscibility between silicate melts and hydrous fluids, and the extreme enrichment of some elements in the supercritical state - consequences for the formation of pegmatites and ore deposits. Ore Geol. Rev. 72, 1088–1101.

Tong, Y., Hong, D.W., Wang, T., Wang, S.G., Han, B.F., 2006. TIMS U-Pb zircon ages of Fuyun post-orogenic linear granite plutons on the southern margin of Altay orogenic belt and their implications. Acta Petrol. Mineral. 25, 85–89 (in Chinese with English abstract).

Tong, Y., Wang, T., Siebel, W., Hong, D.W., Sun, M., 2012. Recognition of early Carboniferous alkaline granite in the southern Altai orogen: post-orogenic processes constrained by U-Pb zircon ages, Nd isotopes, and geochemical data. Int. J. Earth Sci. 101, 937–950.

Tong, L.X., Chen, Y.B., Xu, Y.G., Zhou, X., Liu, Z., 2013. Zircon U-Pb ages of the ultrahigh-temperature metapelitic granulite from the Altai orogen, NW China, and geological implications. Acta Petrol. Sin. 29 (10), 3435–3445 (in Chinese with English abstract).

Tong, Y., Wang, T., Jahn, B.M., Sun, M., Hong, D.W., Gao, J.F., 2014. Post-accretionary Permian granitoids in the Chinese Altai orogen: geochronology, petrogenesis and tectonic implications. Am. J. Sci. 314, 80–109.

Vervoort, J.D., Patchett, P.J., Blichert-Toft, J., Albarède, F., 1999. Relationships between Lu-Hf and Sm-Nd isotopic systems in the global sedimentary system. Earth Planet. Sci. Lett. 168, 79–99.

Wan, B., Xiao, W.J., Zhang, L., Windley, B.F., Han, C., Quinn, C.D., 2011. Contrasting styles of mineralization in the Chinese Altai and East Junggar, NW China: implications for the accretionary history of the southern Altaids. J. Geol. Soc. London 168, 1311–1321.

Wan, B., Xiao, W.J., Windley, B.F., Yuan, C., 2013. Permian hornblende gabbro in the Chinese Altai from a subduction-related hydrous parent magma, not from the Tarim mantle plume. Lithosphere 5, 290–299.

Wang, W., 2011. The Anatexis of Pelitic Rocks and the Genesis of Leucogranite in the Altai Orogen, Xinjiang. A Dissertation Submitted to Peking University for Doctor Degree. pp. 1–104 (in Chinese with English abstract).

Wang, X.J., Zou, T.R., Xu, J.G., Yu, X.Y., Qiu, Y.Z., 1981. Mineral Study of Pegmatites in the Chinese Altai. Science Press, Beijing, pp. 1–140 (in Chinese).

Wang, D.H., Chen, Y.C., Xu, Z.G., 2001. Chronological study of Caledonian metamorphic pegmatite muscovite deposits in the Altay Mountains, northwestern China, and its significance. Acta Geol. Sin. 75, 419–425 (in Chinese with English abstract).

Wang, D.H., Chen, Y.C., Xu, Z.G., 2002. Metallogenetic Series and Regularity of the Altay Metallogenic Province. Atomic Energy Press, Beijing, pp. 1–493 (in Chinese).

Wang, D.H., Chen, Y.C., Xu, Z.G., 2003. $^{40}Ar/^{39}Ar$ isotope dating on muscovites from Indosinian rare-metal deposits in Central Altay, Northwestern China. Bull. Mineral. Petrol. Geochem. 22, 14–17 (in Chinese with English abstract).

Wang, T., Hong, D.W., Tong, Y., Han, B.F., Shi, Y.R., 2005. Zircon U-Pb SHRIMP age and origin of post-orogenic Lamazhao granitic pluton from Altai orogen: its implications for vertical continental growth. Acta Petrol. Sin. 21, 640–650 (in Chinese with English abstract).

Wang, T., Tong, Y., Li, S., Zhang, J.J., Shi, X.J., Li, J.Y., Han, B.F., 2010. Spatial andtemporal variations of granitoids in the Altay orogen and their implications for tectonic setting and crustal growth: perspectives from Chinese Altay. Acta Petrol. Mineral. 29, 595–618 (in Chinese with English abstract).

Wang, R.C., Hu, H., Zhang, A.C., Fontan, F., Zhang, H., De Parseval, P., 2006a. Occurrence and late re-equilibration of pollucite from the Koktokay no. 3 pegmatite, Altai, northwestern China. Am. Mineral. 91, 729–739.

Wang, T., Hong, D.W., Jahn, B.M., Tong, Y., 2006b. Timing, petrogenesis, and setting of Paleozoic synorogenic intrusions from the Altai Mountains, Northwest China: implications for the tectonic evolution of an accretionary orogen. J. Geol. 114, 735–751.

Wang, R.C., Hu, H., Zhang, A.C., Fontan, F., de Parseval, P., Jiang, S.Y., 2007a. Cs-dominant polylithionite in the Koktokay# 3 pegmatite, Altai, NW China: in situ microcharacterization and implication for the storage of radioactive cesium. Contrib. Mineral. Petrol. 153, 355–367.

Wang, T., Tong, Y., Jahn, B.M., Zou, T.R., Wang, Y.B., Hong, D.W., Han, B.F., 2007b. SHRIMP U-Pb Zircon geochronology of the Altai No. 3 Pegmatite, NW China, and its implications for the origin and tectonic setting of the pegmatite. Ore Geol. Rev. 32, 325–336.

Wang, R.C., Che, X.D., Zhang, W.L., Zhang, A.C., Zhang, H., 2009a. Geochemical evolution and late re-equilibration of Na–Cs-rich beryl from the Koktokay# 3 pegmatite (Altai, NW China). Eur. J. Mineral. 21, 795–809.

Wang, T., Jahn, B.M., Kovach, V.P., Tong, Y., Hong, D.W., Han, B.F., 2009b. Nd-Sr isotopic mapping of the Chinese Altai and implications for continental growth in the Central Asian Orogenic Belt. Lithos 110, 359–372.

Wang, W., Wei, C., Wang, T., Lou, Y.X., Chu, H., 2009c. Confirmation of pelitic granulite in the Altai orogen and its geological significance. Chin. Sci. Bull. 54, 2543–2548.

Wang, Y., Yuan, C., Long, X., Sun, M., Xiao, W., Zhao, G., Cai, K., Jiang, Y., 2011. Geochemistry, zircon U-Pb ages and Hf isotopes of the Paleozoic volcanic rocks in the northwestern Chinese Altai: petrogenesis and tectonic implications. J. Asian Earth Sci. 42 (5), 969–985.

Wang, W., Wei, C., Zhang, Y., Chu, H., Zhao, Y., Liu, X., 2013. SHRIMP zircon U-Pb dating of a small tonalite intrusion in metamorphic belt of Chinese Altai orogen and its geological implication. Global Geol. 16, 184–191.

Wang, T., Jahn, B.M., Kovach, V.P., Tong, Y., Wilde, S.A., Hong, D.W., Li, S., Salnikova, E.B., 2014a. Mesozoic intraplate granitic magmatism in the Altai accretionary orogen, NW China: implications for the orogenic architecture and crustal growth. Am. J. Sci. 314, 1–42.

Wang, W., Wei, C., Zhang, Y., Chu, H., Zhao, Y., Liu, X., 2014b. Age and origin of sillimanite schist from the Chinese Altai metamorphic belt: implications for late Palaeozoic tectonic evolution of the Central Asian Orogenic Belt. Int. Geol. Rev. 56, 224–236.

Wei, C.J., Clarke, G., Tian, W., Qiu, L., 2007. Transition of metamorphic series from the Kyanite- to andalusite-types in the Altai orogen, Xinjiang, China: evidence from petrography and calculated KMnFMASH and KFMASH phase relations. Lithos 96, 353–374.

White, R.W., Powell, R., Holland, T.J.B., 2001. Calculation of partial melting equilibria in the system Na_2O–CaO–K_2O–FeO–MgO–Al_2O_3–SiO_2–H_2O (NCKFMASH). J. Metamorph. Geol. 19, 139–153.

White, R.W., Powell, R., 2002. Melt loss and the preservation of granulite facies mineral assemblages. J. Metam. Geol. 20 (7), 621–632.

Wiedenbeck, M., Hanchar, J.M., Peck, W.H., Sylvester, P., Valley, J., Whitehouse, M., Kronz, A., Morishita, Y., Nasdala, L., Fiebig, J., Franchi, I., Giard, J.P., Greenwood, R.C., Hinton, R., Kita, N., Mason, P.R.D., Norman, M., Ogasawara, M., Piccoli, P.M., Rhede, D., Satoh, H., Schulz-Dobrick, B., Skar, O., Spicuzza, M.J., Terada, K., Tindle, A., Togashi, S., Vennemann, T., Xie, Q., Zheng, Y.F., 2004. Further characterisation of the 91500 zircon crystal. Geostand. Geoanal. Res. 28, 9–39.

Windley, B.F., Kroener, A., Guo, J., Qu, G., Li, Y., Zhang, C., 2002. Neoproterozoic to Paleozoic geology of the Altai Orogen, NW China: new zircon age data and tectonic evolution. J. Geol. 110, 719–737.

Windley, B.F., Alexeiev, D., Xiao, W.J., Kröner, A., Badarch, G., 2007. Tectonic models for accretion of the Central Asian Orogenic Belt. J. Geol. Soc. 164, 31–47.

Wu, Y.B., Zheng, Y.F., 2004. Genesis of zircon and its constraints on interpretation of U-Pb age. Chin. Sci. Bull. 49, 1554–1569.

Wu, B.Q., Zou, T.R., 1989. The genesis of granitic pegmatites in Xinjiang Altai. Mineral Geol. Xinjiang 1, 60–70 (in Chinese).

Wu, C.N., Zhu, J.C., Liu, C.S., 1994. A study on the inclusions in spodumenes from Altai pegmatite, Xinjiang. Geotect. Metal. 18, 353–362 (in Chinese with English abstract).

Xiang, L., Wang, R.C., Romer, R.L., Che, X.D., Hu, H., Xie, L., Tian, E.N., 2020. Neoproterozoic Nb-Ta-W-Sn bearing tourmaline leucogranite in the western part of Jiangnan Orogen: implications for episodic mineralization in South China. Lithos 360–361, 105450.

Xiao, W.J., Han, C.M., Yuan, C., Sun, M., Lin, S.F., Chen, H.L., Li, Z.L., Li, J.L., Sun, S., 2008. Middle Cambrian to Permian subduction-related accretionary orogenesis of Northern Xinjiang, NW China: implications for the tectonic evolution of central Asia. J. Asian Earth Sci. 32, 102–117.

Xiao, W.J., Windley, B.F., Huang, B.C., Han, C.M., Yuan, C., Chen, H.L., Sun, M., Sun, S., Li, J.Y., 2009. End-Permian to mid-Triassic termination of the accretionary processes of the southern Altaids: implications for the geodynamic evolution, Phanerozoic continental growth, and metallogeny of Central Asia. Int. J. Earth Sci. 98, 1189–1217.

Xiao, W., Windley, B.F., Sun, S., Li, J., Huang, B., Han, C., Yuan, C., Sun, M., Chen, H., 2015. A tale of amalgamation of three Permo-Triassic collage systems in Central Asia: oroclines, sutures, and terminal accretion. Annu. Rev. Earth Planet. Sci. 43, 477–507.

Xiao, W., Windley, B.F., Han, C., Liu, W., Wan, B., Zhang, J.E., Ao, S.J., Zhang, Z.Y., Song, D., 2018. Late Paleozoic to early Triassic multiple roll-back and oroclinal bending of the Mongolia collage in Central Asia. Earth Sci. Rev. 186, 94–128.

Xu, Z.Q., Fu, X.F., Wang, R.C., Li, G.W., Zheng, Y.L., Zhao, Z.B., Lian, D.Y., 2020. Generation of lithium-bearing pegmatite deposits within the Songpan-Ganze orogenic belt, East Tibet. Lithos 354-355, 105281.

Xue, C.J., Chi, G.X., Zhao, X.B., Wu, G.G., Zhao, Z.F., Dong, L.H., 2016. Multiple and prolonged porphyry Cu-Au mineralization and alteration events in the Halasu deposit, Chinese Altai, Xinjiang, northwestern China. Geosci. Front. 7, 799–809.

Yan, Q.H., Qiu, Z.W., Wang, H., Wang, M., Wei, X.P., Li, P., Zhang, R.Q., Li, C.Y., Liu, J.P., 2018. Age of the Dahongliutan rare metal pegmatite deposit, West Kunlun,Xinjiang (NW China): constraints from LA–ICP–MS U–Pb dating ofcolumbite-(Fe) and cassiterite. Ore Geol. Rev. 100, 561–573.

Yang, F., Mao, J., Liu, F., Chai, F., Guo, Z., Zhou, G., Geng, X., Gao, J., 2010. Geochronology and geochemistry of the granites from the Mengku iron deposit, Altay Mountains, northwest China: implications for its tectonic setting and metallogenesis. Aust. J. Earth Sci. 57, 803–818.

Yang, F.Q., Liu, F., Chai, F.M., Guo, Z.L., Guo, X.J., Zhang, Z.X., Liu, G.R., Zhou, G., Huang, C.K., Qin, J.H., Geng, X.X., Lü, S.J., 2012. Iron Deposit in Altay, Xinjiang, China. Geological Publishing House, Beijing, China, pp. 1–300 (in Chinese).

Yang, F., Mao, J., Liu, F., Chai, F., Geng, X., Zhang, Z., Guo, X., Liu, G., 2013. A review of the geological characteristics and mineralization history of iron deposits in the Altay orogenic belt of the Xinjiang, Northwest China. Ore Geol. Rev. 54, 1–16.

Yang, W.B., Niu, H.C., Shan, Q., Sun, W.D., Zhang, H., Li, N.B., Jiang, Y.H., Yu, X.Y., 2014. Geochemistry of magmatic and hydrothermal zircon from the highly evolved Baerzhe alkaline granite: implications for Zr-REE-Nb mineralization. Miner. Deposita 49 (4), 451–470.

Ye, X.T., Zhang, C.L., Zou, H.B., Zhou, G., Yao, C.Y., Dong, Y.P., 2015. Devonian Alaskan-type ultramafic-mafic intrusions and silicic igneous rocks along the southern Altai orogen: implications on the Phanerozoic continental growth of the Altai orogen of the Central Asian Orogenic Belt. J. Asian Earth Sci. 113, 75–89.

Yin, R., Wang, R.C., Zhang, A.C., Hu, H., Zhu, J.C., Rao, C., Zhang, H., 2013. Extreme fractionation from zircon to hafnon in the Koktokay No. 1 granitic pegmatite, Altai, northwestern China. Am. Mineral. 98, 1714–1724.

Yuan, F., Zhou, T.F., Yue, S.C., 2001. The ages and genetic types of the granites in the Nurt area, Altai. Xinjiang Geol. 19, 292–296 (in Chinese with English abstract).

Yuan, H.L., Gao, S., Liu, X.M., Li, H.M., Gunther, D., Wu, F.Y., 2004. Accurate U-Pb age and trace element determinations of zircon by laser ablation-inductively coupled plasma mass spectrometry. Geostandards Newslett. 28, 353–370.

Yuan, C., Sun, M., Xiao, W.J., Li, X.H., Chen, H.L., Lin, S.F., Xia, X.P., Long, X.P., 2007. Accretionary orogenesis of the Chinese Altai: insights from Paleozoic granitoids. Chem. Geol. 242, 22–39.

Zagorsky, V.Y., Vladimirov, A.G., Makagon, V.M., Kuznetsova, L.G., Smirnov, S.Z., D'yachkov, B.A., Annikova, I.Y., Shokalsky, S.P., Uvarov, A.N., 2014. Large fields of spodumene pegmatites in the settings of rifting and postcollisional shear-pull-apart dislocations of continental lithosphere. Russian Geol. Geophys. 55, 237–251.

Zhang, H., 2001. The Geochemical Behaviors and Mechanisms of Incompatible Trace Elements in the Magmatic–Hydrothermal Transition System: A Case Study of Altay No. 3 Pegmatite, Xinjiang. A Dissertation Submitted to Institute of Geochemistry for the Degree of Doctor of Philosophy, Guiyang. pp. 1–172 (in Chinese with English abstract).

Zhang, A.C., Wang, R.C., Hu, H., Zhang, H., Zhu, J.C., Chen, X.M., 2004. Chemical evolution of Nb-Ta oxides and zircon from the Koktokay No. 3 granitic pegmatite, Altai, northwestern China. Mineral. Magazine 66, 739–756.

Zhang, C.L., Li, Z.X., Li, X.H., Xu, Y.G., Zhou, G., Ye, H.M., 2010. A Permian large igneous province in Tarim and Central Asian orogenic belt, NW China: results of a ca. 275 Ma mantle plume? Geol. Soc. Am. Bull. 122, 2020–2040.

Zhang, C.L., Santosh, M., Zou, H.B., Xu, Y.G., Zhou, G., Dong, Y.G., Ding, R.F., Wang, H.Y., 2012. Revisiting the "Irtish tectonic belt": implications for the Paleozoic tectonic evolution of the Altai orogen. J. Asian Earth Sci. 52, 117–133.

Zhang, C.L., Zou, H.B., Yao, C.Y., Dong, Y.G., 2014. Origin of Permian gabbroic intrusions in the southern margin of the Altai Orogenic belt: a possible link to the Permian Tarim mantle plume? Lithos 204, 112–124.

Zhang, Y., Chen, J.L., Bai, J.K., Tang, Z., 2015. LA-ICP-MS zircon U-Pb dating of gneissic granitic intrusive mass in Wuqiagou on the southern margin of Altay Orogenic Belt and its geological significance. Northwestern Geol. 48 (3), 127–139 (in Chinese with English abstract).

Zhang, X., Zhang, H., Ma, Z.L., Tang, Y., Lv, Z.H., Zhao, J.Y., Liu, Y.L., 2016. A new model for the granite–pegmatite genetic relationships in the Kaluan-Azubai-Qiongkuer pegmatite-related ore fields, the Chinese Altay. J. Asian Earth Sci. 124, 139–155.

Zhang, C., Liu, L.F., Santosh, M., Luo, Q., Zhang, X., 2017. Sediment recycling and crustal growth in the Central Asian Orogenic Belt: evidence from Sr–Nd–Hf isotopes and trace elements in granitoids of the Chinese Altay. Gondw. Res. 47, 142–160.

Zhang, C., Liu, D., Luo, Q., Liu, L., Zhang, Y., Zhu, D., Wang, P.F., Dai, Q., 2018. An evolving tectonic environment of Late Carboniferous to Early Permian granitic plutons in the Chinese Altai and Eastern Junggar terranes, Central Asian Orogenic Belt, NW China. J. Asian Earth Sci. 159, 185–208.

Zhao, Y.M., Peng, G., Zhao, D.L., You, Y.C., 2016. LA-ICP-MS zircon age and geochemistry of the Kezile granite pluton in Altay of China and their geological implications. Geol. Explor. 52 (2), 271–282 (in Chinese with English abstract).

Zhao, J.Y., Zhang, H., Tang, Y., Lv, Z.H., Chen, Y., 2017. Ore-forming elements diffusion and distribution in the altered host rock surrounding the Koktokay No. 3 pegmatite in the Chinese Altay. Acta Geochim. 36 (2), 151–165.

Zheng, J., Chai, F., Yang, F., 2016. The 401-409 Ma Xiaodonggou granitic intrusion: implications for understanding the Devonian Tectonics of the Northwest China Altai orogen. Int. Geol. Rev. 58, 540–555.

Zhou, G., Zhang, Z.C., Luo, S.B., He, B., Wang, X., Yin, L.J., Zhao, H., Li, A.H., He, Y.K., 2007. Confirmation of high-temperature strongly peralumious Mayin'ebo granites in the south margin of Altay, Xinjiang: age, geochemistry and tectonic implications. Acta Petrol. Sin. 23, 1909–1920 (in Chinese with English abstract).

Zhou, G., Dong, L.H., Qin, Q.H., Zhang, L.W., Zhao, Z.H., Li, Y., 2015. The age of the granitoids in the Dolanasayi gold ore district in Xinjiang and its constraints on gold mineralization. Geol. China 42 (3), 677–690 (in Chinese with English abstract).

Zhou, Q., Qin, K., Tang, D., Wang, C., Tian, Y., Sakyi, P.A., 2015a. Mineralogy of the Koktokay No. 3 pegmatite, Altai, NW China: implications for evolution and melt-fluid processes of rare-metal pegmatites. Eur. J. Mineral. 27, 433–457.

Zhou, Q.F., Qin, K.Z., Tang, D.M., Tian, Y., Cao, M.J., Wang, C.L., 2015b. Formation age and evolution time span of the Koktokay No. 3 pegmatite, Altai, NW China: evidence from U-Pb zircon and $^{40}Ar/^{39}Ar$ muscovite ages. Resour. Geol. 65, 210–231.

Zhou, Q.F., Qin, K.Z., Tang, D.M., Wang, C.L., 2018. LA-ICP-MS U-Pb zircon, columbite-tantalite and ^{40}Ar-^{39}Ar muscovite age constraints for the rare-element pegmatite dykes in the Altai orogenic belt, NW China. Geol. Mag. 155 (3), 707–728.

Zhu, J.C., Wu, C.N., Liu, C.S., Li, F.C., Huang, X.L., Zhou, D.S., 2000. Magmatic-hydrothermal evolution and genesis of Koktokay No. 3 rare metal pegmatite dyke, Altai, China. Geol. J. China Univ. 6, 40–52 (in Chinese with English abstract).

Zhuang, Y.X., 1994. The pressure-temperature-space-time (PTSt) evolution of metamorphism and development mechanism of the thermal-structural-gneiss domes in the Chinese Altaides. Acta Geol. Sin. 68 (1), 35–47 (in Chinese with English abstract).

Zou, T.R., Li, Q.C., 2006. Rare and Rare Earth Metallic Deposits in Xinjiang, China. Geological Publishing House, Beijing, pp. 1–284 (in Chinese with English abstract).

Zou, T.R., Xu, J.G., 1975. On the origin and classification of granite pegmatites. Geochimica 3, 161–174 (in Chinese with English abstract).